University of Zurich[UZH]

Assessing RAMMS for Glacial Lake Outburst Floods: A Comparative Study Across Diverse Geographical Regions

GEO 511 Master's Thesis

Author
Noël Baumann
18-110-668

Supervised by
Brian McArdell (brian.mcardell@wsl.ch)

Faculty representative
Prof. Dr. Christian Huggel

03.02.2025
Department of Geography, University of Zurich

Acknowledgments

This thesis would not have been possible without the support of many individuals. First and foremost, I would like to express my deepest gratitude to my supervisor, Dr. Brian McArdell from the Institute for Forest, Snow and Landscape Research (WSL), for his support from the beginning to the finish of my thesis. His valuable insights into my concept and expertise in working with the software RAMMS were instrumental in the progress of my thesis. Beyond his expertise in mass flows and proficiency in modeling them, it was always a pleasure to engage in discussion with him, not only about my thesis but also about the field of natural hazards.

I am also sincerely grateful to Prof. Dr. Christian Huggel, who enabled my connection with Brian and guided me in conceptualizing my thesis. His generous feedback on my initial draft was greatly appreciated. Both Brian and Christian demonstrated a pragmatic working approach, and I thoroughly enjoyed working with them.

Furthermore, I would like to extend my appreciation to:

- Marc Christen from the Institute for Snow and Avalanches Research (SLF), for generously providing me with the RAMMS license.
- My employer, CSD Ingenieure AG, for their understanding of the commitments that came with my master's thesis and continuous support.
- Dr. Holger Frey, who proposed during my concept presentation the idea of examining the South Lhonak GLOF events from October 2023. This study site enabled fascinating insights and valuable lessons on dealing with limited data availability and large-scale GLOF modeling.
- Florian Bissig and Eva Planzer, who always welcomed me with a place to stay in their apartment while I was working on my thesis in Zurich.
- My friends and family, for their support and for offering much-needed distractions throughout my thesis journey.
- The Cantonal Library of Uri, for providing an excellent infrastructure that enabled me to work remotely on my master's thesis.

Abstract

Glacial lake outburst floods (GLOFs) pose significant threats to downstream infrastructure and communities and are considered the most hazardous glacial phenomena globally. GLOFs can occur with minimal forewarning and reach extreme magnitudes due to their capacity to entrain sediments, thereby altering their flow behavior. Since the 2000s, several models have been developed to address the dynamic and complex behavior of GLOFs in terms of inundation extents and runout distances. This thesis investigates the capability of the numerical single-phase model RAMMS to replicate these characteristics. To assess the inundation extent and flow heights of GLOF simulations, the study sites of Weingarten Lake in Switzerland and South Lhonak Lake in India were analyzed. The findings demonstrate that RAMMS can accurately replicate GLOF inundation extents, performing comparably with other models such as HEC-RAS or r.avaflow. Furthermore, the study underscores the critical influence of applied Digital Elevation Model (DEM) and input volumes on modeling outcomes. The scope of the simulations in this study was constrained by limited computational power and data availability. Although the single-phase RAMMS version applied in this research successfully models GLOF characteristics, it remains limited to a single process within the cascading event chain and cannot independently replicate flow transitions. However, the upcoming two-phase version of RAMMS Is expected to address this limitation. Future research should focus on examining this elevated GLOF model. Additionally, a comprehensive literature review of friction parameters used in previous GLOF studies with RAMMS could help modelers select appropriate values for predictive simulations.

Table of Contents

List of Figures

List of Tables

List of Abbreviations

ASCII	American Standard Code for Information Interchange
DEM	Digital Elevation Model
ELM-SWE	Eulerian-Lagrangian Shallow Water Equation
EM-SWE	Euler Method Shallow Water Equation
ESRI	Environmental Systems Research Institute
EUR	Euro
GeoTIFF	Geographic Tag Image File Format
GIS	Geographic Information System
GLOF	Glacial Lake Outburst Flood
GRASS	Geographic Resources Analysis Support System
HEC-RAS	Hydrologic Engineering Center's River Analysis System
HKKH	Hindu Kush-Karakoram-Himalaya
LiDAR	Light Detection and Ranging
MSF	Modified Single-Flow-Direction
NASA	National Aeronautics and Space Administration
QGIS	Quantum Geographic Information System
RAMMS	Rapid Mass Movement Simulation
Sc	Scenario
SDGs	Sustainable Development Goals
SLF	Institute for Snow and Avalanches Research
SRTM	Shuttle Radar Topography Mission
SWE	Shallow Water Equation
URL	Uniform Resource Locator
WGS	World Geodetic System
WSL	Swiss Federal Institute for Forest, Snow and Landscape Research

1 Introduction

1.1 Context

Throughout the globe, the impact of climate change has led to the retreat of glaciers and will be precipitating significant depletion of glacier ice in the years to come (Zemp *et al.*, 2015). The receding of mountain glaciers is one of the most dependable indicators of shifting patterns in the Earth's climate (Kumar and Murugesh Prabhu, 2012). In high mountain terrains, the risk of glacial-related hazards increases due to melting glaciers. Glacial lakes pose significant challenges due to their high water volume content and fragile structures, as they can threaten villages and infrastructure located several kilometers along potential outflow routes. They can form through different processes such as over deepening in former glacier beds due to glacier retreat, which allows meltwater to collect as glacial lakes. In addition, glacial lakes can also be formed through dammed moraines (Richardson and Reynolds, 2000) or via the growth and coalescence of supraglacial ponds on debris-covered glaciers (Benn *et al.*, 2012). The expansion of glacial lakes is promoted by positive feedback effects through calving and subaqueous melting, causing additional melt and retreat of the glacier (King *et al.*, 2019). Sudden drainage of Glacial lakes occurs due to an impulse, where large water volumes can be released leading to glacial lake outburst floods named GLOFs (Harrison *et al.*, 2018). The impulsive initiation phase can differ from a mass movement-induced impulse wave, an extreme precipitation event causing overtopping of the dam to ice dam degradation (Clague and Evans, 2000; Westoby *et al.*, 2014; Rounce *et al.*, 2016).

GLOFs have the potential to be highly damaging, often striking with minimal forewarning, leading to substantial destruction of infrastructure and property resulting in widespread loss of life. According to Taylor *et al.* (2023), 15 million people globally are endangered today by the impacts of potential GLOFs. People in high-mountain Asia are especially exposed to GLOFs, where 1 million live within 10 km of a glacial lake (Taylor *et al.*, 2023). However, the impact of GLOFs varies considerably worldwide. Over the past 70 years, several thousand individuals have lost their lives due to GLOFs in the Cordillera Blanca alone, with the majority of fatalities occurring from a small number of incidents (Emmer *et al.*, 2020). Controversy, GLOF activity in European Alps over the past millennium has directly resulted in 393 deaths (Carrivick and Tweed, 2016). The ongoing melting of glacier ice and the consequent growth of glacial lakes, driven by climate change, thus present a significant global natural hazard.

Not only natural factors favor the risk of GLOFs but also socio-economic. This can be illustrated in the Hindu Kush-Karakoram-Himalaya (HKKH) where population and economic growth are trending in catchment areas where potential GLOFs are located (Taylor *et al.*, 2023). Houses and other infrastructures are built closer to river valleys, leading to a loss of vegetated river banks, reducing the natural buffer to flooding. This trend is observed generally in the HKKH, where the inexistence of expansion regulations and poorly built infrastructure increases the risk to GLOFs (Ziegler *et al.*, 2014). The coupling of the climate-driven expansion of glacial lakes and socio-economic development amplifies the exposure to GLOFs. Addressing this challenge aligns with the United Nations Sustainable Development Goals (SDGs), particularly Goal 11 (sustainable cities and communities), Goal 13 (climate action) and Goal 15 (life on land). Especially Goal 11 emphasizes disaster risk reduction, highlighting the need for

sustainable urban planning that balances growth while preventing unnecessary construction in GLOF-prone areas.

The term GLOF has been used differently in literature. Some authors refer to GLOF as an event of compromising a series of different, cascading processes (e.g. Worni *et al.*, 2014), whereas some refer to different types of outburst floods from glacial sources (e.g. Westoby *et al.*, 2014). In this study, the definition of a GLOF refers exclusively to the flow behavior and propagation.

1.2 Problem Statement

Outburst floods originating from glacial lakes consist of extremely mobile mixtures of water and sediment. They have the potential to travel long distances, ranging from tens to hundreds of kilometers, at velocities exceeding tens of kilometers per hour (Iverson, 1997; Worni *et al.*, 2014). As the flow distance increases, valley characteristics such as topography, vegetation and sediment availability become increasingly influential (Richardson and Reynolds, 2000). The flood volume and peak discharge can triple or more compared to initial values due to erosion and the incorporation of sediment, making these events highly dynamic (Mergili *et al.*, 2011). GLOFs can change their fluid and solid content from 10%, classified as a mudflow, to 60% for a granular debris flow (Hungr, Leroueil and Picarelli, 2014). This change leads to flow transitions with significant fluctuations as they propagate downstream. Such transitions are determined by sediment deposition and bulking processes, influenced by the slope of the flood path and mixing the flow with stream water called dilution (Smith and Lowe, 1991). Generally, sediment is entrained on steep slopes and deposited in shallow slopes (Iverson *et al.*, 2011). The hydrographs of GLOFs undergo attenuation as the slopes flatten and extend in duration as they flow downstream (Cronin *et al.*, 1999), making GLOFs highly dynamic and challenging to comprehend.

A persistent problem in mountain regions is modeling and predicting the possible inundation and deposition area of GLOFs (Emmer *et al.*, 2022). Water floods are well understood and model results based on the one-dimensional St. Venant equations or two-dimensional SWE (shallow water equation) can therefore be considered reliable (Worni *et al.*, 2014). However, when sufficient amounts of sediments are entrained into a flow, process descriptions are based in part on empirical relations. Therefore, simulations of hyperconcentrated flows and debris flows are generally less accurate than simulations of pure water flows, due to their more complex behavior influenced by additional sediment parameters (Worni *et al.*, 2012). However, several existing modeling software such as HEC-RAS (e.g. Sattar *et al.*, 2021), r.avaflow (e.g. Zhang, Wang and An, 2025) or RAMMS (e.g. Frey *et al.*, 2018) are used today to model GLOFs in various regions across the globe. Since it is challenging to define the parameters of a GLOF, especially if there is small data available, potential GLOF sites have to be calibrated first at other sites or through retrospective simulations of past events. This methodology is commonly used in literature (e.g. Mergili *et al.,* 2011; Frey *et al.*, 2016; Iribarren Anacona *et al.*, 2018) and poses a challenge to generate realistic simulations and predictions. However, the modeling and prediction of GLOF play a crucial role in natural hazard engineering and designing adaptation measurements.

In the scope of this study, GLOF simulations are conducted with the software RAMMS for two case studies in different geographical settings in Switzerland and Sikkim Himalaya. The simulation results, especially the inundation extent and flow heights are exploited and discussed with other modeling software available namely HEC-RAS and r.avaflow. The goal of the thesis is not only to exploit the GLOF sites in Switzerland and Sikkim Himalaya but also to the model performance of RAMMS regarding GLOFs. Moreover, the comparison to the other models allows making statements about the strengths and weaknesses of each model. Equations and calculation domains of each model are not exploited, as the focus lies more on the performance of the model in a practical view. The thesis aims to help practical engineers in the decision-making process regarding models for the GLOF sites under investigation.

1.3 Research Question

An analysis of models is essential for future hazard management regarding GLOFs. A more accurate simulation model enables engineers to formulate effective adaptation and mitigation strategies, protecting infrastructure and human lives. Consequently, the following research question arises:

- To what extent can the present modeling tools, such as RAMMS, effectively replicate the complex flow dynamics and transformation processes of glacial lake outburst floods (GLOFs) across diverse geographical settings?

2 Scientific Background

2.1 Causes and Cascading Processes of GLOFs

The causes and cascading processes of GLOFs are interconnected and complex, influenced by climatic, hydrological, geological and anthropogenic factors. Ongoing climate change leads to retreating glaciers and the formation of glacial lakes, as the expected frequency and magnitude of GLOFs will increase. Glacial lakes occur in the alpine and high-mountain regions around the globe. According to Grove (2019), a greater part of lateral and terminal moraine complexes impound present-day glacial lakes were formed in the so-called Little Ice Age. This period is a globally-synchronous time where glacial advance occurred between the 15th and the end of the 19th century. Glacial lakes form between the glacier terminus and the moraine, when the moraine is sufficiently consolidated and stable. For this development, an over-deepened glacier bed is required (Frey *et al.*, 2016). The permeability of the moraine determines the growth of the lake, the volume increases until piping or overtopping occurs (Worni *et al.*, 2014). However, the lake's volume can naturally be regulated through seepage through the moraine structure or over the dam crest (Costa and Schuster, 1988) or through technical adaptations as done in at the Lago Effimero in the Monte Rosa region in Italy (Voigt *et al.*, 2010).

The extent of the glacial lakes is strongly variable and can differ regarding the geographical setting of the surrounding environment. GLOFs are distinctive occurrences that take place in various geographical regions, exhibiting different manifestations. For instance, Jökulhlaup events are occurring in Iceland, characterized by glacial lake outburst floods triggered by volcanic subglacial activity (Hungr, Leroueil and Picarelli, 2014). Conversely, in Huaraz (Chile), glacial lake outburst floods were initiated by ice mass movement flowing into glacier lakes (Frey *et al.*, 2018; Motschmann *et al.*, 2020; Meyrat *et al.*, 2024). Nevertheless, GLOFs include a sequence of processes, structured into three key phases: trigger mechanism and the resulting wave propagation or piping through the dam (Phase 1, Figure 1), dam breach initiation (Phase 2, Figure 1) and the actual flood from the glacial lake (Chapter 2.1.3). These key phases, in turn, encompass distinct mechanisms that can be identified (Worni *et al.*, 2014).

In this study the focus is on a European and an Asian GLOF event, thus the investigation centers on GLOF initiated by mass movement or dam breaches. The following Sections 2.1.1 – 2.1.3 elaborate on the primary and subordinate mechanisms involved in GLOFs. Since the study focuses on flood propagation and its modeling approaches, only brief explanations are provided for the trigger and the breaching or overtopping processes.

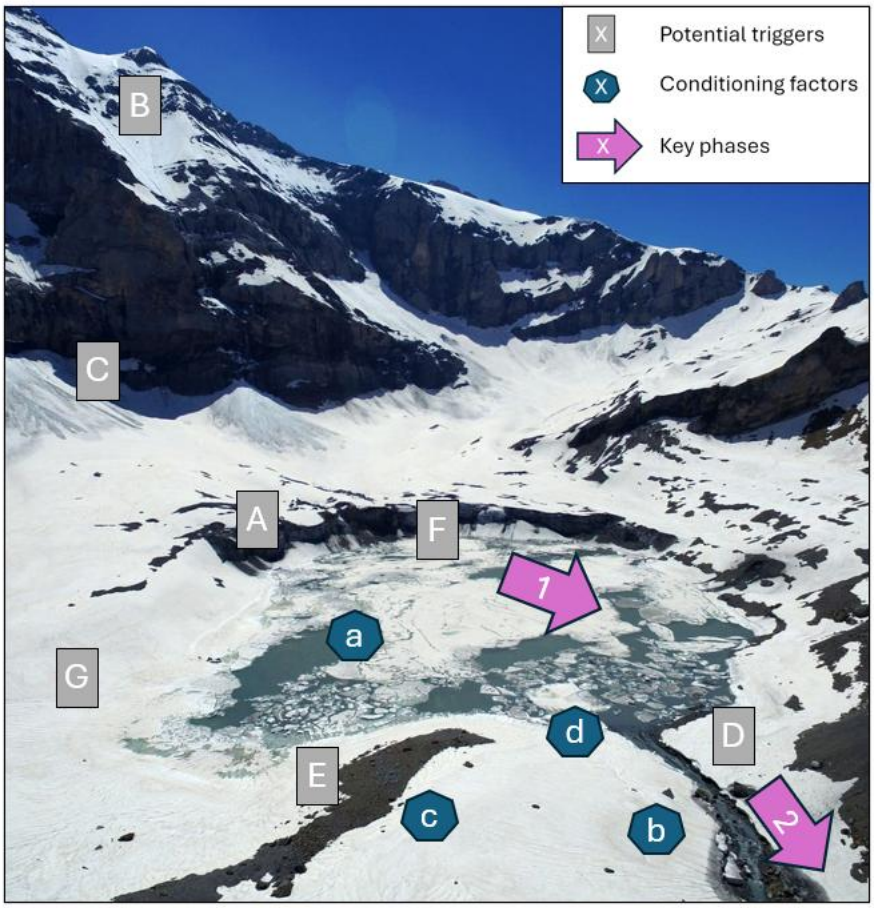

Figure 1: Picture of Griesssee near Klausenpass (Canton Uri, Switzerland) as a visualization of potential triggers, conditioning factors, and key phases in a GLOF event according to Richardson and Reynolds (2000). Potential triggers for a GLOF are: A) glacier calving; B) icefall from hanging glacier; C) rock/ice/snow avalanches; E) ice-cored moraine degradation; F) rapid input from glacial water from supra-, en- or subglacial sources; G) seismic activity. Conditioning factors for dam failure, especially for seismic activity: a) great lake volume; b) decreased width-to-height dam ratio; c) degradation of permafrost ice in moraine structure; d) limited dam freeboard. Key phases in GLOF events are: 1) Propagation of waves in the lake and piping through dam; 2) breach initiation and formation; excluded is the the propagation of the flood itself. The picture is obtained from Stefan Simmen 17.06.2019 (URL: https://www.urnerzeitung.ch/zentralschweiz/uri/gletschersee-sorgt-fur-bange-stunden-ld.1128445, last access: 20.04.2024)

2.1.1 Trigger Mechanism of GLOFs

GLOFs are complex natural hazards that can be triggered by several mechanisms and governed by various conditioning factors. Figure 1 presents a visualization through the glacial lake Griesssee near Klausenpass in Uri of potential triggers, conditioning factors and key phrases in a GLOF event described by Richardson and Reynolds (2000).

Several potential triggers can result in a GLOF event, which include glacier calving (A), icefall from hanging glaciers (B), rock, ice and snow avalanches (C), ice-core moraine degradation (E), rapid input from glacial meltwater from supra-, en- or subglacial sources (F) and seismic activity (G). Among these, mass movement triggers such as ice and rock avalanches or glacier calving are particularly significant. These

triggers can produce impulsive waves in the glacial lake, with their characteristics dependent on the volume and type of the triggering mass, its velocity and the angle of impact (Heller and Hager, 2011; Worni *et al.*, 2014).

Conditioning factors that incline a moraine-dammed lake to failure are also important in understanding GLOFs. Richardson and Reynolds (2000) identify conditioning factors such as large lake volume (a), a decreased width-to-height dam ratio (b), permafrost within the moraine structure (c) and limited freeboard (d). These factors in combination with potential triggers can significantly increase the likelihood of a dam failure and therefore of a GLOF, especially in response to seismic activity (G) (Osti, Bhattarai and Miyake, 2011). In moraine-dammed glacial lakes, the structural stability of the dam of the dam is further determined by the sedimentological composition and the potential presence of degrading permafrost, which can undermine the dam over time (Westoby *et al.*, 2014).

Additional triggers for GLOFs, which are not highlighted in Figure 1, include dam settlement, internal erosion (piping) and temporary blockages of spillways due to ice or debris accumulation (Huggel *et al.*, 2004). Extreme weather events, for instance heavy precipitation, can further intensify these conditions by enhancing spillway erosion and increasing lake levels (Clague and Evans, 2000). Understanding trigger mechanisms and their conditioning factors is essential for assessing GLOF hazards and implementing mitigation strategies in vulnerable GLOF environments.

2.1.2 Dam-Breach Mechanisms

As GLOFs can develop through dam-breaching it is important to understand briefly the dynamics and fundamentals of a dam-breach. The stability of and dam consisting of moraine material is strongly dependent on its geometry, internal structure, material properties and the distribution of particle sizes (Richardson and Reynolds, 2000). According to Massey *et al.* (2010), the failure of a moraine dam occurs when its material strength is surpassed by driving forces. These forces included shear stresses induced by overtopping flows or displacement waves. Overtopping is considered the most common trigger for moraine dam breaching (Richardson and Reynolds, 2000) and initiates dam erosion which can lead to increased forces that progressively help the dam breach (Singh, 1996). The eroded sediments are transported within the outflow as bedload. The dam-breaching process is irreversible and leads to partial or total emptying of the glacial lake.

2.1.3 Flood Propagation and Behavior

Sudden drainage of large water volumes during GLOF events in high mountain terrain leads to sediment entrainment into the flow. The interaction between particles governs the behavior of the flow, making it crucial to understand the key parameters that influence sediment content, particle type and size (Iverson, 2009). Glacier lake outburst floods can exhibit long runout distances, which makes the flows highly unsteady. This variability is influenced by factors such as topography, vegetation and sediment availability. Over the routing of the event, the flow can transition from a hyper-concentrated to a

sediment-laden debris flow (Worni *et al.*, 2012), influenced by the slope gradient of the route and the dilution of the flow by downstream streams (Smith and Lowe, 1991). However, sediment-laden flows achieve far greater runout distances than clear water flows. This is due to increased momentum afforded by the combination of fluid and solid forces as well as the continuing addition of material through bed and bank erosion (Iverson, 1997).

2.1.3.1 Sediment Entrainment in GLOF Events

Glacial Lake outburst floods can entrain huge amounts of sediment while flowing down the outflow valley. The degree of sediment entrainment relies on the availability of unconsolidated sediments in the riverbed and the velocity of the flow. Bolch *et al.* (2012) identify the slope gradient of the riverbed as the primary factor controlling the mass flow. If the average channel slope gradient is lower than 10 degrees, the flow typically entrains fewer sediments and can cease if the slope gradient is too gentle (Huggel *et al.*, 2002; Westoby *et al.*, 2014). This indicates that the composition of GLOFs can vary, with flows transitioning into debris flows as they erode material from both the lateral sides and the riverbed (Narama *et al.*, 2018).

Flow characteristics are closely tied to the evolving solid content within the mass movement, with the highest flow height usually occurring at the front of the flow (McArdell, Bartelt and Kowalski, 2007). The front of the mass flow plays an essential role in sediment entrainment, as its height directly controls the erosive processes on the outflow bed (Schürch *et al.*, 2011). This is highlighted by Berger, McArdell and Schlunegger (2011), who state that sediment entrainment predominantly occurs at the front of the flow, where basal shear stress is significantly increased due to larger solid fractions and higher flow depth (Stock and Dietrich, 2006). Therefore flow depth has a crucial impact on sediment entrainment and flow characteristics, channel geometry and slope angle further influence the flow dynamics. As a result, GLOFs can experience transitions, with flatter channels or reduced flow momentum leading to a potential stop of the mass flow (Schürch *et al.*, 2011).

The combined effects of sediment entrainment factors can enhance floods into large, destructive debris flows (Huggel *et al.*, 2003). Such transformations can result in peak flow volumes and discharges by a factor of three (Mergili *et al.*, 2011), underscoring that GLOFs are highly unpredictable. This escalation is driven through positive feedback mechanisms, where increased solid fractions enhance erosion, leading to higher velocities and further sediment entrainment into the mass flow (Breien *et al.*, 2008). To conclude, runout distances and flow momentum are substantially influenced by these processes (Westoby *et al.*, 2014).

Terrain properties also play an essential role in determining sediment entrainment and flow behavior. Iverson *et al.* (2011) highlight that wet terrain generally enhances mass flow propagation, whereas dry terrain hinders flow development. The dynamic interplay between erosion and deposition during mass flow further complicates predictions in flow propagation. The alternating patterns of sediment entrainment and deposition result from geomorphic landforms and frictional forces, which produce spatial variability in flow characteristics along the outflow channel (Carrivick *et al.*, 2010).

Overall, the sediment entrainment process in GLOFs is determined by a complex interplay of factors, including channel slope, sediment availability, flow height and terrain characteristics. Together these factors influence the evolution of GLOFs, resulting in significant variations in flow behavior and presenting challenges in analyzing outflow propagation and therefore prediction.

2.1.3.2 Behavior of Sediment-Laden Flows

GLOFs can undergo transition during their propagation, changing from pure water flows to hyper-concentrated or debris flows as they entrain sediment and interact with water sources beyond the glacial lake water itself (Figure 2). The definition of these transitions poses a challenge, as the behavior of mass movements during GLOF events depends on various factors such as trigger mechanism, velocity, composition and environmental conditions (Coussot and Meunier, 1996). These factors make it challenging to distinguish between different flow types during the event, as the characteristics of the flow change multiple times during the GLOF propagation due to channel topography and the amount of available sediments (Westoby *et al.*, 2014). These highly dynamic transitions can occur at various sections along the flow path, complicating the description and modeling of GLOF events (Coussot and Meunier, 1996; Meyrat *et al.*, 2023).

One key distinction between different types of sediment-laden flows is the concentration of solids in the flow. As water flows out of the glacial lake, the flow initially consists of primarily water with small amounts of sediments. As sediments are entrained during the flow, the flow transitions into a hyper-concentrated flow, characterized by a solid fraction of less than 25% regards the volume (Coussot and Meunier, 1996). If the solid fraction exceeds 50%, the flow can be classified as a debris flow, which can consist of up to 90% solids in extreme cases with large sediment availability within the flow path (Coussot and Meunier, 1996). Mudflows are classified by the same proportion as debris flow, although with higher amounts of fine sediments compared to coarse sediments (e.g. boulders, rocks) of debris flows (Cui *et al.*, 2010). The ratios between the solid and liquid phases in the flow vary along the flow propagation, with the front of the flow generally containing greater concentrations of solid materials, while the tail becomes more liquid (Meyrat *et al.*, 2023). Pierson (2020) emphasizes that the front of debris flows often is the most intense, characterized by the highest flow depth and the coarse solids, which significantly contribute to the flow's erosive power (Hungr, 2000). However, when the front of the debris flows cease, the flow can continue with particle sizes tend to decrease. This dewatering process can result in a mudflow, characterized by its fine sediments and the high liquid content (Cui *et al.*, 2010).

The behavior of debris flows and other mass movements during a GLOF event remains challenging to classify and predict due to multiple factors driving the solid-fluid ratios and sediment entrainment along the outflow path. Although several studies provide the classification of different mass flows (Coussot and Meunier, 1996; Hungr, Leroueil and Picarelli, 2014), the distinction between them remains difficult. Especially during rapid flow transitions, these uncertainties complicate the modeling and prediction of GLOFs.

Depending on the scale and characteristics of the GLOF event, debris flows are typically shorter than other mass movements, potentially lasting from several minutes to hours (Coussot and Meunier, 1996).

Pierson *et al.* (1996) identify two key characteristics of debris flows that impact their behavior: first, the velocity discrepancy is minimal between solid and liquid particles, and second, the entire mass moves uniformly. These features allow debris flows to be modeled with a simplified single-phase model such as RAMMS (Bartelt *et al.*, 2017). However, due to the varying characteristics of the outflow channel and the changing solid-liquid ratio, it is challenging to simulate debris flow or other mass movements with a single-phase model (Meyrat *et al.*, 2022). This challenge is particularly of interest when modeling GLOF events, where flow transitions can occur quickly between different mass movement types.

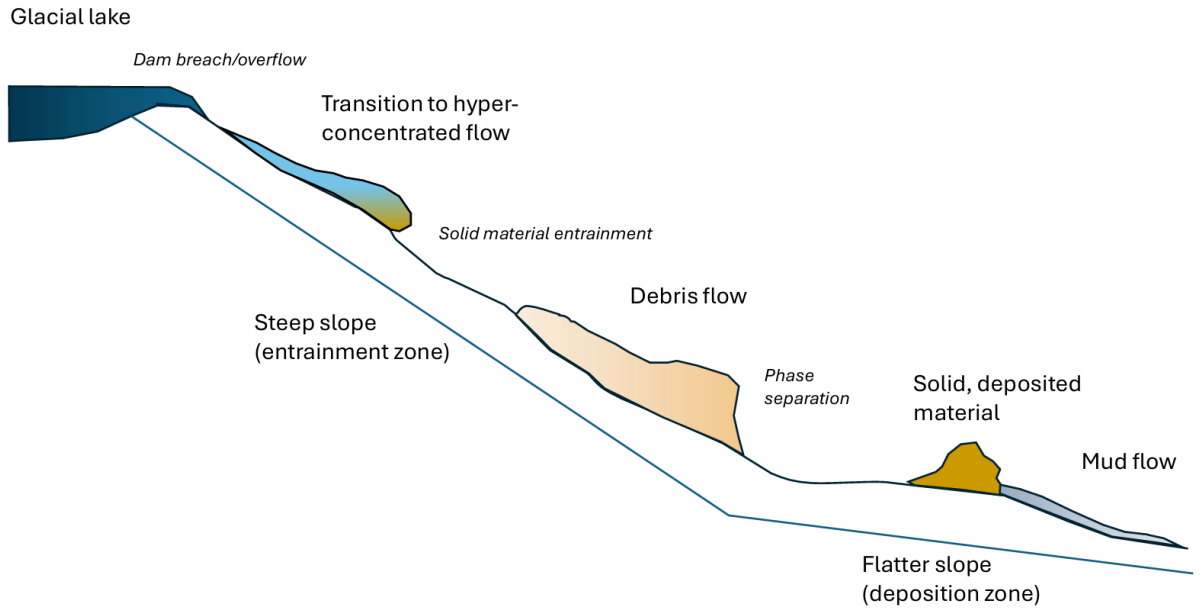

Figure 2: Conceptualized outflow of a GLOF event. The initial overflow or dam breach leads to a highly water-concentrated outflow which entrains sediment from the dam itself and later downstream. Occurring transitions from hyper-concentrated flows to debris flows can change several times depending on the available amount of erodible material and the topography. After stopping the sediment-laden mass flow, phase separation occurs, leading to a phase separation between the solid and fluid phase.

2.2 GLOF Modeling Approaches

The modeling and simulations of GLOFs have evolved since the early 2000s. Initial modeling efforts primarily focused on simple empirical models, such as the single-flow-direction (MFS) model (Huggel *et al.*, 2003). These early models were well-suited for small-scale applications and provided valuable insights into GLOF examination. Over time, more sophisticated models have been developed, applying physically based simulation tools tailored to individual cascades of the GLOF process chain. This approach has been demonstrated in several studies (e.g. Worni *et al.*, 2014), highlighting the growing complexity and adjustment of GLOF modeling techniques.

Building on these advancements, the introduction of two-phase (Pudasaini, 2012) and later the three-phase (Pudasaini and Mergili, 2019) mass movement models has been a significant step in the field. These models enable the comprehensive representation of GLOF characteristics by accounting for interactions between liquid and solid phases. The latest trend in GLOF modeling is moving toward integrating all components of the process chain within a single simulation step (Emmer *et al.*, 2022). This integrated approach, requiring the application of only one model (e.g. r.avaflow), not only reduces the complexity but also lowers the costs. The financial benefit makes these models highly interesting for private companies and institutions by minimizing the requirements for software licenses.

Despite these advancements, several difficulties can be addressed in the current state of the art. As underscored by (Emmer *et al.*, 2022), the definition of GLOF scenarios and balancing physical accuracy with practical applicability remain key concerns in the field. One of the main challenges lies in the transition from successful retrospective simulations of past events to robust predictions for future scenarios. In the context of GLOF risk management, worst-case scenarios are generally prioritized. However, defining which scenarios represent plausible worst-case input values versus conservative scenarios remains a subject of debate (Worni *et al.*, 2014).

Significant progress has been made in understanding the processes of GLOFs, including multi-phase flows, sediment entrainment and deposition, interactions between mass movement and lakes, and phase separation in debris flows (Pudasaini, 2020; Pudasaini and Fischer, 2020; Meyrat *et al.*, 2023). Furthermore, traditional depth-averaged models are being increasingly complemented and sometimes challenged by machine learning techniques and comprehensive 3D models. While these advanced models can simulate the phenomena with high realism (e.g. Gaume *et al.*, 2018), their computational demands currently limit their operational use for complex, long-runout distances. However, this limitation is expected to diminish over the coming years and decades as computational capabilities will improve (Emmer *et al.*, 2022).

2.2.1 Overview of Existing GLOF Models

This thesis applies the RAMMS software to model GLOF propagation and compares it with simulation results conducted with HEC-RAS and r.avaflow (see Chapter 5.1). While RAMMS and HEC-RAS are suitable for modeling the flood propagation of GLOFs, r.avaflow offers a more comprehensive solution, covering the entire process chain of GLOF events, including the triggering and breaching processes. Other specialized models, such as those for dam breaching (Singh, 1996) or impact wave modeling (Heller, Hager and Minor, 2008), also offer GLOF process modeling but fall outside the scope of this thesis and are not further discussed.

There are various existing modeling tools, ranging from empirical approaches to physically-based dynamic models, which can be used to model GLOFs. Unlike empirical models, advanced physical models can capture complex flow behaviors, accounting for fluid-solid interactions and varying flow dynamics (Worni *et al.*, 2014). These models are based on mass and momentum conservation principles, incorporating numerical methods and flow resistance quantification to solve partial differential equations.

In addition, they take into account the floodplain and channel geometries of the GLOF (Manville, Major and Fagents, 2013). GLOF modeling tools are generally categorized based on their dimensionality (Worni *et al.*, 2014; Westoby *et al.*, 2014), therefore the following sections provide an overview of one-dimensional and multi-dimensional models.

2.2.1.1 One-Dimensional Models

In contrast to GIS models (Huggel *et al.*, 2003), one-, two- and three-dimensional models attempt to calculate the modified Navier-Stokes equations (Batchelor, 2000). One-dimensional models are based on the St-Venant or so-called shallow water equations (SWE) of de Saint-Venant (1871). The specific details of these equations are beyond the scope of this thesis. However, one-dimensional models often rely on the step-backwater method, which automates and numerically adapts the slope-area technique (Westoby *et al.*, 2014). This method generates energy-balanced water surface profiles based on discharge, channel roughness and geometry. Additionally, they can provide cross-sectionally averaged velocities and discharge values (Brunner, 2002).

The cross-sectional profiles can be derived from field surveys or satellite images. These models can simulate subcritical, supercritical or mixed flow regimes and incorporate initial boundary conditions, such as input hydrographs or downstream water profiles based on past flood events. This approach is typically used for GLOF reconstruction (e.g. Kershaw, Clague and Evans, 2005), as the dynamic behavior of GLOFs poses challenges to accurate modeling. Flow velocities, high discharge rates, erosion and sediment transport further complicate simulations. Due to often limited direct measurements of GLOF events, hydrographs can be obtained from downstream locations where flow conditions enable easier data collection (Richardson and Reynolds, 2000). Popular one-dimensional models used in modeling GLOFs include for instance HEC-RAS (1D) (e.g. Brunner, 2002; Carling *et al.*, 2010).

2.2.1.2 Multi-Dimensional Models

Two-dimensional models rely on a depth-averaged version of the shallow water equation, integrating the Reynolds-averaged Navier-Stokes equations over flow depth (Chanson, 2004). In contrast to one-dimensional models, which only capture flow in a single direction, two-dimensional models allow for multi-directional simulations (Pitman *et al.*, 2013). Their ability to model hydraulic jumps and transitions between different flow regimes makes them particularly valuable for simulating the turbulent and dynamic behavior of GLOFs. The two-dimensional models are especially useful for modeling non-Newtonian flow behaviors, where debris entrainment from moraine dams and valley beds significantly alters flow rheology (Rickenmann *et al.*, 2006; Stolz and Huggel, 2008). Widely used two-dimensional models include IBER (IBER, 2010) and FLO2D (O'Brien, Julien and Fullerton, 1993).

Three-dimensional models are the only models capable of solving the full Navier-Stokes equations (Westoby *et al.*, 2014), allowing for detailed modeling of velocity distributions across flow depth and width. Despite their ability to capture the complex flow behavior of GLOFs, high computational power and the lack of high-resolution DEMs currently limit their practical application. However, future advances in computational power are expected to reduce these limitations, making three-dimensional models more accessible for both practical and research applications (Emmer *et al.*, 2022).

2.2.1.2.1 HEC-RAS for GLOF Simulations

The software HEC-RAS (Hydrologic Engineering Center's River Analysis System) is a free, open-source software for modeling water flow. The U.S. Army Corps of Engineers developed the application and supports one-dimensional and two-dimensional flow simulations, enabling the analysis of complex hydraulic systems. The implemented two-dimensional modeling capabilities allow the simulations of unsteady water flow scenarios, making it useful for floodplain management, dam breaches and sediment-laden flows like GLOFs (*HEC-RAS User's Manual*, 2025). Later is applied in several GLOF studies (e.g. Klimeš *et al.*, 2014; Sattar *et al.*, 2021; Hazra and Krishna, 2022; Yu *et al.*, 2024) for modeling dam-breaching and outflow processes.

A considered strength of HEC-RAS is the integration ability of one- and two-dimensional modeling within a single simulation. For instance, users might apply one-dimensional modeling to great river channels while exploiting two-dimensional modeling for detailed analysis of areas with complex flow dynamics. The software lies down to advanced numerical methods, solving the shallow water equations (SWE), which are fundamental for simulating unsteady flow dynamics. According to the *HEC-RAS User's Manual* (2025), the software offers two primary solvers for the SWE, the Eulerian-Lagrangian (ELM-SWE) and the Euler Method (EM-SWE). The ELM-SWE handles the advection terms effectively, generating stability and accuracy in complex flow scenarios. Whereas the EM-SWE discretizes the governing equations over a fixed spatial grid, fitting for a wide range of hydraulic modeling. Users can incorporate digital elevation terrains and land cover data to create realistic simulations over different kinds of landscapes.

Generally, HEC-RAS is known for its accessibility and easy application for engineers and researchers and hydraulic modeling, as there is a lot of knowledge freely accessible. The performance of HEC-RAS is compared with other models in Chapter 5.1.1, including the results of the South Lhonak GLOF (Sattar, Goswami, *et al.*, 2021) with the simulations conducted in this study with RAMMS.

2.2.1.2.2 R.avaflow for GLOF Simulations

The software r.avaflow is an open-source software that is GIS-supported and designed for modeling complex mass flows. It is known for its ability to model cascading mass flows, including rapid mass movement such as avalanches, debris flows and landslides making the software highly interesting for modeling GLOFs. R.avaflow has been used in various GLOF case studies across the globe (e.g. Mergili *et al.*, 2020; Rinzin *et al.*, 2024; Zhang, Wang and An, 2025).

The software uses advanced numerical schemes, including the scheme named NOC-TVD (Wang, Hutter and Pudasaini, 2004), and employs models such as the Voellmy-type and the elevated version of the Pudasaini multi-phase model (Pudasaini and Mergili, 2019). These models enable r.avaflow to simulate processes such as dispersion, sediment entrainment, phase transformations and deposition. Therefore the initial mass distribution is defined through hydrographs and the base is built through a raster map (e.g. digital elevation map). The software incorporates features for conducting parameter sensitivity analysis by exploiting multi-core environments to run multiple simulations simultaneously. The results can be visualized through generated layers, maps, diagrams and further explored by using 3D tools like Paraview, Unreal Engine and Blender enabling immersive virtual reality experiences. R.avaflow offers

different versions to accommodate various user preferences and system environments. For example, r.avaflow 4.0W offers a stand-alone alternative for Windows users, while 4.0G is available for Linux users with integrated GRASS GIS. Both software versions are open source and provide equivalent functionalities.

The user's manual offers practical guidance and there is also a web interface available with an integrated manual called r.avaflow.direct which offers the simulation process step-by-step instructions (Mergili, 2014).

Overall, r.avaflow is known for its usage in various system environments and its ability to model cascading processes in complex terrains. The performance of r.avaflow regarding GLOF simulations is compared to the simulations conducted in this study with RAMMS in Chapter 5.1.2.

2.3 Overview of the Study Areas

2.3.1 South Lhonak Lake (Sikkim Himalaya)

The area of interest lies in Sikkim, a federal state of India (Figure 3, left panel). Geographically, Sikkim is situated to the west of Nepal and the north of Bangladesh. In comparison to other Indian states, Sikkim is relatively small in size and inhabitants. The state is further divided into four districts, with North Sikkim which is notable for several glacial Lakes as well as the Lake of interest South Lhonak.

The glacial Lake South Lhonak is located in the Teesta Basin, Sikkim, Himalaya (27°54’20’’N and 88°10’20’’). At an elevation of 5’200 m a.s.l. the lake lies at the front of the South Lhonak glacier (Figure 4, A), which had a total area of 12.5 km when last mapped in 2019 (Sattar, Goswami, *et al.*, 2021). According to Sattar *et al.* (2021), the glacier changed its length from 6.4 km to 5.1 km and its overall area shrank by approximately 0.96 km^2. With retreating glaciers, the South Lhonak Lake significantly grew from 0.42 km^2 in 1990 to 1.35 km^2 in 2019 (Kumar and Murugesh Prabhu, 2012; Sattar *et al.*, 2021). The lake is dammed by a moraine which is about 500 m as it gets narrow towards the north, where also the surface outflow is located. The damming morain is cut through by the surface outflow in the north-northeast direction and the main valley is oriented towards the east. Sharma *et al.* (2018) measured the crest height of the frontal section of the damming moraine, located south of the outflow channel and found it to be 7 m above the lake level. This portion of the moraine features a hummocky surface, suggesting the presence of ice in the dam. Additionally, several small lakes, likely formed by thermokarst processes and filled with precipitation, dot the moraine surface, which lacks any vegetational cover (Sattar, Goswami, *et al.*, 2021).

According to Sattar *et al.* (2021), the South Lhonak Lake outflow flows into the Goma Channel, which 36 km downstream joins the Zemu River. Further downstream, the outflow joins the Lachen River at Hema 40 km away from the South Lhonak Lake. The outflow valley is moderately populated until the first major town Chuangthang with the Teesta Stage III hydropower dam is located 62 km downstream. Sattar *et al.* (2025) state that Chungthang has more than 10’000 inhabitants and over 1’900 households

(Figure 4, B). According to Sattar *et al.* (2021), the village has seen rapid growth over the years, especially since the construction of the hydropower station (see Appendix D)). The hydropower station was built due to the increased demand for energy with the growing urbanization in the South Lhonak Valley and the constant discharge generated from the glaciers in the catchment area. Moreover, the hydropower station is expected to attract more small-scale industries, fostering economic growth in the region. However, population growth could lead to building houses and infrastructure closer to the riverbed, increasing the risk of floods reaching vulnerable constructions (Sattar *et al.*, 2025).

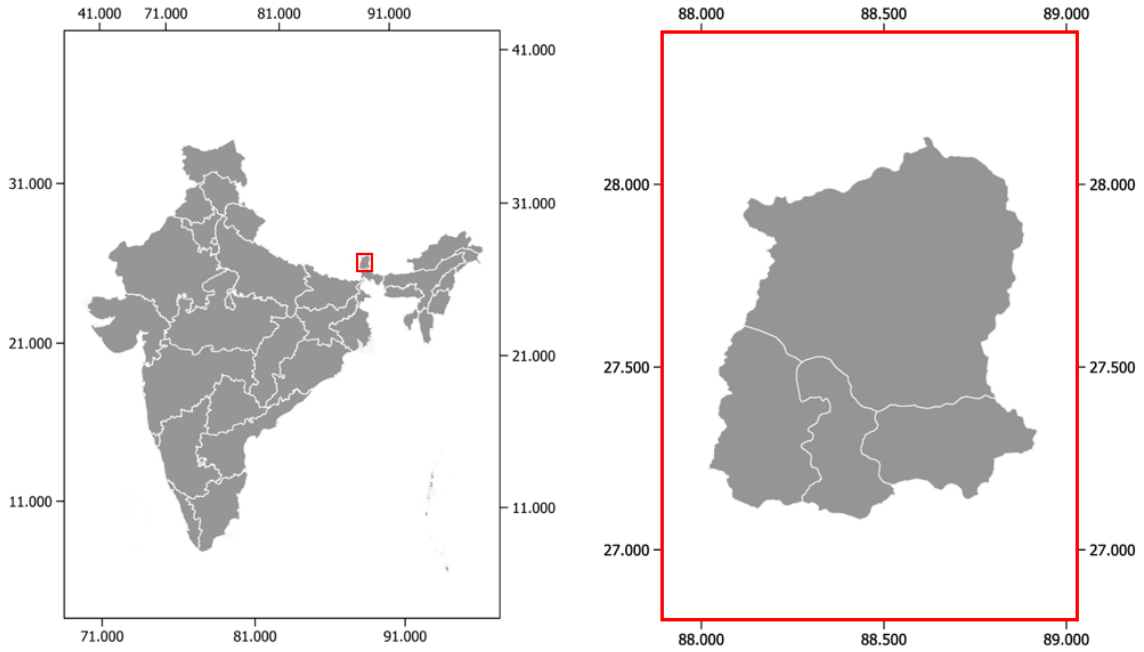

Figure 3: Overview of the study area in the federal state of Sikkim, India. The left panel shows the Sikkim within India (red box), while the right panel visualizes a detailed view of Sikkim with its district boundaries.

The geological framework of Sikkim Himalaya consists of lithologically arranged units in a regional fold pattern (Neogi, Dasgupta and Fukuoka, 1998). Lesser Himalayan rocks including low-grade metapelites and interbedded metapsammite are predominantly in the central area of Sikkim. In contrast, a Higher Crystalline Complex, consisting of medium to high crystalline rocks is occurring in the northern part of Sikkim Himalaya (Nath, 2005). The outflow channel of the South Lhonak Lake is characterized by steep slopes on the sidelines of the channels and varied land cover. The terrain is complex with a paleo-glaciomorphic feature crossing the channel. Sattar, Goswami and Kulkarni (2019) elaborated on the flow channel in their study with satellite imagery. They managed to identify a surface depositional landform in the form of a lateral moraine. The moraine crosscuts the outflow channel at 15.5 km downstream the South Lhonak Lake. Sattar, Goswami and Kulkarni (2019) state that it is important to know such morphologic phenomena, as they can act as a topographic barrier and minimize the impact of a flood.

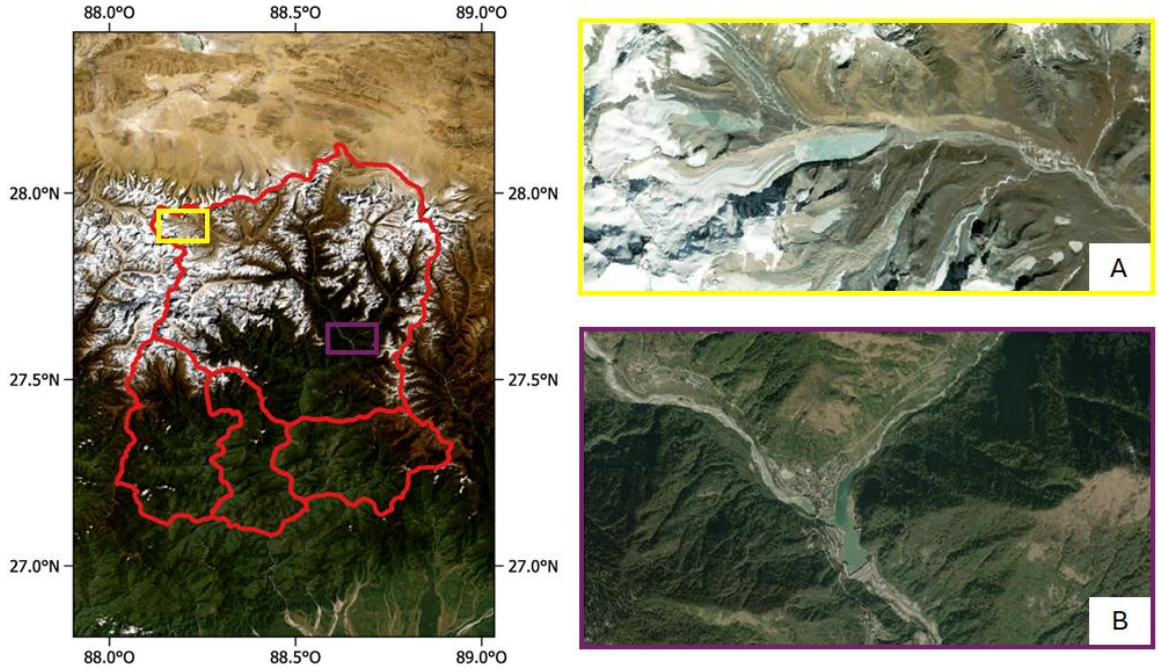

Figure 4: Overview of Sikkim with its district visualized on the left. The yellow and purple outline shows the area of interest. The right panels provide close-up views of Noth Sikkim, with South Lhonak Lake (A) and the village of Chungthang (B). Satellite imagery is sourced from ESRI.

2.3.1.1 Climate of Sikkim Himalaya

The region of Sikkim lies in the eastern part of the Himalayas and is subject to complex weather patterns due to significant altitude variations, as the elevations range from 280 m to 8'586 m above sea level. The weather in the region is influenced by the convergence three of climatic systems: dominated by the monsoon of the southwest, the limited winter rain from the Mediterranean from the west and the north-east monsoon (Kumar *et al.*, 2020). This tri-junction of climatic influences underlines the complex weather of Sikkim Himalaya.

From May to October, during the monsoon and summer periods, Sikkim experiences the majority of its annual precipitation. The climate varies across the different altitudinal zones, with higher elevations receiving more rainfall. The highest temperatures are recorded in summer between June and August, while the coldest temperatures, along with snowfall, occur during the winter months of December to January (Kumar *et al.*, 2020). Sikkim is located in a transitional zone between the Arabian Sea branch and the Bay of Bengal branch of the Indian monsoon. Due to its location, heavy orographic rainfall can occur during the monsoon season. Furthermore, the topography, including the aspect and elevation of the valleys, plays a significant role in determining the distribution of rainfall.

2.3.1.2 Reported GLOF Events of South Lhonak Lake

Until the autumn of 2023, no GLOF event at South Lhonak Lake has been recorded. However, there were concerns about a potential GLOF. In the Sikkim Himalaya, there are 14 glacial lakes potentially

vulnerable to GLOFs out of 320 (Raj, Remya and Kumar, 2013). According to Yu *et al.* (2024), the South Lhonak Lake is one of the 14 and a potential hazard with a high probability of flowing out. Kumar and Murugesh Prabhu (2012) presented a report to the Government of Sikkim, indicating that the lake outlet shows evidence of a previous GLOF. In addition, Sattar, Goswami and Kulkarni (2019) investigated the glacial lake and modeled its outflow with the software HEC-RAS. Later Sattar *et al.* (2021) mapped three scenarios of potential GLOF in their work at Chungthang, being conscious of a potential GLOF event happening in the future. However, the suggested implementation of an early warning system seemed to be ignored.

In the autumn of 2023, several floods occurred from the South Lhonak Lake, resulting in 55 fatalities, 74 missing people and over 7'025 displaced individuals (Sattar *et al.*, 2025). The floods from the 4th and 5th of October 2023 were caused by the failure of a lateral moraine north of the South Lhonak Lake, generating wave impulses that led to a dam breach (Yu *et al.*, 2024). The lateral moraine collapsed due to heavy rainfall when the area of Sikkim received more than double its normal rainfall (Yu *et al.*, 2024). Satellite images of the Indian Space Research Organisation's RISAT-1A show that the surface of the south Lhonak Lake decreased by 100 hectares (Figure 6). At Chungthang the dammed lake was at full capacity the days before the event (Figure 3). During the event, the gates of the Hydropower dam were opened too late, leading to the destruction of the dam. The dam failure led to high water levels further down the valley. The Teesta River rose by 4.6 to 6.1 m on average, flooding many areas in Mangan, Gangtok, Pakyong, and Namchi districts in Sikkim, and Kalimpong, Cooch Behar, Jalpaiguri and Darjeeling districts in West Bengal (Sattar *et al.*, 2025). The flood also went onwards to Bangladesh, where hundreds of villages were affected along the Teesta River.

Satellite image of before the GLOF event

Satellite image 10 days after the GLOF event

Figure 5: Satellite images from the village Chungthang captured before and after the GLOF event on the 4th of October 2023. The dammed lake is at full capacity with the dam intact (left), while the right pictures highlight the inundation outlines and the destroyed dam. The images are adapted from the BBC report (URL: https://www.bbc.com/news/world-asia-india-67678440, last access: 30.04.2024)

This GLOF event highlights the critical necessity for introducing a robust early warning system. Alerts on time could have facilitated the earlier opening of the hydropower station gates, potentially lowering

the impact of the flood. In addition, proactive measures such as keeping the lake at a lower water level could have enhanced the capacity to function as a retention basin, breaking the outflow peaks. Such adaptations would have reduced the downstream impact of the GLOF event, supporting greater protection for vulnerable villages. The high magnitude of the event is underscored by the fact that its effects were observed in Bangladesh, approximately 400 km from the Glacial Lake South Lhonak. This demonstrates the far-reaching consequences of the event and highlights the importance of comprehensive risk management strategies in high-altitude, alpine regions.

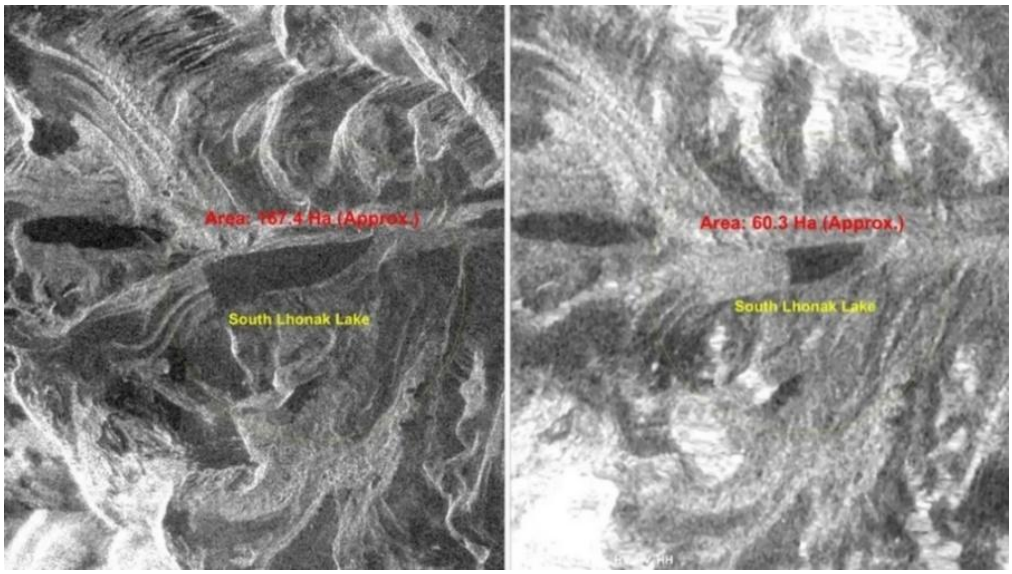

Figure 6: Satellite Images of the South Lhonak Lake pre- and post-GLOF event, highlighting the huge loss in water area respectively volume. The images are adapted from the BBC report (URL: https://www.bbc.com/news/world-asia-india-67017845, last access: 25.04.2024), originally from ISRO, India's space agency.

2.3.2 Weingarten Lake (Valais, Switzerland)

The area of interest for this study lies in the Canton of Valais, specifically the commune of Täsch, located in the southern part of Valais (Figure 7). The village holds 1'200 inhabitants and features significant infrastructure including parking facilities for tourists visiting Zermatt. According to the local hazard map (URL: https://www.vsgis.ch/, last access 22.12.2024), Täsch is threatened by several natural hazards such as snow avalanches, floods and debris flows. Later occurred in combination with a GLOF event that happened in 2003 from the Glacial Weingarten Lake.

The glacial lake Weingarten is situated below the Täschhorn and the Alphubel in the Alps of Valais (46°06'35"N and 7°83'91"S). At an elevation of 3'056 m a.s.l., the lake lies east of the Weingarten Glacier, which covers an area of approximately 0.42 km^2, according to the Swisstopo map (URL: map.geo.admin.ch, last access: 11.07.2024). The Lake is formed at the end moraine of the deposited material from the 1850 glacial maximum. The blue shading illustrated in Figure 8 indicates the glacial maximum extent of the year 1850, whereas the light blue represents the 1973 glacial maximum, and the turquoise the

current extent. According to the Swisstopo map, the glacier changed its area from 0.8 km^2 in 1973 to 0.42 km^2 today (Figure 8). The lake's surface outflow is oriented westward, cutting through the damming moraine with a bedrock depth of 70 to 120 m (Huggel *et al.*, 2003).

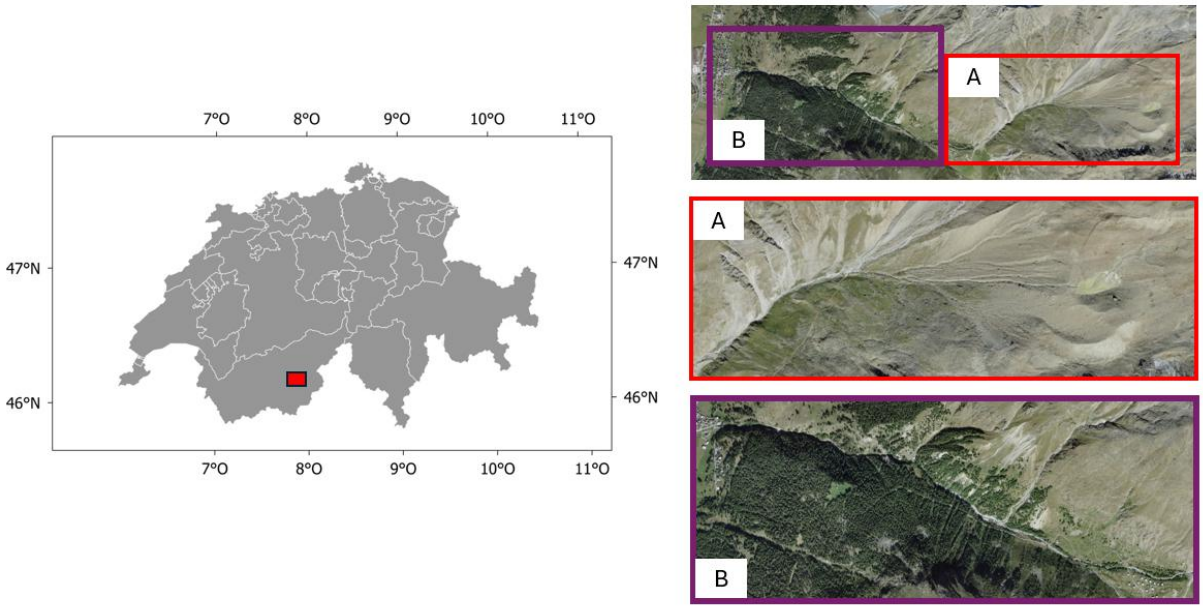

Figure 7: Overview of the glacial Weingarten Lake outflow downstream to Täsch. The left panel shows the study area (red box) within Switzerland, while the right panel shows a detailed view of the outflow path. Part A represents the outflow section with unconsolidated material, whereas Part B indicates the section with solid material. Satellite imagery is sourced from ESRI.

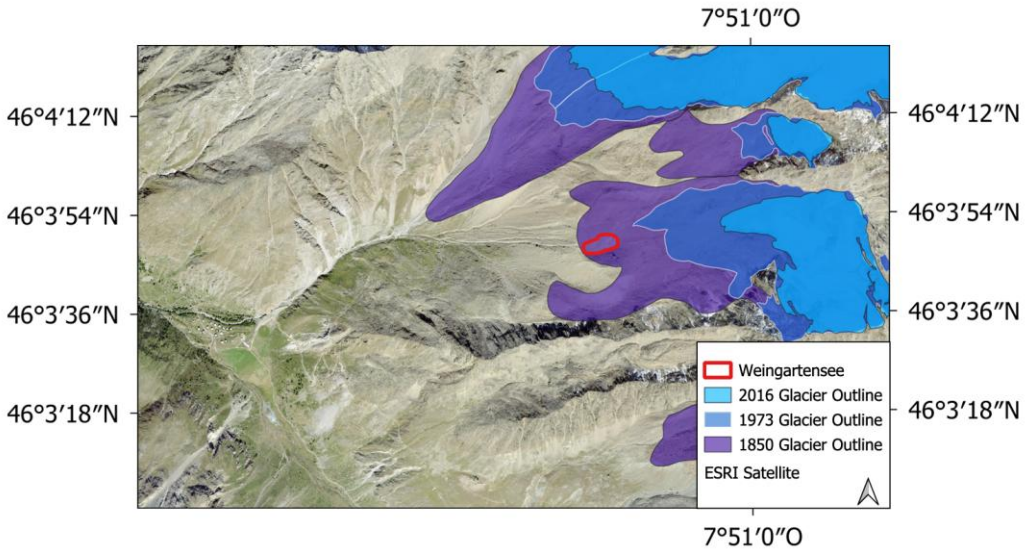

Figure 8: Glacier extent changes for Weingarten Glacier over the years, with maximum extents visualized for the years 1850 (dark blue), 1973 (light blue), and 2016 (turquoise) based on data from Swisstopo (URL: https://map.geo.admin.ch/, last access: 20.08.2024). The red outline depicts the location of Weingarten Lake. The glacier extent layers are obtained from (URL: https://www.glamos.ch/downloads#inventories/A50d-01, last access: 22.08.2024), and the background is an ESRI satellite image.

The river bed is divided into two parts, A and B (Figure 7), because of its differences in morphology. Part A consists of the outflow of Weingarten Lake to the village of Täschalp, as this section consists of very unconsolidated moraine material. The damming material originates from the Alphubel and Täschhorn mountains, located east of Weingarten Lake. The moraine has a 700 m long slope which is up to 36° steep (Huggel *et al.*, 2003) and consists of loose material of crystalline rock, primarily Gneis from the Briançonnais unit (see Appendix B)). At this elevation and orientation, permafrost is widespread and its thickness is decreasing (see Appendix C)). Part B describes the flow propagation from Täschalp downwards to Täsch. The morphology of the riverbed consists of less sediments and more rough material such as blocks and boulders in comparison to part A. The outflow of the Weingarten Lake flows into Rotbach which 2 km later joins the Täschbach at the Täschalp. Further downstream in the village of Täsch the Täschbach merges with the Matter Vispa.

2.3.2.1 Climate of Valais Switzerland

The climate in Valais is characterized by variable and localized conditions, typical for the Alpine region. Generally, the climate is influenced by the Atlantic and even more by the Mediterranean Sea. The Rhone Valley reports the highest number of heat days per year in Switzerland. According to (Nauser, 2016), the heat days are averaging approximately 16 days during the period 1981-2010, and currently exceeding 20 days annually.

Precipitation in Valais varies significantly between the wet high mountains and the dry valley floors, influenced by its complex high topography and local climatic factors. For instance, the average annual precipitation in the central part between Sion and Visp drops below 600 mm, highlighting Valais's unique climatic characteristics compared to other regions of Switzerland. Central Valais is the driest region in the country, with less rain during the summer half-year (April-September) compared to the winter half-year, a pattern which is reversed in other parts of Switzerland. The region also experiences more frequent and pronounced dry periods, with greater year-to-year variability in precipitation, with Visp recording minimal annual rainfall below 400 mm (Nauser, 2016).

Extreme weather events, particularly warm extremes, summer heatwaves, and dry periods in summer and autumn, are expected to become more frequent in the future. While extreme cold temperatures in winter will become less common according to Nauser (2016). The development of heavy precipitation events, including intense snowfalls and associated avalanche risks, remains highly uncertain in the short to mid-term. However, in the long term, heavy precipitation in spring and autumn and dry periods, especially in summer, are projected to increase.

2.3.2.2 Reported GLOF Events of Weingarten Lake

In literature, there is one GLOF event for Weingarten Lake recorded which happened on the 25th of June 2001. Despite any significant rainfall around that time recorded, a debris flow had significant damage to buildings and other installations in Täsch. The cost of the damages was about 12 million EUR (Hegg *et al.*, 2002). Luckily, no fatalities occurred, thanks to the evacuation of 150 people in Täsch. Persons who observed the debris flow in Täschalp alarmed the people in Täsch just in time.

According to Huggel *et al.* (2003), inspections after the event at Weingarten Lake revealed that the shoreline was 0.4 to 0.5 m above the water level. Based on the lake size of 16'000 km^2, it is estimated that the amount of water overtopping the dam was between 6'000 and 8'000 m^3. Elevated air temperatures and during days before the event led to a high meltwater flow into the lake.

The following scenario was drawn from Huggel *et al.* (2003), based on the intact drainage channel and the presence of the shoreline. The lake was likely dammed by a blockage of water caused by pieces of lake ice and snow deposits. At the time of the event, the lake was partially covered by snow and ice due to seasonal snow and ice cover at that elevation. The higher water levels could have led to increased hydraulic pressure in the moraine dam body which eventually caused piping processes. This is highlighted by the observation of the outer side of the moraine. The outburst did not lead to a dam breach, as there was not a full erosive cut-through observed, even though the water volume was enough to initiate a debris flow. The amount of debris deposited in Täsch was estimated between 20'000 and 50'000 m^3.

3 Methodology

3.1 RAMMS Software for GLOF Simulations

The software RAMMS is a numerical modeling tool and was developed by the Institute for Snow and Avalanches (SLF), an organization within the Swiss Federal Institute for Forest, Snow and Landscape Research (WSL). Originally designed for simulating snow avalanches, RAMMS has since been extended and adapted to model debris flows (Christen, Kowalski and Bartelt, 2010; Bartelt *et al.*, 2017). The software is widely used for research on natural hazards, mitigation planning and hazard mapping. It is applied globally by academic institutions, governmental authorities and private-sector natural hazard bureaus. In the context of GLOF modeling, RAMMS is frequently applied to simulate triggering mechanisms such as rock or snow avalanches that may impact glacial lakes (e.g. Sattar *et al.*, 2021). Although originally developed for debris flow modeling, RAMMS has also been successfully used for simulating the hydrodynamic routing of GLOFs, as demonstrated by various scholars (e.g. Mergili *et al.*, 2011; Frey *et al.*, 2016; Iribarren Anacona *et al.*, 2018; Sattar *et al.*, 2022)

According to Christen, Kowalski and Bartelt (2010) and Bartelt *et al.* (2017), the software lies down to the following parameters. Mass transfer from the release zone to the deposition zone is calculated within the three-dimensional terrain framework, using numerical depth-averaged equations of motions. The frictional behavior is described by using the Voellmy-fluid model. This model separates frictional resistance into two components: a turbulent friction parameter ξ [m s^{-2}] and a Coulomb friction parameter μ [-] (Salm, Burkhard and Gubler, 1990; Salm, 1993). The velocity-dependent turbulent friction parameter ξ regulates frictional resistance during high-speed mass movement. In contrast, the velocity-independent coefficient μ predominates during slow motions (Frank *et al.*, 2015). Erosive processes can be simulated using the integrated entrainment model, which is crucial during flow transformations, as they often occur when modeling GLOFs. The erosion is influenced by the shear stress and the erosion rate, according to Bartelt *et al.* (2017). To simulate the discharge of a mass movement, the software allows users to start the simulation with a block release or by defining an input hydrograph to control discharge over time (Bartelt *et al.*, 2017).

As multiple scholars describe the underlying equations and assumptions (e.g. Christen, Kowalski and Bartelt, 2010; Frank *et al.*, 2017), this thesis will not delve into the detailed mathematical formulations behind the software. Instead, the study focuses on evaluating the performance and practical application of the new RAMMS, particularly in terms of model output accuracy and efficiency regards GLOF modeling.

3.1.1 Key Features of the Upcoming Two-Phase Model in RAMMS

The SLF is currently developing a new RAMMS software which is almost finished and soon be available for users. As Chapter 3.1 explained, the existing RAMMS version treats debris flow as a single, homogenous phase. Adapted from the snow avalanche modeling, it enables the simulation of run-out

distances, pressures and velocities. The new version, however, introduces the capability to simulate dewatering and sedimentation processes, allowing the modeling of flow transitions from debris flows to hyper-concentrated flows. These different flow types can soon be simulated within a single model step.

The new features in upcoming RAMMS-Version are being developed and examined at the WSL in Birmensdorf and Davos. The most significant innovation is introducing a dilatant two-phase debris flow model, as proposed in several studies (Meyrat *et al.*, 2022; Meyrat *et al.*, 2023; Meyrat, Bartelt and McArdell, 2023). Meyrat *et al.* (2023) conceptualize debris flow as a matrix of solid materials - rocks and boulders - within a muddy fluid. However, Meyrat *et al.* (2023) make a key distinction by separating the muddy fluid into two fractions, the intergranular fluid and the so-called free fluid (see Figure 9). The intergranular fluid is bonded to the solid matrix, filling the void space between the rocks and boulders. This combination is considered as the first layer of the debris flow and is building the nose of it. The free fluid, understood as the second layer of the debris flow, is not bonded to the solid matrix and can flow independently of the first layer (Meyrat *et al.*, 2022). During the flow, the rocky particulate material undergoes shearing, which triggers dilatant movements, altering the solid-fluid concentration of the first layer and subsequently affecting its density.

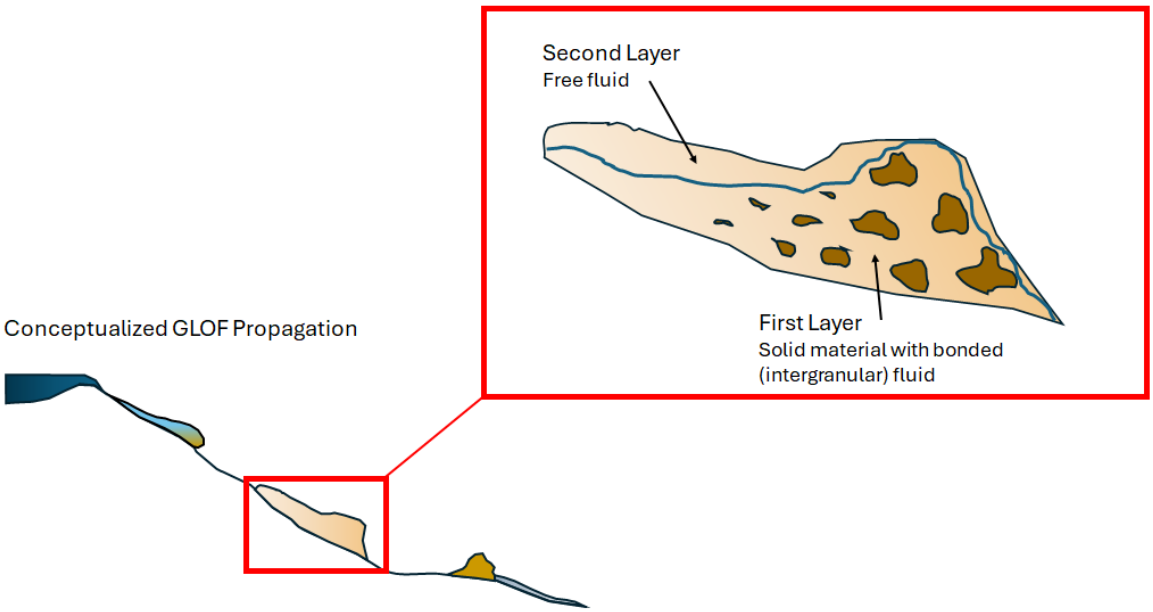

Figure 9: Visualisation of the two-phase layer approach adapted from Meyrat et al. (2023). The first layer consists of solid material with bonded intergranular fluid, while the second layer represents the free fluid. The blue line depicts the boundary between the solid phase at the front, consisting of boulders and rocks, and the free fluid phase a the tail of the mass flow.

The dilatant two-layer phase approach is being tested at the Illgraben (Valais, Switzerland) study site, where the model has successfully replicated an event involving dewatering and sediment processes with high accuracy. The results of Meyrat *et al.* (2023) demonstrate that friction decreases with

increasing volumetric fluid concentration. The extent of this reduction is influenced by factors such as pore pressure and the agitation in solid particles. Quantifying these effects is challenging, as they render friction in debris flows highly nonlinear.

3.1.1.1 Expected Advantages of the Two-Phase Model

The introduction of the two-phase layer approach in mass flow modeling has several advantages over the currently in RAMMS implemented single-phase models. This approach, which distinguishes between the solid matrix and free fluid phase enables a more accurate and detailed representation of the complex dynamics within debris flows, as shown by Meyrat *et al.* (2024).

The two-phase layer approach provides a more accurate prediction of debris flow behavior by accounting for the distinct interactions between solid and fluid components (Meyrat *et al.*, 2022). The currently implemented single-phase model in RAMMS treats debris flows as a homogeneous mixture (Bartelt *et al.*, 2017), oversimplifying the internal dynamics. By differentiating between the solid matrix and the free fluids, the two-phase model captures the variability in flow characteristics. In particular, the simulations of flow transitions are enhanced. For instance, the two-phase model should be able to represent transitions from debris flows to hyper-concentrated. These transitions are often recognized in GLOF events with a long-distance outflow, as they can change several times during the natural setting. During these transitions, changes in water, sediments and slope angle can occur, which can only be captured by two-phase models. In addition, the model is expected to simulate sedimentation and dewatering processes, which are crucial to deposition patterns of mass flows. Not only is this important for the final deposition of sediments during a GLOF event but also during an event, as the mass flow can dewater and behave as a hyper-concentrated flow and later form a debris flow. The model enables realistic behavior of sediment settlement and allows for independent movement of the fluid phase. In comparison to the one-phase models, these processes are neglected and inadequately represented.

3.2 Model Setup and Configuration

The general setup of the model RAMMS to simulate GLOF events involves several steps, ensuring the generated simulations' reliability. The description of the process of configuring the model, including choosing the input parameters, the calibration and the validation as well as the preparation of simulation scenarios.

3.2.1 Hydrograph Setting and Input Data

The software RAMMS allows the initiation of a simulation with either a block release or a hydrograph. A block release scenario can be simulated when a mass, like a snow avalanche, starts to slide at the time of initiation (Bartelt *et al.*, 2017). This option fits simulations where the depth of the potential gliding, continuous layer is known and in the absence of great water volumes, often referred to rock avalanches or dry granular flows (Hungr, Leroueil and Picarelli, 2014). The block release is usually used in GLOF literature to simulate triggering events for snow-, rock- and ice avalanches (e.g. Lala, Rounce and McKinney, 2018; Somos-Valenzuela *et al.*, 2016). According to the RAMMS user manual, it can also

distinguished between unchanneled and channelized debris flows. Whereas it is recommended to use a block release for an unchanneled and a hydrograph for a channelized debris flow (Bartelt *et al.*, 2017). In the case of GLOF modeling, deploying a hydrograph fits better with the characteristics of a GLOF outflow event. GLOFs often occur in large-scale valleys with high water volumes and channelized torrents (e.g. Meyrat *et al.*, 2024). In addition, discharges at certain locations are often known, because of landmarks, observations, photography or GPS. RAMMS Users can determine both the volume of water entering the system and the amount discharged at the release, as well as for subsequent time intervals.

For RAMMS simulation of GLOFs initiated with an input hydrograph, knowledge about the discharge at a given location is required (Bartelt *et al.*, 2017). Knowledge can be obtained, when the discharge at a given location is known, through measured flow heights and corresponding channel cross-sections. The estimated total volume is known with empirical relationships between total volume and maximum discharge of Rickenmann (1999). The hydrograph options require the number of discharges as well as the velocity for each, defined time step. The hydrograph setting in RAMMS lays down a simplified equation clarified in Rickenmann (1999), which describes the flow velocities of debris flows in dependence of discharge and slope.

In the scope of this thesis, two approaches to define the input hydrograph are applied. At the Täsch site, outflow volumes are known as the water level of the glacial Weingarten Lake were examined before and after the event (see Chapter 2.3.2). Whereas in South Lhonak reports of the flow height during the event are known for a defined location through reports (see Chapter 2.3.1). With the equation of Rickenmann (1999), it is possible to define a hydrograph through both approaches in RAMMS. This reduces the difficulty for practical users to define water volumes with small data available. Moreover, the implemented equation simplifies and optimizes the efficiency of conducting the simulations.

3.2.2 Topographic Data Processing (DEM)

According to Bartelt *et al.* (2017), the topographic data is the most important input parameter for simulations with RAMMS. The accuracy and resolution of the DEM significantly influence the simulation results (Westoby *et al.*, 2014). To generate reliable modeling outputs, Bartelt *et al.* (2017) recommend that all important terrain features be integrated and represented into the DEM before applying simulations. In addition, all georeferenced datasets, including the DEM, must be applied in a Cartesian coordinate system, as RAMMS does not support degree-based coordinate systems. The software is capable of several DEM formats, including ESRI ASCII, ASCII XYZ and GeoTIFF.

Given that the DEM is one of the most influential input parameters for modeling with RAMMS, careful processing is required, especially when working with low-powered systems. The general topographic data processing workflow applied in this thesis consists of several key steps, as illustrated in Figure 10:

1. Generating raw DEM: The first step involves acquiring and selecting the most suitable DEM for the study area, considering the factors of data availability and resolution.

2. Processing DEM: The acquired DEM undergoes reprocessing, including shading adjustments, gap-filling, and resampling to a coarser resolution if necessary to balance computational demands with result accuracy.
3. Framing: Definment of calculation area by framing the DEM focusing on the specific region of interest, ensuring that unnecessary data is excluded regards the computational demand.
4. Cutting: Further refinements involve cutting the DEM to the exact area needed for simulation (e.g. channel bed), reducing computational power and enabling to run simulations on low-powered systems such as standard laptops.
5. Refinement: Finally, the DEM undergoes a refinement process, addressing any remaining gaps, no-value areas or sinks to improve the model outputs. This is done after several model simulations.

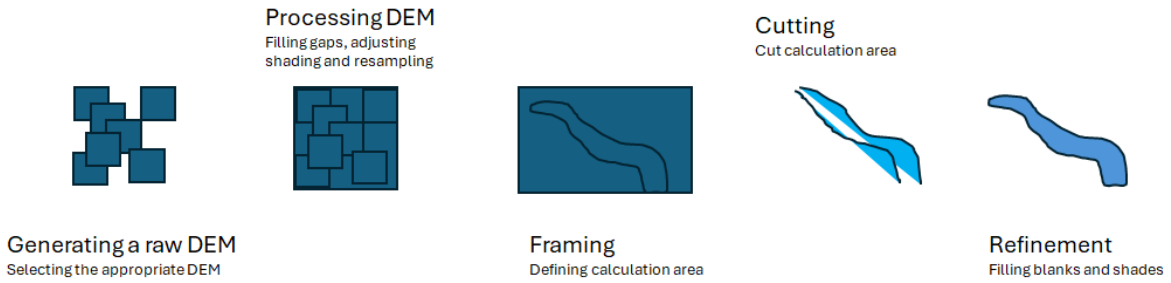

Figure 10: Schematic overview of the DEM processing workflow. The process includes 5 key steps: Generating raw DEM (1), processing DEM (2), framing (3), cutting (4) and refinement (5), ensuring a suitable input for RAMMS simulations.

These processing key steps are important in preparing the DEM for accurate simulations, as they act beneficial for optimizing computational efficiency while maintaining the data quality. Details on the specific processing techniques applied to the DEMs in this study are provided in Chapter 3.3.1 for the Weingarten Lake site and 3.4.1 for the South Lhonak site.

3.2.3 Calibration and Validation of the Model

Calibration and validation are important steps in generating reliability of the model simulations for GLOFs, especially when limited empirical data is available. This section shows the general process for calibration and validation and focuses on two case studies conducted in this thesis.

Model calibration involves the best-fit approach, adjusting model parameters to improve the relationship between simulated results and observed data. This enables the model to reflect the real-world processes under examination. This approach has been successfully conducted in several studies (e.g. Cao and Carling, 2002; Mergili *et al.*, 2011; Frey *et al.*, 2016). In the context of GLOF modeling, finding the best fit is often challenging due to the lack of measured data such as discharge records. Therefore, calibration can rely heavily on secondary data sources, such as eyewitness accounts, deposition volumes or satellite imagery. For GLOF modeling, key parameters include the input hydrograph, DEM and friction coefficients that determine the flow behavior. These parameters can be adjusted using the trial-

and-error approach, tuning them until the model best reproduces the past event. In retrospective GLOF modeling, for example, parameters like friction coefficients are tuned to simulate the flow's characteristics, such as flow heights or inundation extents.

For the Weingarten Lake and South Lhonak case studies, calibration is based on site-specific literature (Huggel *et al.*, 2003; Huggel *et al.*, 2004; Sattar *et al.*, 2021), as well as secondary data such as reported outflow volumes and deposition. Despite the lack of direct discharge records, these sources provided crucial information on peak discharges and total outflow estimates. For the South Lhonak site, additional qualitative data were adapted from local reports and news articles, which helped to calibrate the model despite being not precise (Chapter 2.3.1.3). Given the unique characteristics of both sites, calibration is focused on tuning the friction coefficients μ and ξ to reflect the specific conditions of the Weingarten and South Lhonak Lake outflow valley. The default values $\mu = 0.2$ and $\xi = 200\ m/s^2$ for these parameters in RAMMS were initially used (Bartelt *et al.*, 2017). However, these settings are recommended for debris flows with small specific information, and therefore need to be adapted to reflect the more water-saturated GLOF routings at both sites. In particular, higher values for ξ and lower values for μ are found to replicate the most accurate simulations of the past events, as detailed in the baseline simulations sections 3.3.1 for Weingarten Lake and 3.4.1 for South Lhonak Lake.

To validate and further calibrate the model, satellite imagery and photographs can be used to compare model outputs with observed flood extents and deposition patterns of past events. This visual comparison helps to ensure that the model accurately captures the spatial distribution and flow dynamics of the sediment-laden flows, tuning friction coefficients to match the observed flow height and inundation extent along the outflow path.

Calibration of models is not only important for retrospective GLOF analysis but also provides valuable insights for predictive modeling on other potential GLOF sites with similar characteristics. By tuning friction coefficients and input hydrograph to the best fit of past events, these calibrated models serve as a baseline for evaluating the risk of future GLOFs or back-calculations of past events. Therefore, it is recommended that model parameters are well described in GLOF sites under examination. While the calibration process helps to reduce uncertainty in retrospective modeling, it is important to acknowledge the limitations of this technique. As discussed in Chapter 5.3.2, the lack of precise data and the uniqueness of events result in some degree of uncertainty, which can influence the accuracy of models.

3.3 Simulation Scenario Weingarten Lake

The glacial lake Weingarten presents a persuasive case study for the simulations of GLOFs due to its history of a past event and the mitigation measurements currently in place. This section outlines the methodologies and considerations involved in providing realistic simulations for the lake outflow, leveraging state-of-the-art digital elevation models and the modeling tool RAMMS.

The scenario definition aims to understand the GLOF behavior under varying conditions, providing insights into simulation setup and hazard mitigation. This is carried out by calibrating the baseline scenario to the GLOF event of 2001 and exploiting alternative scenarios with modified input parameters, investigating the sensitivity of these parameters and the factors influencing the flow dynamics and the inundation extent.

3.3.1 DEM Processing and Preparation

The DEM applied in the simulations is accessed from the Swiss Government of Topography (URL: https://www.swisstopo.admin.ch/de/hoehenmodell-swissalti3d, last access: 17.05.2024). The DEM is called swissALTI3D and describes the Swiss surface without any vegetation and construction. The model is actualized every 6 years for the whole of Switzerland, meaning one-sixth of the Switzerlands area is actualized yearly. The structure can be provided as a 2 m or 0.5 m raster, whereas the latest is utilized for the simulations with RAMMS in this study. The provided data contains completed tiles with an area of 1 km^2. As the area of the outflow of the Weingarten Lake is several kilometers long, the tiles are merged within the software QGIS.

After the GLOF event of 2001, explained in Chapter 2.3.2.2, two dams were installed in the outflow routing of the glacial Weingarten Lake (see Appendix A)). One was built in 2006 above the Täschalp at 2'250 m a.s.l.. The dam protects the houses of Täschalp and reduces the outflow volumes from Weingarten Lake before entering the Täschbach. The construction of the dam allows the outbreak of the Rotbach during an extreme event in a designated runout zone, depositing the material where no houses or infrastructure are endangered. The second dam is located at the fan apex of the Täschbach, above the village of Täsch at 1'472.7 m a.s.l.. The dam protects Täsch and holds back solid material in the river bed, allowing the water to travel further downstream. As the Baseline Scenario (Chapter 3.3.1) lays down to the GLOF event of 2001, the DEM had to be adapted in QGIS to the outflow topography of this time. Due to the lack of a precise DEM at that time, today's DEM was modified by excluding the dams to represent and approximate the terrain of 2001.

The process of modifying the DEM to replicate the terrain during the past GLOF event involves several steps in QGIS, which are detailed in the following section. First, polygon shapefiles are drawn to delineate the locations of the dams. The DEM is then cut by utilizing the "*cut by layer mask"* tool along the polygon shapefiles. As a result, the cut DEM contains nodata values in the corresponding areas of the dam locations, which allows for interpolation to represent the terrain of that time. The interpolation of the nodata areas is performed by utilizing the QGIS tool "*r.fillnulls*" (URL: https://grass.osgeo.org/grass-stable/manuals/r.fillnulls.html, last access: 08.08.2024), which fills pixels with no value in the input rater and provides a completed output raster. The tool "*r.fillnulls*" uses the bilinear interpolation method, which calculates the value of a null cell by taking a weighted average of the values of its four nearest neighbors in the grid. In this method, values closer to the null cell have a greater influence on the final interpolated value, while more distant values contribute less.

Furthermore, the interpolated DEM was tested with success through initial model simulations using RAMMS. Nevertheless, the validation was based only on the behavior of the simulated outflow. As a result, the DEM remains an uncertain variable, due to the approximation of the terrain at that time of the past event.

3.3.2 Baseline Scenario Setup

The Baseline Scenario of Täsch represents a retrospective simulation of the GLOF event that happened in 2001. The goal of the Baseline Scenario is to provide a solid, realistic scenario that can be adapted to different scenarios with various input values. However, as this thesis aims to investigate to what extent RAMMS can model GLOF events, the Baseline Scenario was calibrated qualitatively and no quantitative sensitivity analysis of friction parameters has been made on the Baseline Scenario itself. However, multiple simulations were conducted to explore the best fit of parameters regarding the past GLOF event. Precisely, the Baseline Scenario was calibrated regarding photographs (Figure 11) and the volumetric estimation of the outflow of Huggel *et al.* (2003). The parameter values used for the basis simulation are presented in Table 1.

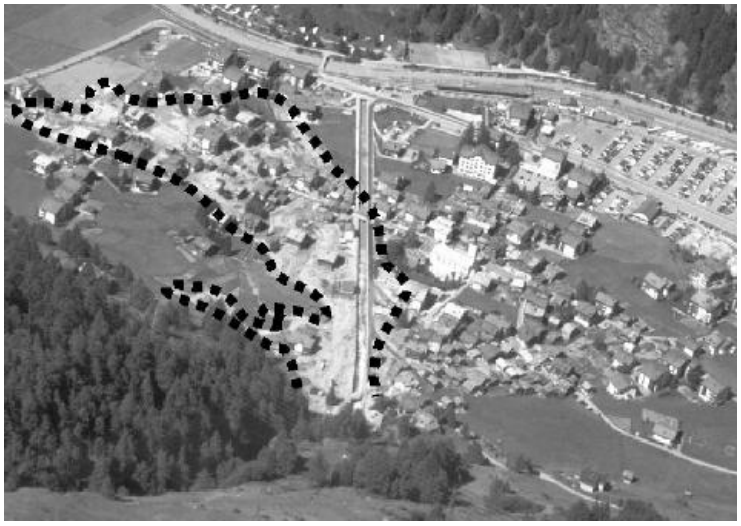

Figure 11: Overview of the deposited debris flow material in Täsch. The dashed black line represents the maximum deposition extent in Täsch of the Weingarten GLOF event in 2001. The picture is adopted from Huggel et al. *(2004).*

The relatively small-scale GLOF in Täsch allows for a detailed simulation of the entire outflow path. To optimize computational efficiency, the resolution of the simulation was increased to 5 meters. This can be adjusted directly in the RAMMS software. Initially, a 0.5 m DEM was used for the simulations. While this finer resolution, would provide more precise results (Westoby *et al.*, 2014), it was not feasible for this study due to the significant increase in computational demand that comes with a higher resolution. RAMMS calculates the mass flow for each cell, smaller cell sizes improve accuracy, but they also require more computational resources, which were not available in this study.

The input hydrograph parameters lie down to the numbers considered by Huggel *et al.* (2003). They estimated an outflow of the Weingarten lake of 6'000-8'000 m^3. In this Baseline Scenario, 8'000 m^3 is chosen for the hydrograph volume, as it fits best to the event from 2001. Regarding the relationship between the maximum peak discharge and maximum volume of Rickenmann (1999), the peak discharge is set right at the input hydrograph with 178.400 m^3/s. For the simulation, the hydrograph is located directly under the Weingarten Lake, as the highest volumes are expected to emerge right at the beginning of the lake outflow.

The density is set to 2'000 kg/m^3 for mass movement, which is the recommended default value for a debris flow (Bartelt *et al.*, 2017). As Huggel *et al.* (2003) stated a range of deposited volume in Täsch of 20'000 to 30'000 m^3, the GLOF is considered a debris flow in this baseline simulation. Hungr, Leroueil and Picarelli (2014) describe debris flows as very rapid to extremely rapid surging flow of saturated debris in a steep channel, with strong entrainment of material from the flow path. This is true for the first part of the outflow path above Täschalp, where great amounts of sediment are available (Huggel *et al.*, 2003). The material consists of unconsolidated moraine material, which holds small cohesion. This is taken up in the simulations with an erosion polygon in this section of the flow path (Figure 7, Part A). However, the erosion polygon is set to the default values as there was no field survey conducted (Table 1). In contrast, in the second part after Täschalp, the river bed consists of big boulders and blocks that are considered as not erodible (Figure 7, Part B). Therefore no erosion polygon is applied in the simulations for the second part of the GLOF routing in Täsch.

Parameter	**Value**
Simulation resolution [m]	5
Stopping criteria [%]	5
Density [kg/m^3]	2000
Lambda [-]	1
Hydrograph volume [m^3]	8000
Inflow direction [°]	180
Time to peak discharge [s]	1
Peak discharge [m^3/s]	178.400
μ [-]	0.200
ξ [m/s^2]	4000
Erosion polygon	
Maximal eroded rate	0.025
Shear factor	0.100
Critical shear	1.00
Limit erosion	0.00

Table 1: Input parameter values of the basis simulation for the Weingarten Lake.

To calibrate the Baseline Scenario to the real event, multiple simulations were made to simulate the real event. The simulation is compared to the real event and the parameters are set to get the nearest to the real event with the "best fit" approach (Cao and Carling, 2002). For this, available literature (Huggel *et al.*, 2003; Huggel *et al.*, 2004) about outflown water volumes and the picture of the deposited material in Täsch (Figure 11) were used to ensure a realistic baseline model. The values of the friction parameters μ and ξ are set to 0.20 and 4'000 m/s^2, respectively. A high-value ξ is chosen, as this parameter regulates the frictional resistance during high-speed movement, expecting to match the high flow velocities during the real event mentioned by Huggel *et al.* (2003). The μ value is set to the default value μ = 0.2 because the GLOF outflow is described as a debris flow. However, the discrepancy of ξ to the default does not affect the simulations significantly, indicating a low sensitivity of the friction parameter ξ.

3.3.3 GLOF Event Scenarios for Weingarten Lake

The goal of defining scenarios is to exploit the different input volumes, density and mitigation measurements and their behavior regarding the inundation extent and flow heights occurring. To achieve this, scenarios with different input hydrographs, density and mitigation measurements are chosen (see Table 2), based on the reports of the real event observed in 2001. The other parameters, such as the friction parameters ξ and μ or DEM, are based on the Baseline Scenario and remain unchanged (see Table 1). This also includes the location setting of the hydrograph, right under Weingarten Lake.

Scenario	Hydrograph volume [m^3]	Peak Discharge [m^3/s]	Density [kg/m^3]	DEM *
Baseline Scenario	8'000	178.40	2'000	Without Dams
Sc_2	6'000	140.00	2'000	Without Dams
Sc_3	8'000	178.40	1'000	Without Dams
Sc_4	8'000	178.40	1'000	With Dams

*Table 2: Summarized input parameters for the scenario simulations in Täsch. *: The DEM without dams represents the DEM from 2001 which was modified in QGIS by excluding the obstacles from the terrain, whereas with dams represent today's terrain.*

In Scenario 2 the input volume is decreased to 6'000 m^3, as stated by Huggel *et al.* (2003), this is the minimum volume released during the observed event in 2001. The inundation extent and flow heights are expected to be smaller regarding the baseline scenario.

Scenario 3 relates strongly to the Baseline Scenario as the input hydrograph values are kept the same. However, the density is decreased to 1'000 kg/m^3 to exploit the flow behavior of a more fluid mass flow in comparison to the Baseline Scenario. As the default value of 2'000 kg/m^3 relates strongly to debris flows, a value of 1'000 kg/m^3 relates more to a water flow.

Scenario 4 includes the same input parameters and friction coefficients as Sc_3. However, for Sc_4 today's terrain is used as the input DEM, representing the adaptation measurements in the terrain model. The

goal of this scenario is to make statements about GLOF dynamics with the implemented dams at Täschalp and the fan apex in front of Täsch. The results of the scenario simulations are presented in Chapter 4.2 and further discussed in Chapter 5.2.

3.4 Simulation Scenario Lake Lhonak

This chapter provides a detailed exploration of GLOF simulations in the South Lhonak region, leveraging RAMMS to model and study the flood dynamics and potential risks. The objective is to provide a comprehensive understanding of the methodology, varying event conditions and scenario development using the latest version of RAMMS. The gained insights aim to contribute to future research and improve GLOF hazard assessments with RAMMS from a modeling point of view.

3.4.1 DEM Processing and Preparation

The digital elevation model (DEM) is a fundamental input parameter for simulations procured with RAMMS (Bartelt *et al.*, 2017). To ensure the accuracy and reliability of the simulations, a detailed methodology is followed to process and prepare the DEM of South Lhonak using QGIS.

The DEM utilized for the simulations in this study is obtained from the USGS Earth Explorer platform (URL: https://earthexplorer.usgs.gov/, last access: 16.07.2024), specifically from NASA's SRTM3 SRTMGL1 satellite dataset. The dataset is identified as N27E088.SRTMGL1 was originally collected between February 11th and 21st in the year 2000 and was recently updated on the 30th of November 2023. Since RAMMS requires DEMs in the Cartesian coordinate system, the original projection of WGS84 was reprojected to the WGS 84 N84 coordinate system using the software QGIS. To improve the understanding and interpretability of the terrain, a hillshade layer was generated within the RAMMS software.

To increase the precision of the simulations, the original DEM resolution was resampled from 30 m to 12.5 m. This resampling was done by using the tool "*Warp (reproject)"* in QGIS, with the target resolution set for both the X and Y axes. Bilinear interpolation was chosen as the resampling method, as it averages the values of the surrounding pixels, generating a smooth and continuous dataset suitable for modeling GLOF events. The updated resolution was confirmed by inspecting the metadata of the DEM and the performance of the initial debris flow simulations with RAMMS. A higher resolution is essential for accurate modeling because RAMMS performs calculations for each cell, as smaller cell sizes lead to a more detailed representation of the terrain and therefore for the simulations (Westoby *et al.*, 2014). The level of detail is particularly important for the studies of localized mass flows, such as GLOFs, as the flow dynamics are captured in narrow valleys and other complex terrains.

Because of the computational demands of working with large GLOF areas and therefore with large datasets, the DEM was clipped to focus on the Chungthang village. Initially, the DEM encompassed a 60 km stretch of the valley from the South Lhonak Lake to Chungthang, containing approximately 30'000 cells. However, the availability of a standard laptop was unable to process simulations of this scale of dataset. By reducing the area of interest to the Village of Chungthang, the computational load

was lowered to approximately 5'000 cells. The reduction of cells not only allowed for manageable simulations but also enabled the use of a finer resolution of 12.5 m, as opposed to the coarser 100 m resolution used for the entire Teesta Valley from the South Lhonak Lake to Chungthang.

The DEM resolution was considered to meet simulation quality criteria. According to Bartelt *et al.* (2017), the resolution should be at least four times smaller than the width of the channel being modeled. For the Teesta River, with a channel width of approximately 70 to 80 m in the 1 km calculation domain of Chungthang, the 12.5 m resolution fits this requirement. This ensures that the terrain features are captured accurately by the DEM.

Further refinements were made to the DEM, addressing potential errors. First RAMMS simulations were made to identify issues such as sinks or depressions in the river bed. This again was cross-validated with satellite imagery of the riverbed. Any erroneous sinks were corrected using the GRASS GIS tool "*r.fill.dir"*, which produces a depressionless DEM. These corrections ensured the accurate representation of the terrain without distortions that could compromise simulation results.

To model the dammed lake around Chungthang, a polygon shapefile was created. Based on satellite imagery, an elevation attribute of 1'574 m a.s.l. was attributed. The polygon was integrated into the DEM using the QGIS tool "*cut by layer mask"* and the "*rastercalculator"* was used to establish a uniform elevation for the lake. The following expression ensured the lake surface was flat and impermeable:

("DEM_mit_rfilldir" < 1574) * 1574 + ("DEM_mit_rfilldir " >= 1574) * " DEM_mit_rfilldir "

Equation 1: Applied equation with the rastercalculator in QGIS for generating a flat area, which represents the lake in the DEM.

This step ensured that the mass movement did not sink into the dammed lake during simulations. Although this behavior is unrealistic, it is assumed that the mass movement would float slightly over the lake or remain suspended at least during the initial stages of entering the dammed lake. Given that Chungthang is surrounded by the lake, this dynamic increases the risk of inundation, especially if the lake is at full capacity.

3.4.2 Baseline Scenario Setup

The Baseline Scenario of Lhonak represents a retrospective simulation of the GLOF propagation that happened on the 4th and 5th of October 2023. The goal of the Baseline Scenario is to provide a solid, realistic simulation that can be adapted to different scenarios with varying input volumes. However, as this thesis aims to investigate to what extent RAMMS can model GLOF outflow events, the Baseline Scenario was evaluated and calibrated qualitatively on reports and satellite images and no quantitive sensitivity analysis has been conducted on the baseline scenario itself. The Baseline Scenario was calibrated regarding journal articles mentioned in Chapter 2.3.1.1. The articles hold pieces of information from civilians who saw the floods. Moreover, satellite images from before and after the event helped the optimal parameters to fit the event observed (Figure 6). The parameter values used for the basis simulation are presented in Table 3.

The Baseline Scenario is limited to the village of Chungthang, as the computational power is too demanding to simulate the whole valley (Chapter 3.4.1). The village of Chungthang is of special interest because of its socio-economic development and the hydropower station damaged in the 2023 event. The hydrograph is set 500 m before the Teesta River reaches Chungthang.

The hydrograph input parameters, namely the volume and the peak discharge are reconstructed from reports from the inhabitants of Chungthang of the 4th October event (see Chapter 2.3.1.1). A 6 m flood is reported and noted in a journal article (URL: https://www.bbc.com/news/world-asia-india-67017845, last access: 25.04.2024). Regarding the common discharge equation Q [m^3/s] = a [m^2]*v [m/s], the peak discharge at Chungthang can be estimated. With a given channel width of approximately 80 m and 6 m height of the flood wave parameter a, the cross-sectional area of the flow (wetted area), is denoted with 480 m^2. The velocity of the GLOF is down to assumptions from Meyrat *et al.* (2024) and Sattar, Goswami and Kulkarni (2019), who state a flow velocity of 6 to 9 m/s for their large-scale GLOF simulations. For the Baseline Scenario in the present study, a velocity of 6 m/s is chosen. Putting all values in the discharge equation 2'880 m^3/s results. RAMMS uses the equation of Rickenmann (1999) to calculate the peak discharge respectively the input hydrograph volume. Rickenmann (1999) describes the estimated total volume in combination with empirical relationships between total volume and maximum discharge. Because of this relationship the input hydrograph volume of 225'000 m^3 results regarding the wetted area and flow velocity.

The density of the moving mass is set to 1'200 kg/m^3, as the GLOF consists relatively small amount of solid material regarding the almost pure liquid outflow of the South Lhonak Lake. Despite the dam breach which entrains great amounts of solid material right from the start (Richardson and Reynolds, 2000), the default density for debris flows of 2'000 kg/m^3 is considered too high. The entrained breach material is assumed to have been deposited earlier on in the flow channel of the GLOF.

Parameter	**Value**
Simulation resolution [m]	12.5
Stopping criteria [%]	5
Density [kg/m^3]	1'200
Lambda [-]	1
Hydrograph volume [m^3]	225'000
Inflow direction [°]	320
Time to peak discharge [s]	1
Peak discharge [m^3/s]	2'873.20
μ [-]	0.04
ξ [m/s^2]	500

Table 3: Input parameter values applied in RAMMS for the basis simulation of South Lhonak Lake.

The process of erosion is neglected in the simulations of South Lhonak, due to the lack of information on the geology of the valley as well as the availability of sediments in the river bed. The entrainment of the solids is therefore not further evaluated, as this would have been a vague parameter and affected the results strongly without fundamental information on erosion.

Scholars from Iribarren Anacona *et al.* (2018) and Frey *et al.* (2018) show that setting $\xi = 500$ m/s^2 represents the turbulent friction during debris flow events accurately. The parameter $\mu = 0.04$ is considered reasonable for hyperconcentrated flows according to Stricker (2010). Multiple simulations were applied with changes in ξ and μ values. However, in this Baseline Scenario, the parameters of $\xi = 500$ and $\mu = 0.04$ are chosen, as the simulations resulted in promising inundation extents and flow heights.

3.4.3 GLOF Event Scenarios for South Lhonak Lake

The objective of defining multiple GLOF scenarios is to examine how varying input volumes, based on the peak discharges, influence the inundation extent and flow heights at Chungthang. These scenarios are defined based on reports from the 2023 event, supplemented by velocity ranges observed from similar large-scale GLOF events globally (e.g. Frey *et al.*, 2016; Meyrat *et al.*, 2024).

The four modeled scenarios (Sc_1, Sc_2, Sc_3 and Sc_4) visualized in Table 4 are built on the Baseline Scenario described in Chapter 3.4.2. The DEM of the riverbed topography and the hydrograph location remain the same as the Baseline Scenario. The friction coefficients $\xi = 500$ and $\mu = 0.04$ are kept unchanged regards the Baseline Scenario to isolate the effects of varying flow parameters on inundation extents and flow heights. A similar scenario definition approach was successfully applied in the study of Sattar *et al.* (2021), demonstrating the validity of defining multiple scenarios for GLOF event examination.

Scenario	Velocity [m/s]	Discharge [m^3/s]	Wetted Area [m^2]	Flow Height [m]	Input volume* [m^3]
Sc_1	8	3’840	480	6	319’000
Sc_2	6	4’800	800	10	420’000
Sc_3	8	6’400	800	10	590’000
Sc_4	8	7’680	960	12	730’000

*Table 4: Summarized parameters for the input hydrograph of the simulated scenarios. *: Input volume calculated utilizing the equation of Rickenmann (1999) within RAMMS.*

In Scenario 1, the flow velocity is increased to 8 m/s compared to the Baseline Scenario. Due to the absence of measured data from October 4th, this value aligns with literature, such as Sattar, Goswami and Kulkarni (2019), who documented velocities between 7.4 and 7.6 m/s for GLOF events in the Alaknanda basin, Uttarakhand, India. The flow height remains at 6 m, consistent with the Baseline

Scenario, resulting in a calculated discharge of 3’840 m³/s at Chungthang. The wetted area is estimated at 480 m^2, corresponding to the assumed cross-section of the riverbed.

Scenario 2 explores the influence of flow height, increased flow heights to 10 m are chosen, reflecting the vague eyewitness reports from the 4th of October 2023. With an assumed riverbed cross-section of 80 m, the wetted area expands to 800 m^2, leading to a peak discharge of 4’800 m³/s, while velocity is set to 6 m/s to examine a lower energy flow condition.

Combining the parameters from Scenarios 1 and 2, Scenario 3 maintains the increased flow height of 10 m while applying a higher velocity of 8 m/s, resulting in a peak discharge of 6’400 m³/s. The wetted area remains at 800 m^2, consistent with the adjusted flow conditions.

Scenario 4 demonstrates the most extreme conditions, with flow height assumptions increased to 12 m, resulting in a wetted area of 960 m^2. The velocity remains at 8 m/s, generating the highest discharge of 7’680 m³/s. This scenario provides an extreme case estimation for the potential GLOF impact at Chungthang.

4 Results

4.1 Simulation Results for South Lhonak Lake

The results of the South Lhonak GLOF simulations provide critical insights into the inundation patterns, flow heights, flow dynamics and sediment deposition characteristics at Chungthang. Applying the RAMMS model, four scenarios (Sc1 to Sc4) were developed in Chapter 3.4.3 to simulate the retrospective GLOF event of autumn 2023. The scenarios enable the comparison of observed event values with modeled outputs, underscoring the key differences in inundation extent, flow dynamics and heights.

The following sections begin with an analysis of simulated flow heights and inundation extents, contributing to a quantitative and visual comparison of the four scenarios to the real event. It examines the runout characteristics and flow behavior, stressing variables such as momentum, velocity, pressure and shear stress. This provides a deeper understanding of the GLOF behavior and its destructive potential at Chungthang. Finally, the section evaluates the deposition patterns of sediments and discusses uncertainties within the simulation process, reflecting the model assumptions and the limitations of the input data.

4.1.1 Inundation Extent and Flow Heights

The results of the RAMMS simulations for the four scenarios Sc1 to Sc4 are shown in Figure 12, illustrating both the flow heights and the inundation extents at their maximum extents occurring during the flow. The flow heights are depicted with a color gradient, where violet indicates smaller depths from 0.2 m to 3 m and orange/red represents the highest depths, reaching a maximum of 18 m. The red, dashed line indicates the maximum inundation extent of the observed event of the 3rd of October 2023, allowing the comparison of the simulation results with the real event.

The simulated scenarios, Sc1 to Sc4, reveal notable variations in distribution and extent of inundation, underscoring the influence of differing input volumes on flood dynamics. Generally, the inundation expands from Sc1 to Sc4 progressively, with a significant increase in Sc3 and Sc4 compared to Sc1 and Sc2. This progression reflects the increased input volumes in the applied RAMMS simulations.

Regarding the spatial distribution, the inundation patterns are concentrated in the main river bed and its adjoining floodplains. The upstream and downstream sections exhibit variations in inundation extent, reflecting the scenario-specific conditions (input volume) and the influence of the local topography (DEM). The scenarios Sc3 and Sc4 inundated area extends more widely into the riverbeds surrounding terrain, affecting broader areas of the landscape compared to Sc1 and Sc2. While south of the riverbed the inundation areas are similar across all scenarios, differences appear northwest, with greater inundation extents occurring in Sc3 and Sc4. This suggests that not only do these scenarios with higher input values involve higher flood discharges but also result in more widespread flooding affecting more infrastructure. Therefore, Sc3 and Sc4 underscore the increased risk to critical infrastructure and human settlements.

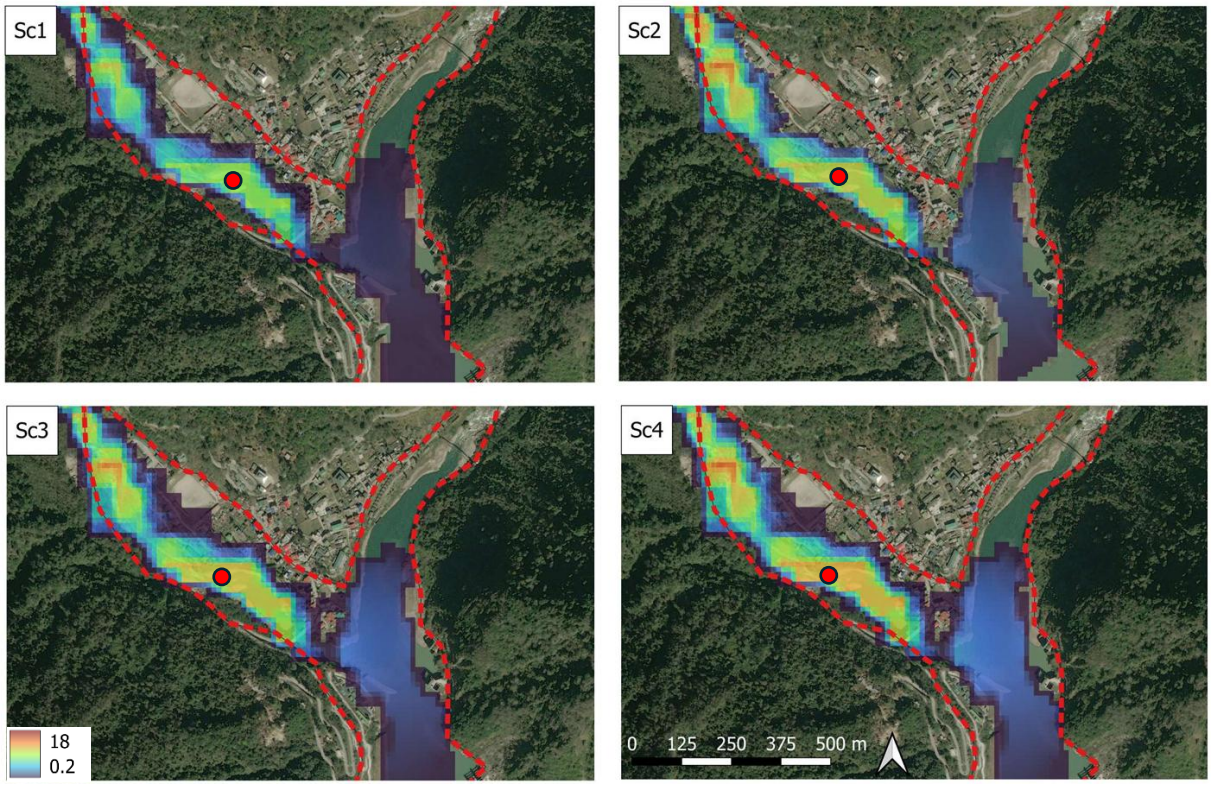

Figure 12: The red line is the maximum inundation area of the event on the 3rd of October obtained from satellite images after the event. Scenarios 1-4 the spatially distributed flow height. The red point indicates the location of the simulated flow heights in Figure 13.

The overall inundation distribution remains consistent across all scenarios within the river bed. The varying extents reflect the system's sensitivity due to changes in input volumes. These results emphasize the importance of considering a range of scenarios in flood risk assessment and provide valuable insights for informing mitigation strategies, land-use planning, and emergency response measures.

The relationship between resulting flow heights and input volume in the simulation scenario Sc1 to Sc4 reveals a strong linear trend, as indicated in Figure 13 by the regression line (dashed purple line). Flow heights increase with higher input volumes progressively, ranging from 8.64 m in Sc1 to 11.76 m in Sc4 at the measuring point located south of Chungthang in the river bed (red point in Figure 12). This consistent upward trend represents how the changes in input volumes directly influence the hydraulic response of the model.

High flow height hotspots are concentrated within the river channel, where the terrain constrains the flow, causing water levels to rise significantly, as indicated by the orange color in Figure 12. These areas experience the greatest rise in flow height and and volumes. However, flow heights out of the river bed are of special interest, as the infrastructure and settlements of Chungthang are affected. Especially, Sc4 depicts flow heights between 0.2 m and 3 m, colored violet, affecting the village of Chungthang northwest of the riverbed. Emphasizing the heightened exposure to GLOF risk in this urban and infrastructural zone. In contrast, lower flow heights in scenarios Sc1 and Sc2 result in more localized inundation patterns, with maximum flow heights confined to the river channel.

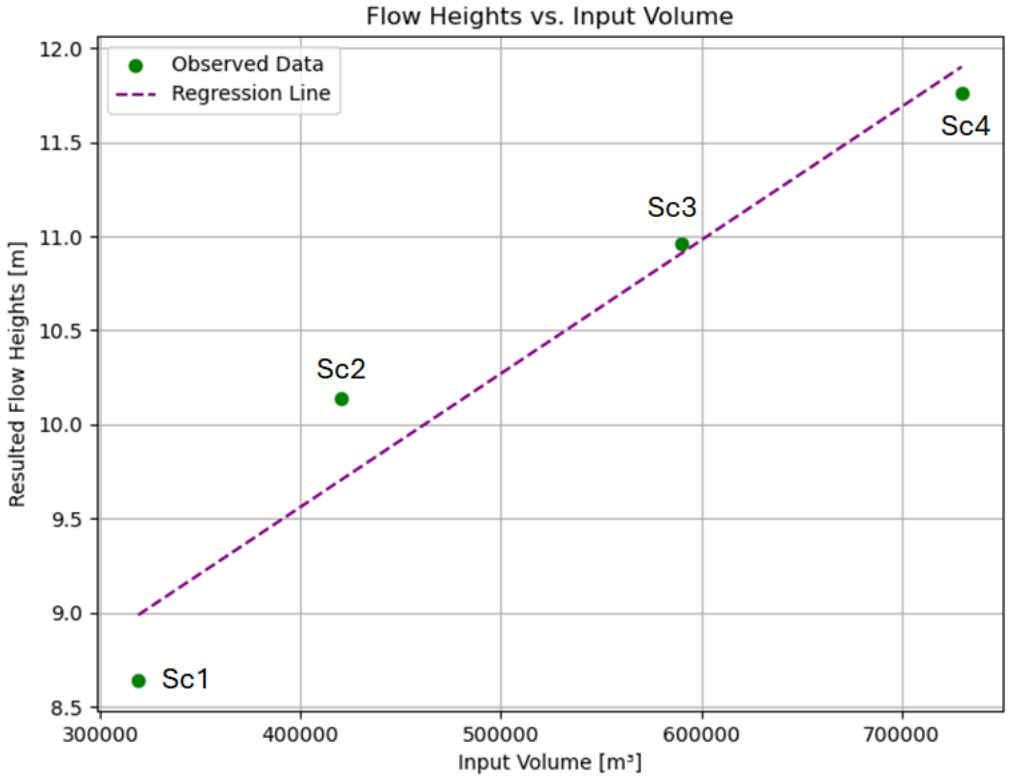

Figure 13: Relationship between input volume [m³] and simulated flow heights [m] for the applied scenarios 1-4 in the riverbed of Chungthang (red point in Figure 12). The green points are the observed flow heights, and the purple dashed line represents the linear regression line fitted to the data, illustrating the correlation between input volume and flow height.

Overall, the results show a progression in both flow heights and inundation extents from Sc1 to Sc4, with Sc1 showing the lowest and Sc4 the most extensive inundation and highest flow depths. However, the results all show smaller extents than the real-world event. A comparison of the flow heights and the observed event seems to be challenging, as there is no data available regarding occurred flow heights.

4.1.2 Flow Dynamics and Runout Characteristics at Chungthang

The results of Scenario 4 (Sc4) are illustrated in Figure 14, displaying the spatial distribution of maximal momentum, maximum velocity, maximum pressure and maximum shear stress across the area of interest. Every variable is represented with color gradients indicating the magnitude of the respective values.

Maximum momentum combines both flow velocity and flow depth into a single measure, allowing insights into the force and energy carried by the water during a simulated event. Momentum indicates the potentially destructive force and energy of the water, which is of importance regarding risk assessment. Moreover, the momentum allows us to make statements about the flow behavior of the GLOF. High momentum often occurs when the velocity and flow depth are increased, such as in more narrow channels, steep terrain gradients or constricted riverbeds. The maximum momentum, the top left

panel, is concentrated along the river bed and adjacent areas. In the upstream section of the river, northwest of Chungthang, higher momentum values are observed in areas where the cross-section is narrower. The momentum decreases gradually as the simulated flow moves downstream towards wider cross-sections and the dammed lake.

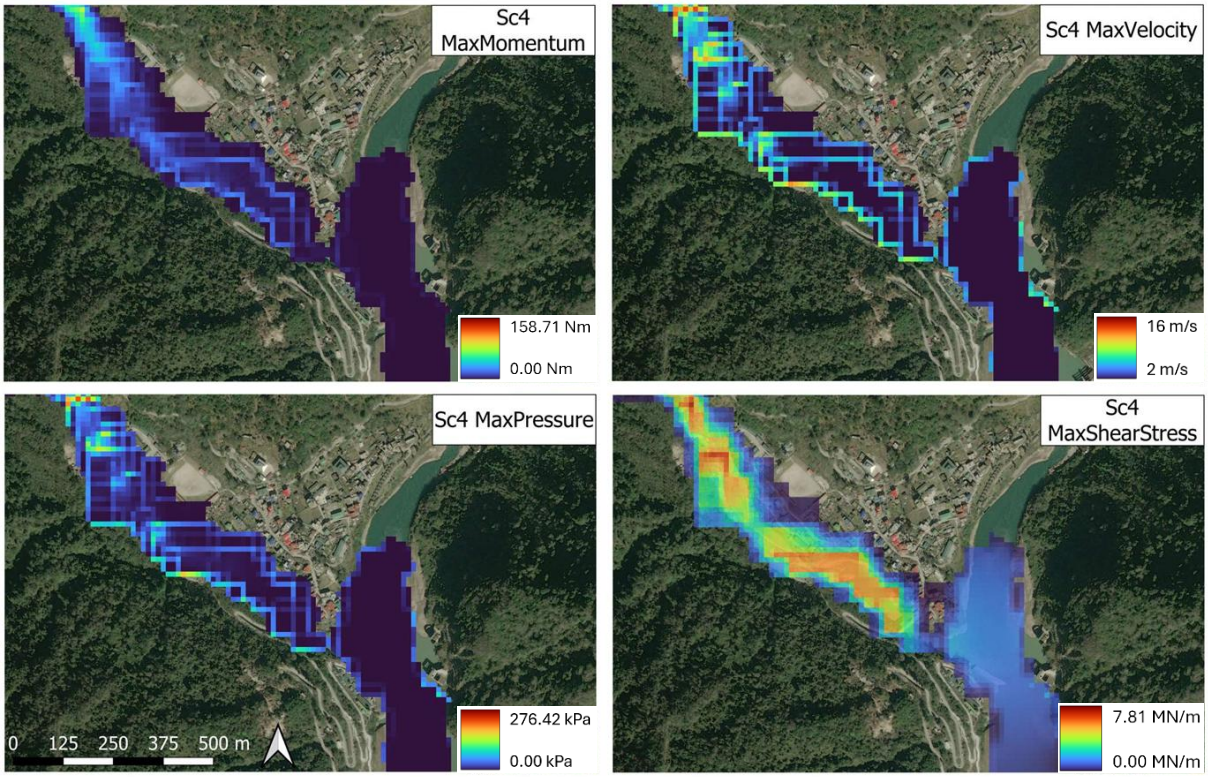

Figure 14: Different variables are displayed for Scenario 4, with the maximal momentum (top left panel), maximal velocity (top right panel), maximal pressure (bottom left panel) and maximal shear stress (bottom left panel).

The maximum velocity is shown in the top right panel of Figure 14 and provides information about the speed and dynamics of water flow during the simulated GLOF event. High-velocity areas typically occur where the water has the greatest kinetic energy. Allowing the analysis of the flow behavior of the water flow. For instance, how the water moves through different topography, how it accelerates in a narrower cross-section and how it slows down in wider, open floodplains. The simulated results of the maximum velocity follow a similar spatial pattern as the maximum momentum. The highest velocities occur along the river channel and in confined areas of the flow. Elevated velocities are occurring in the northwest of Chungthang in the upstream section of the area of interest. In the downstream section, before the river enters the dammed lake, the velocity is reduced across the broader floodplain. Lower velocities are noticeable in the dammed lake because the lake is considered a flat area in the DEM.

The maximum pressure is shown in Figure 14 in the bottom left panel because the pressure directly relates to the force exerted by water during the flow. High-pressure areas not only allow statements about the flow behavior but also how flows can cause damage to infrastructure. The highest pressures are evident in the upstream section and along narrow parts of the floodplain, with pressure values

decreasing as the flow expands downstream. A few isolated areas with elevated pressure can also be seen further along the floodplain. Especially on the right edge of the riverbed high-pressure values are occurring, because the river changes slightly in its direction and centrifugal forces are higher.

The maximum shear stress is directly related to the force exerted by flowing water on the river bed or the surfaces that are overflown. It can be seen as a key factor for erosion and sediment transport and is therefore important to understand the flow behavior and the potential erosion and deposition areas. In Figure 14 bottom right panel, two distinct areas of higher values can be seen. One section can be identified in the northwest and the other in the southwest part of the area of interest. Primarily the high values are concentrated in the river bed. The magnitude of the simulated flow is high just before the river joins the dammed lake, where values decrease.

Overall, the maximal momentum, maximum velocity, and maximum pressure behave strangely, as in localized strings high values occur. This indicates that either RAMMS is not capable of simulating the exact variables or the DEM applied is leading to misinterpretation of the results. A precise interpretation of these simulations is therefore not possible.

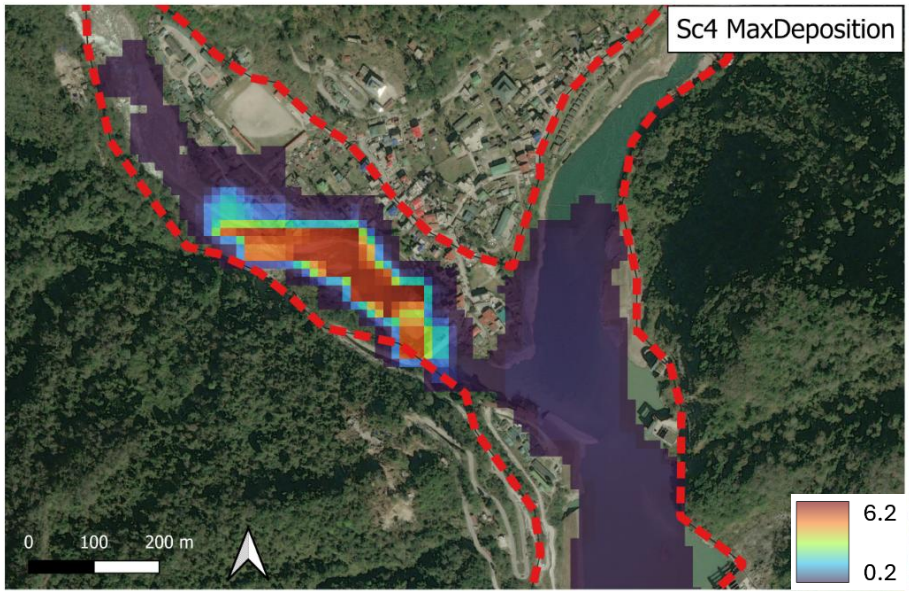

Figure 15: Maximum deposition [m] displayed at the Village of Chungthang for Scenario 4.

The maximum deposition height in Scenario 4 is shown in Figure 15. The deposition layer illustrates the spatial distribution of sediment deposition in the study area, represented as a color gradient from low deposition heights in purple and high deposition heights in red. The darkest red regions within the deposition layer indicate that the maximum deposition height reaches 6.2 m. The spatial distribution shows the highest deposition occurs primarily when the river enters the dammed lake, following the natural terrain where the route is flattening and the velocity of the flow decreases. This suggests that the hydrodynamic forces play a significant role in controlling the deposition of the sediments and its

deposition. The upstream section experiences small amounts of deposition, as the river bed still has a terrain gradient that is high enough to transport sediments. The deposition expands out of the river channel and floodplain, reaching houses in Chungthang. The deposition heights reach some houses heights of 2 m, whereas most houses are affected by small deposition values as indicated by the purple shading. The observed inundation boundary (red dashed line) and the deposition simulation do not match, as the simulated deposition area is smaller than the ones from the real event. However, there is no data available on deposition values from the real event, which only allows the comparison of the deposition extent.

4.1.3 Uncertainty in Simulation Results

For the simulation of the GLOF routing at Chungthang, several uncertainties have to be addressed. The uncertainties affect the DEM, input hydrograph and the friction parameters used.

As the DEM is one of the most important parameters in GLOF modeling according to Bartelt *et al.* (2017) the DEM has to be critically analyzed with the variable of the simulated GLOF case. Regarding the flow heights of the applied scenarios 1 to 4 (Figure 12) as well as the deposition map of Scenario 4 (Figure 15) no anomalies can be observed. However, maximum pressure, maximum momentum and maximum velocity (Figure 14) behave strangely. For instance, one would expect higher velocities in the middle of the flow, as friction is lower than towards the riverbanks. In the simulations at Chungthang velocities are highest at the riverbanks, implicating that something is wrong with the DEM applied. The maximum momentum underscores this statement, as there are some strands where higher momentum values are recognizable. The exported layer of maximum pressure therefore is possible to occur as displayed in Figure 14, since high-pressure zones occur at the riverbanks on the outside of the river curve. Moreover, in the applied DEM the dammed lake is oversimplified. The DEM sees the lake as a flat area at an elevation of 1’574 m a.s.l.. This means that the simulated movement flows over the lake, and not like in the real event into the lake. That’s also the reason why values are occurring on the lake of the different variables shown in Figure 12, Figure 14 and Figure 15. In addition, the lake is set to an elevation of 1574 m a.s.l., which is set to this value according to the satellite images available. The elevation of the dam could have been way higher before the GLOF event on the 3rd of October. This can have a great impact on the inundation behavior, leading to an earlier flow into the lake and therefore backwash the mass movement more upstream. Leading to an earlier outflow of the GLOF, affecting more infrastructure northeast of the river.

Regarding the input hydrograph values, several assumptions had to be made (Table 4). Beginning with the wetted area as the base of the discharges applied in the simulations. The wetted area was defined through satellite images and reported flow heights, 80 m for the cross-section and 6 m of flow heights. Both values are locally rooted and therefore can change along the projected area at the village of Chungthang. Especially, it is unknown where the 6 m of flow height has been seen and if they took into account that the river in a normal situation already has its flow depths. The volume has been adjusted, so the peak discharge fits the calculated discharge generated from the wetted area and the expected

flow velocity. The values of the flow velocity are based on the literature of similar GLOF cases (Sattar, Goswami and Kulkarni, 2019; Meyrat *et al.*, 2024), which is therefore also just an assumption and a vague variable.

Friction parameters are set according to the “best fit” method, which is seen as a standard practice in retrospective modeling (Cao and Carling, 2002). The pros and cons of this method are explained in Chapter 5.3.2, simulations are done with friction parameters on default values and then changed to the optimal behavior of the flow simulations. To examine the values of the parameters, several simulations are applied and changed to the best fit. This is only possible for retrospective modeling, whereas in prediction modeling other GLOF events that seem similar to the investigated GLOF are chosen to examine the friction parameters. However, the sensitivity of these parameters is low regarding the sensitivity of the DEM or the flow discharges.

Generally, there is widespread uncertainty as there was little information available for the GLOF event of South Lhonak Lake at the time when the simulations were conducted in this thesis. This is true for reports in journals or also in literature, as the first scholars on the GLOF event from 2023 are now available (Yu *et al.*, 2024; Zhang, Wang and An, 2025; Sattar *et al.*, 2025).

4.2 Simulation Results for Weingarten Lake

This section exploits the results of the different scenarios modeled with RAMMS at the Weingarten Lake GLOF site. As the flow propagation from the origin to Täsch is about 5 km, the results are shown for two sites of interest, due to visualization purposes. The two sites Täschalp and Täsch are of special interest because of the houses and infrastructure and the implemented dams after the GLOF event 2001.

4.2.1 Inundation Extents and Flow Heights at Täschalp

The results of the RAMMS simulations for the four scenarios at Täschalp, from the Baseline Scenario to Scenario 4, are shown in Figure 16. The results illustrate both the flow heights and the inundation at their maximum extents occurring during the flow for the outflow Part A (Figure 7) from Weingarten Lake to Täschalp. The flow heights are depicted with a color gradient, where violet indicates minimal depths of 0.5 m to 2 m and orange/red represents the highest depths, reaching a maximum of 8 m.

In the Baseline Scenario and Scenarios 2 and 3, similar flow dynamics can be observed with slightly different values in flow heights and inundation extents. These scenarios show the inundation of the houses in Täschalp with depths reaching up to 3 m at some houses (see Sc3, Figure 16). All scenarios show the exceeding of the riverbed right above Täschalp with increased values in the riverbed. Continuing flowing downstream to Täsch occurs in all scenarios except Scenario 4. In addition, maximum flow heights occur at the same places in the riverbeds, where smaller cross-sections define the terrain. These smaller cross-sections are recognizable when a resource management pathway crosses the riverbed. The cross-section is smaller because of the natural terrain and an existing river correction enabling crossing the riverbed to manage resources. While Scenario 2 has the smallest values with a maximum flow height of 5.5 m above Täschalp, Scenario 3 shows a flow height of 8.5m and the Baseline Scenario 7 m.

Scenario 4 with the present DEM, including the mitigation measurements, behaves significantly differently regarding the Baseline and Scenarios 2 and 3. The GLOF outflow stops right before entering the village of Täsch, with maximum flow heights of 13.5 m occurring at the implement dam. The mass flow exceeds the riverbed southwards with values between 0.5 m to 1.5 m, as the slope flattens the flow height values decrease. The houses of Täschalp are not affected by the GLOF propagation, as the implementation of the dam stops the flow and directs it to the designated runout zone. Despite the low density (1’000 kg/m^3, see Table 2) of the mass flow, the propagation of the GLOF does not continue flowing downstream towards Täsch. However, the simulated outflow in Scenario 4 behaves the same as the other scenarios regarding its dynamic and the occurring flow height hotspots.

The deposition of the solid material is occurring in the riverbed and especially at the implemented dam. The values are between 0.5 m within the riverbed and a maximum of 13.5 m at the dam. Almost no deposition occurs at the beginning of the outflow, the values range under 0.5 m and increase when the cross-section gets smaller.

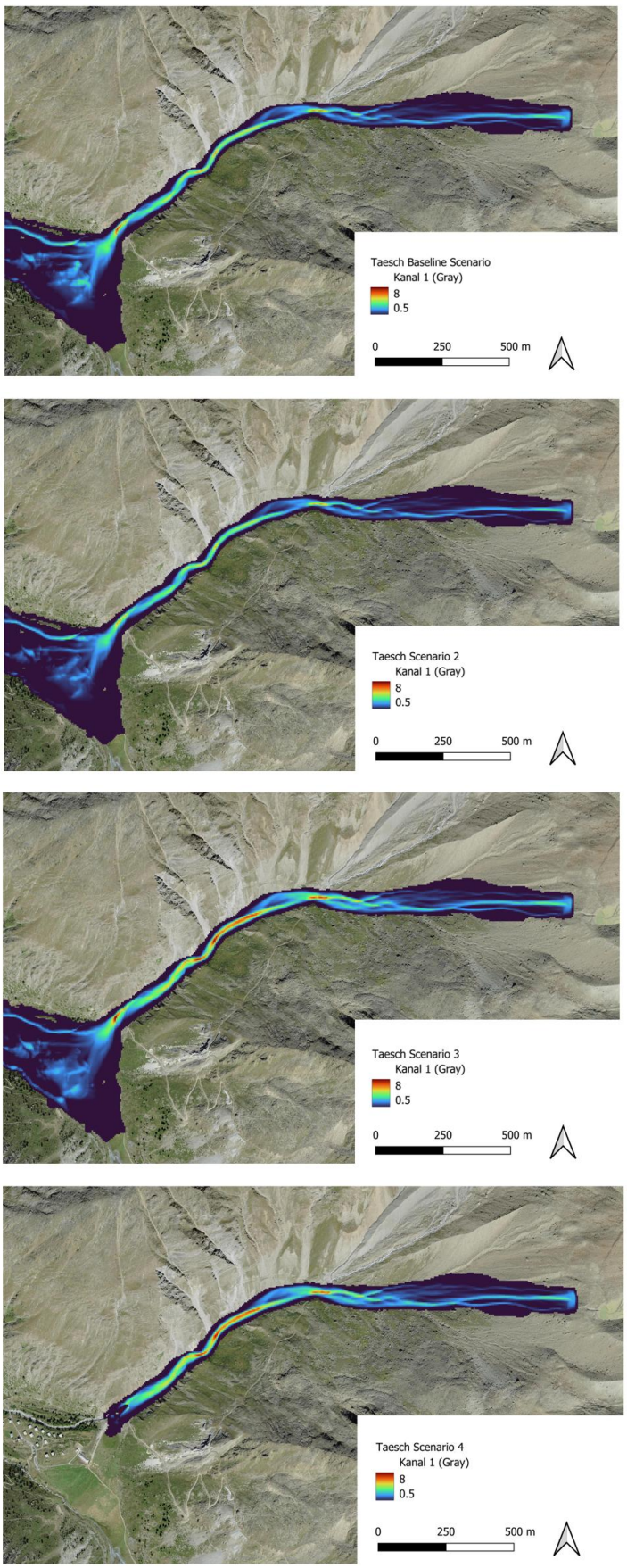

Figure 16: Inundation extent and flow height for Baseline Scenario, Scenario 2, Scenario 3 and Scenario 4 at Täschalp.

4.2.2 Inundation Extents and Flow Heights at Täsch

The results of the RAMMS simulations for the four scenarios at Täsch, from the Baseline Scenario to Scenario 3, are shown in Figure 17. The Scenario 4 is not mentioned in these results, as the GLOF already stops at Täschalp and does not affect the village of Täsch (see Figure 16). The simulated results illustrate both the flow heights and the inundation extents at their maximum extents occurring during the flow for the outflow Part B (Figure 7) from Täschalp to Täsch. The flow heights are depicted with a color gradient, where violet indicates minimal depths of 0.5 m to 2 m and orange/red represents the highest depths, reaching a maximum of 8 m.

All three scenarios show similar inundation extents with the smallest extent of Scenario 2, thus it is only a few meters overall, the extent north of the river is 30 m smaller compared to Scenario 3 and about 10 m smaller compared to the Baseline Scenario. In all scenarios, high flow height values are occurring the gorge at the fan apex before Täsch, where the present dam is situated. The highest values occur for Scenario 3 and the Baseline Scenario, both with values of approximately 5.2 m whereas Scenario 2 has about 4.5 m. The flow initially appears to follow the main, channeled river but spreads extensively into residential areas. In all scenarios the mass flow exceeds the river bed south- and northwards the riverbed, with the higher values occurring south of the riverbed. With flow height values of up to 1.5 m by the houses nearest to the river bed (turquoise color). Regarding the event of 2001 (Figure 11), the GLOF outflow exceeds the riverbed mainly southwards, with a small extent affecting houses north of the riverbed. However, the simulations show a similar behavior of the GLOF south of the riverbed regarding the real event. Thus the outflow towards the north of the village does not correspond to the event of 2001.

The comparison of the applied scenarios highlights the importance of defining the input hydrograph and the flow density. While the Baseline Scenario presents extensive inundation and high flow heights across the village of Täsch, Scenarios 2 and 3 show significant improvements in flow containment. Particularly Scenario 3.

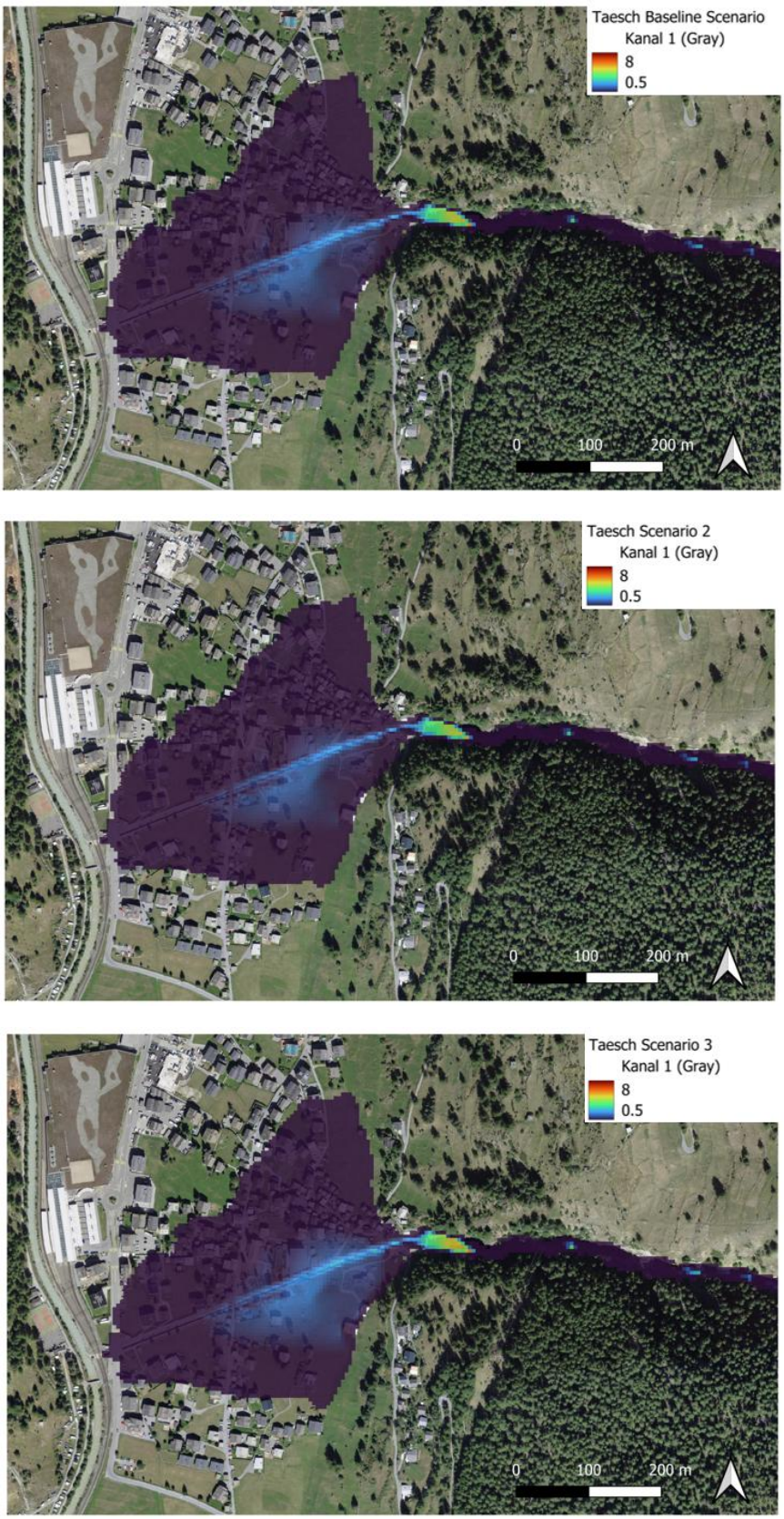

Figure 17: Inundation extent and flow height for Baseline Scenario, Scenario 2 and Scenario 3 at Täsch.

4.2.3 Uncertainty in Simulation Results

For the simulations of the GLOF propagation of the Weingarten Lake, several uncertainties have to be addressed. Despite the inexistence of discharge measurements, the uncertainties can be addressed mainly by the DEM used, as the volume of the lake was known before and after the outflow the input hydrograph is quite evident.

The DEM plays a crucial role in modeling GLOFs with RAMMS, as it is the base and calculation domain of the simulations. To compare the simulations with the real event of 2001, the DEM was modified in QGIS to replicate the terrain in 2001 because of the inexistence of a high-resolution DEM. The modification involves some uncertainties, despite being tested several times. This affects mainly the location of dams, which had to be excluded from the present DEM. Regarding the location above Täschalp (Figure 16), the simulations show high flow height values where the present dam is located, indicating that the dam is still present in the DEM or the cross-section is too narrow. However, the flow continues to propagate downstream to Täsch within the riverbed as visualized in the simulations with higher volumes. Regarding the second location, at the fan apex of the village of Täsch (Figure 17), the flow seems to be dammed as the flow height values are high. However, before the dam implementation, there was an existing natural gorge with a small terrain gradient, which can also be seen as a reason for the high occurring values. In addition, the used swissALTI3D DEM does not account for houses and infrastructure which allows the simulated flow to run through the houses. The presence of houses in the DEM would lead to different behavior of the flow, especially regarding the GLOF exceeding south of the riverbed in Täsch.

The friction parameters were defined with the best-fit approach (Cao and Carling, 2002). Multiple simulations were executed to generate the best fit for the coefficients, however, as there is not a lot of information about the GLOF of Weingarten Lake despite the input volumes, the definition of friction parameters has to be seen critically.

As no field observation is conducted in the scope of this thesis, the erosion polygon at the outflow part above Täschalp (Figure 7, Part A) is set to the default values of RAMMS (Bartelt et al., 2017). Therefore uncertainties regarding the decision of the erosion parameters can be asked. However, because of the unconsolidated material, the erosion polygon seems to be the right decision despite being set to default.

The simulation resolution of 5 m impacts the outflow behavior, as RAMMS calculates the flow for each cell. A better resolution of the simulations would allow a more precise result, despite that, the computational power limits the resolution conducted in this thesis.

5 Discussion

5.1 Model Comparison: South Lhonak Lake Simulations

The South Lhonak GLOF simulations serve as a tool for mitigating and comprehending the potential impacts of catastrophic events. This section discusses the retrospective modeling outcomes of this study with simulations from other established models namely HEC-RAS (Sattar, Goswami, *et al.*, 2021) and r.avaflow (Zhang, Wang and An, 2025). By analyzing these comparisons, the strengths and limitations of different modeling approaches emerge, emphasizing their ability to replicate real-world events like the GLOF in autumn 2023.

The employed RAMMS software enabled the simulation of outflow dynamics of the South Lhonak GLOF, focusing on its propagation and the downstream area, specifically at Chungthang. In contrast, the previous studies incorporated a more holistic or cascading approach to model GLOFs, including moraine breaches and triggering events (Sattar *et al.*, 2021; Zhang, Wang and An, 2025). These diverse methodologies and scopes allow one to examine distinct modeling tools' performance, assumptions and simulation outcomes. The comparison explores differences and similarities in simulated inundation extents and underscores significant variations in flow depths and methodological assumptions. While simulations conducted with HEC-RAS provide valuable insights into the water flow dynamics, they neglect the influence of sediments and debris, as modeled by RAMMS. Similarly, r.avaflow takes on a hybrid approach but exhibits an overestimation of flow heights and inundation extents, due to differences in terrain treatment and model assumptions.

The first section examines the comparison of the results with HEC-RAS simulations in Section 5.1.1, followed by the discussion of r.avaflow outcomes in Section 5.1.2. Through the comparisons, the practical application, limitations and relative accuracy of each model are explored, offering advancements and challenges and a comprehensive understanding of GLOF modeling.

5.1.1 Comparison with HEC-RAS Model

Sattar *et al.* (2021) simulated the potential GLOF as a cascading process, involving not only modeling the outflow of the glacial lake South Lhonak but also triggering mass movement, such as the moraine breach process or an avalanche bursting into the lake. Their approach combined simulations using RAMMS::Avalanche for the avalanche process and HEC-RAS (2D) for the subsequent breach and outflow routing. On the other hand, this study focuses solely on the retrospective simulation of the outflow using RAMMS.

In Sattar *et al.* (2021), the wave impulse and the subsequent overtopping of the dam caused by the triggering mass movement were used as input hydrographs for the HEC-RAS simulations to model the downstream flow dynamics. A roughness coefficient was applied within the simulations, ranging from 0.034 to 0.11, with higher values representing vegetated areas. However, their simulations consider water-only flow dynamics, as HEC-RAS does not account for suspended debris or deposition processes.

The DEM used applied is a 30 m SRTM resampled to 12.5 m. The radiometrically terrain-corrected elevation product was released by the Alaskan Satellite Facility in October 2014. The dammed lake surface is treated as a flat area solid area in the DEM.

The comparison between the software HEC-RAS (2D) and RAMMS is facilitated by the near-identical DEM with the same resolution used in both studies. However, a key distinction is the temporal approach. Sattar *et al.* (2021) conducted a predictive simulation, in contrast to the retrospective in this study, aligning the model output with the real event that happened in 2023. Furthermore, erosion processes are neglected in both studies due to the lack of available field observations and data. For visualization purposes, the symbology used by Sattar *et al.* (2021) was adopted in QGIS to match the presentation style for easier comparison between the results (see Figure 18). For the result comparison, Scenario 4 (Sc4) from this study was selected alongside the Scenarios (SC-1_p, SC-2_p, SC-3_p) from Sattar *et al.* (2021), as both scenarios closely match the observed inundation extent of the real event.

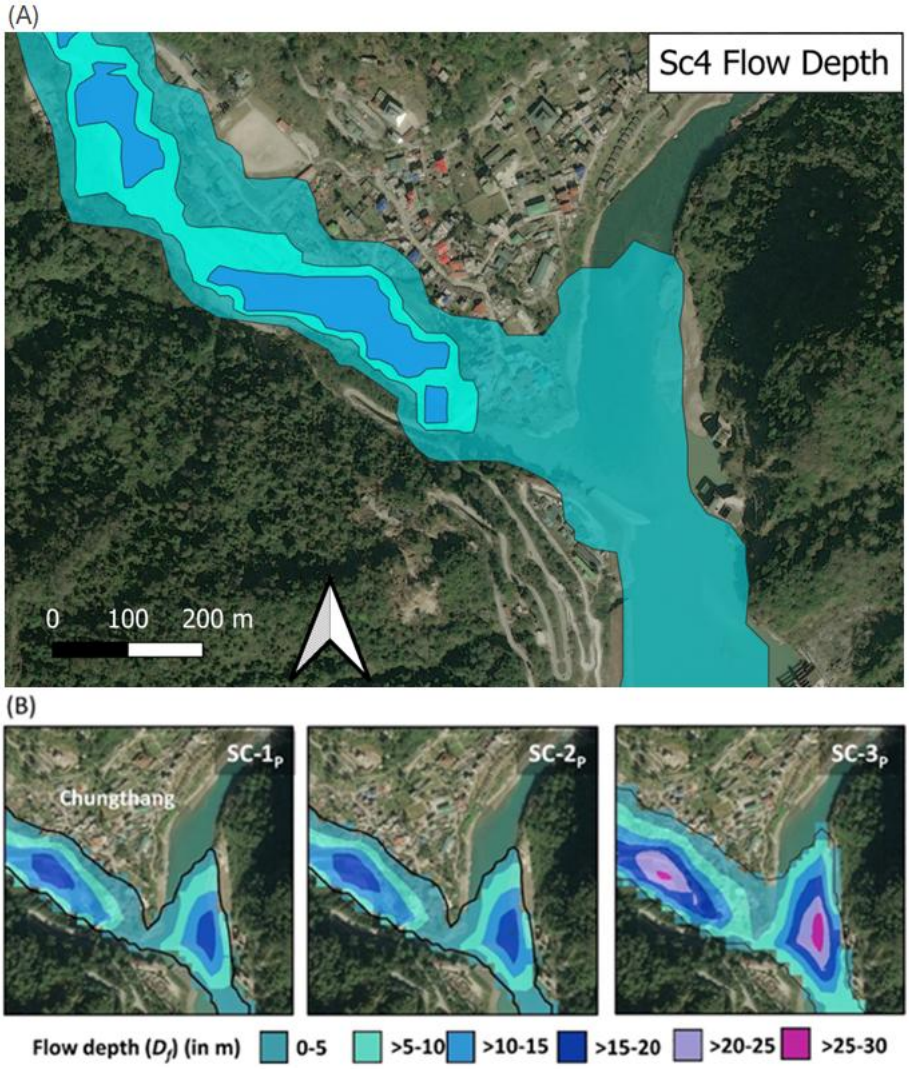

Figure 18: Simulated flow depth and inundation extent with RAMMS (A) and HEC-RAS (B) adopted from Sattar et al. *(2021) at Chungthang.*

Both simulations show a similar inundation extent in the Village of Chungthang, demonstrating general agreement in terms of spatial coverage. However, significant differences appear when analyzing the flow depths of the simulations. The RAMMS simulation results for Sc4 fall between the outputs of SC-2_p and SC-3_p from Sattar *et al.* (2021). Within the village, the extents simulated by Sc4 and SC-2_p are nearly identical, signifying a consistent spatial pattern. However, on the lake surface, Sc4 results align closely with SC-3_p, as both models treat the lake surface as a flat and constant elevation in their DEMs.

However, flow heights vary strongly regarding the two flow models. As in general the simulations done with HEC-RAS show higher flow depth values. Results done with RAMMS do not exceed 15 m of flow depths, whereas the results of HEC-RAS exceed 30 m of flow, despite having almost the same inundation extent. The concentration of higher flow depth in both simulations is notable west of Chungthang. Note that maximum values of over 20 m occur in SC-2_p and SC-3_p 30 m HEC-RAS simulations, compared to Sc4 where smaller heights are detected with a maximum of 15 m. The occurrence of the same spatial concentration maximum flow heights west of Chungthang is certainly due to the DEM used in both models. Two assumptions can be drawn about why the concentrated high values occur in both simulations. One is that both DEMs have sinks in the riverbed. As the DEM is the base of all the simulations applied, the simulated flow fills up the sinks in the riverbed, resulting in high flow heights. Two, the river enters at this location dammed lake which can lead to a backwash of flowing water, leading to elevated flow heights. Explaining the same spatial concentration and the high differences in maximum flow heights is challenging, as there is no further information in Sattar *et al.* (2021) about hydrodynamic modeling with HEC-RAS. An assumption can be that the used DEM has deeper sinks in the riverbed for the HEC-RAS results. The sinks in the DEM are smoothened in QGIS for the simulations of this study (Chapter 3.4.1), as the flow depth transition was too high regarding the first applied simulations.

A great difference between the results is recognizable on the lake's surface. The results of HEC-RAS simulations show a concentration of high-depth values, reaching up to 30 m in SC-3_p. In contrast, the applied RAMMS simulation shows small values on the lake with a maximum of 5 m. Therefore it can be assumed that the lake surface was threatened differently in the simulations of Sattar *et al.* (2021) compared to the simulations of this study.

5.1.2 Comparison with r.avaflow Model

Zhang, Wang and An (2025) simulated the South Lhonak GLOF event of 2023 as a cascading process including the failure of the lateral moraine, dam breach and outflow with r.avaflow. Their study approach was to simulate the whole GLOF process chain with one model. In the scope of this thesis, the focus lies on flood propagation and the modeling performance of r.avaflow compared to RAMMS.

Zhang, Wang and An (2025) used a cell size of 40 m due to the computing power limitations. Despite the GLOF being a mixture of mobile water and sediment, the solid and fluid phases were simulated separately. The entrainment for each basic cell was calculated by multiplying the total kinetic energy of the flow with the entrainment coefficient. The deposition was calculated using the simplified Pudasaini

and Krautblatter (2021) model. The simulation outcomes were evaluated based on the difference between the simulated and the observed inundation extent. Zhang, Wang and An (2025) utilized 11 crucial parameters and 6 of them were recognized as sensitive and crucial for the simulations of the South Lhonak GLOF event (see Appendix E)). Through an expert-based local optimization strategy, the best combination of these sensitive parameters was selected.

The comparison between r.avaflow and RAMMS is possible since both models are applied in retrospect and share simulation results at Chungthang. However, the key distinction can be made as Zhang, Wang and An (2025) modeled the whole cascading GLOF process as well as the entire flood routing from the South Lhonak Lake to Chungthang. Whereas the simulations applied in this study focus only on the village of Chungthang, due to computing power limitations.

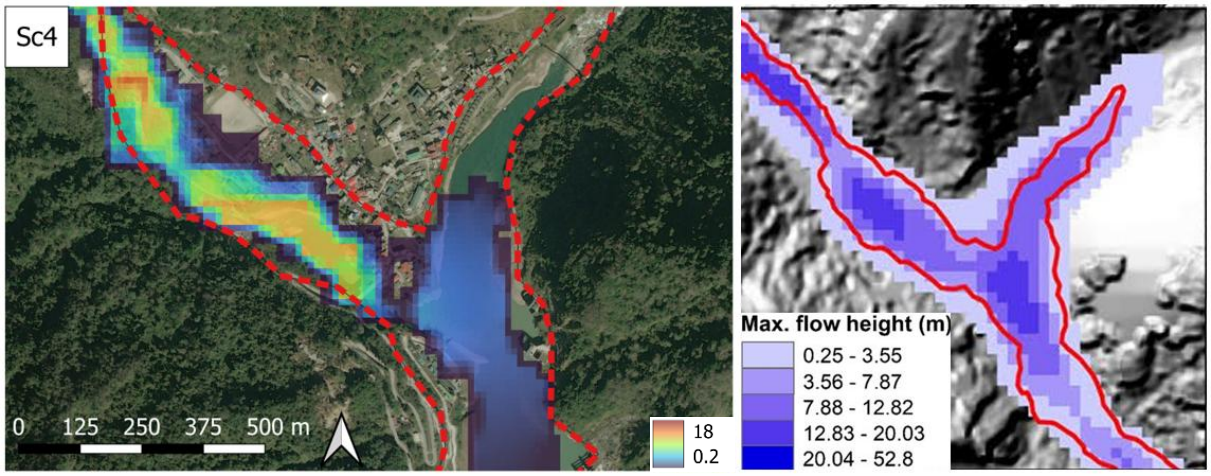

Figure 19: Comparison of simulated flow heights between RAMMS (left panel) and r.avaflow (right panel) at Chungthang. The red lines in both panels indicate the inundation extent of the observed event.

The two panels in Figure 19 present the inundation extent and maximum flow heights simulated using RAMMS (left panel) and r.avaflow (right panel). Both models capture the general flow pattern and underline the key areas affected in Chungthang. However, notable differences emerge regarding the extent and the flow height distribution. The simulation scenario Sc4 is chosen for the comparison, as it matches the closest real event.

The r.avaflow simulations show a significantly greater inundation extent, covering the entire village of Chungthang and extending up the surrounding steep valley flanks. The simulated extent goes beyond the real inundation extent of the 2023 GLOF event. The simulations suggest, that all infrastructure of Chungthang is affected by the GLOF, which overestimates the impact area. The overestimation of the inundation extent is also recognizable in areas downstream of the existing dam, where the simulated GLOF covers the entire valley, exceeding the observed flow pathway of October 2023. The simulations with r.avaflow produce significantly higher values regarding flow heights, with maximal peaks exceeding 50 m in certain areas. These extreme values are particularly concentrated in the riverbed and the

lake, producing two distinct hotspots of high flow values. The first hotspot occurs upstream, northwest of Chungthang within the riverbed, where the riverbed is more channelized. The second hotspot is observed south of Chungthang, where the dammed lake is located, with flow height values ranging between 20 and 50 m. Such high values are notable, as they suggest that the lake is treated without a waterbody. This modeling approach appears to inflate the simulated flow heights within the lake and also for the downstream areas.

In comparison, the conducted RAMMS simulation recorded a more constrained and smaller distribution of flow heights. Maximum values are smaller with 15 m and are strongly concentrated in the riverbed. Smaller values occur in the immediate surroundings. However, both simulations show a gradual decrease in flow heights away from the riverbed, which aligns with the observed real event. The treatment of the dammed lake is a critical distinction between the simulated GLOFs. R.avaflow apparent treatment of the lake as part of the dynamic flow introduces the potential of a different treatment of the dammed lake. One to be noted is that Zhang, Wang and An (2025) do not mention how the dammed lake is treated in their simulations. However, it seems that the lake is not treated as a flat area, as it is done in the simulations conducted with RAMMS. This modeling assumption likely provides not only inflated flow heights but also the overestimation of inundation in the downstream area of the river. In contrast, assumptions of a stabilized lake in the simulations conducted with RAMMS result in moderate flow heights with smaller inundation extents.

This discrepancy might be due to differences in how the two models handle terrain resolution, input parameters, and assumptions about dam interaction with floodwaters. For instance, r.avaflow may incorporate less detailed information on the dam's structural integrity and overtopping dynamics, leading to an unrealistic expansion of the inundation extent. Additionally, the broader extent observed in the r.avaflow results could stem from its hybrid modeling approach that combines fluid and solid phase dynamics, possibly amplifying the spatial spread of simulated debris-laden flows.

These differences underscore the importance of model selection and calibration for simulating glacial lake outburst flood (GLOF) events. While r.avaflow's expansive predictions highlight areas of potential maximum impact, they may overestimate real-world hazards, potentially leading to excessive conservatism in risk management strategies. On the other hand, RAMMS provides a more conservative and event-specific estimate that aligns closely with the observed flood dynamics, making it a valuable tool for localized hazard assessments. To improve accuracy, future applications of r.avaflow could benefit from more precise input data on terrain, dam structure, and flow dynamics to refine its predictive capabilities.

Ultimately, the contrasting results from the two models highlight the need for a nuanced approach to GLOF hazard modeling, combining the strengths of different simulation tools while carefully accounting for their assumptions and limitations.

5.2 Interpretation of Results: Weingarten Lake

The RAMMS simulation results demonstrate the effectiveness of dam mitigation measures. Focusing on GLOF behavior above Täschalp (Figure 7, Part A), the installed dam is leading the GLOF to stop right above Täschalp, with small margins exceeding the riverbed in the intended runout zone (Figure 16, Scenario 4). Moreover, the GLOF does not continue downstream to Täsch which can be seen critically, as a real event water levels in the riverbed would surely rise downstream to Täsch. Despite the density being set at 1000 kg/m^3 for a more fluid GLOF, the flow stops at the implemented dam. A separation of the granular and fluid phases in the simulations may overcome this problem. The new version of RAMMS under development can simulate this separation, enabling a more realistic simulation of the outflow of Weingarten Lake (Chapter 3.1.1). The second dam, present at the fan apex above Täsch is therefore not even affected by GLOF outflow simulated with the input hydrograph set at 8'000 m^3 representing the maximum outflow volume of the event of 2001. Therefore, it can be assumed that also higher input values would not affect the village of Täsch regarding the simulations conducted, as the first dam at Täschalp already stopped the GLOF. Thus this assumption only regards GLOF and does not take into account the coupling of multiple hazards such as extreme precipitation events or snow/rock avalanches blocking the river routing.

The results of the applied RAMMS simulations provide valuable insights into the hydrodynamic behavior and potential impacts of GLOFs at Täschalp and Täsch under various scenarios. Therefore, the influence and sensitivity of the density and input values can be examined. Focusing on the Village of Täsch (see Figure 17), the influence of flow density is evident when comparing the Baseline Scenario with Scenario 3, which assumes a lower density of 1000 kg/m^3. The reduced density of the flow results in slightly dispersed flow behavior, especially near the gorge at the fan apex and the inundation area at the village of Täsch, although maximum flow heights remain comparable across all scenarios. This suggests that density primarily affects the distribution of the inundated area rather than the maximum flow depths. The influence of increased input values is apparent regarding the Baseline Scenario and Scenario 2, both characterized by the same density of 2000 kg/m^3, depicting similar flow dynamics, with extensive extents and flow depths. However, Scenario 2 with a reduced input hydrograph volume of 6000 m^3 and a lower peak discharge of 140 m^3/s, shows the smallest inundation extent and flow heights across all scenarios. Particularly this is evident in the northwest spread of Täsch, which is approximately 30 m smaller than Scenario 3 and 10 m smaller than the baseline scenario. These findings underscore the sensitivity of inundation extents and flow heights to variations in hydrograph volume.

Comparing the simulations to the event of 2001 event, the simulations align partially with the observed flow behavior. The increased flow heights within the riverbed and the southward spread of the outflow are consistent across all scenarios at the village of Täsch, as there is no information available for the location of Täschalp. The consistent inundation extent validates the model's ability to replicate the primary flow paths of the 2001 event. However, the northward inundation extension simulated does not fully correspond to the 2001 event. Despite the northward inundation of the real event, the simulations depict a larger area of inundation affecting a greater number of houses. This discrepancy may result from differences in the terrain model or parameters such as sediment transport, which were not fully

accounted for in the simulations because of small data availability. Focusing on the terrain model, blockages within the riverbed are neglected in the simulations.

In summary, the simulation results demonstrate the sensitivity of GLOF dynamics to the presence of mitigation strategies, input volume and flow density. They also highlight the importance of continued model refinement and calibration, particularly to account for topographic changes, to enhance predictive accuracy for other GLOF sites with the same rheology.

5.3 General Limitation in GLOF Modeling

5.3.1 Challenges in Modeling Transitional Flow Behavior

The RAMMS model in its current version is not able to simulate the flow transition of GLOFs autonomously, as it considers only one phase in its calculation baseline. This limitation requires RAMMS users to manually change friction parameters to simulate transitions to other mass movements. This approach was applied in the work of Frey *et al.* (2018), where friction parameters were manually adjusted at a defined river bed section to represent the transformation into a hyperconcentrated flow. According to Mergili *et al.* (2011), this is a common challenge in modeling GLOFs, as models are often limited regarding the transitional behavior of pure water flows and debris flows.

Although GLOFs are initially released with high liquid content, the entrainment of solids during breaching and flow propagation makes models that can capture multi-phase flows more appropriate (Worni *et al.*, 2014). Currently, the SLF is developing a new version of RAMMS (see Chapter 3.1.1), which incorporates an improved calculation approach based on the separation of the granular and liquid phases (Meyrat *et al.*, 2022; Meyrat *et al.*, 2023). The upcoming version is expected to better capture transitional flow behaviors, which is often addressed as a challenge in GLOF modeling. In particular, the new model is anticipated to effectively demonstrate dewatering processes. Regarding the Täsch study site Scenario 4 in Figure 16, such improvements would result in a more realistic behavior of the outflow, allowing the liquid phase to continue downstream beyond the implemented dam, rather than stopping at the dam as in the present model setup.

However, despite the potential improvements of two-phase models, their application is constrained by the limited availability of detailed field data of GLOF sites. This is pointed out by Mitchell *et al.* (2022), while two-phase models can produce more precise results compared to single-phase models, they require a larger number of input parameters, demanding extensive field data. Besides data availability, the application of advanced models requires increased user expertise and comprehensive knowledge of material characteristics, which can only be obtained through challenging and resource-intensive field observations. This study underscores that such data limitations are common in GLOF modeling, making single-phase models a more practical choice in engineering practice. Consequently, the current available RAMMS software applied to both study sites Täsch and South Lhonak is considered appropriate, given the small data available and the accurate model output in both cases.

Nevertheless, the omission of dynamic aspects of GLOF behavior, such as turbulent, supercritical or transcritical flow and transient flow rheologies continues to limit the accuracy and reliability of these single-phase modeling approaches. Single-phase models assume that the solid and liquid particles are identical in velocity and that the whole mass flow behaves as a bulk flow. In addition, the density of the mass flow stays constant during the simulation, which does not reflect the real-world GLOF behavior. In reality, the front and tail of the outflow exhibit different solid-liquid ratios, as highlighted by Meyrat *et al.* (2023). These limitations must be considered when interpreting simulation results of single-phase models, as they potentially impact the accuracy of hazard assessments.

5.3.2 Retrospective Modeling of GLOFs

In this thesis, the retrospective modeling approach was applied to reconstruct past GLOFs, providing insights into inundation extent, flow heights and behavior of such extreme events. The retrospective modeling approach involves the simulation of past events based on observed data which enables an improved understanding of flood dynamics and facilitates the calibration of predictions.

The strength of retrospective modeling lies in the reconstruction of past GLOF events with higher accuracy, relying on field observations and measurements. Through this approach, parameters such as the natural terrain, friction parameters, input volumes and sediment transport processes can be fine-tuned to achieve the "best-fit" model calibration. As underscored in previous studies (e.g. Cao and Carling, 2002; Kidson, Richards and Carling, 2006), systematic calibration of the natural terrain and friction parameters is crucial to enhance model reliability and help decide parameter choices for potential future events. Nevertheless, model calibration is commonly conducted and tested in laboratory settings (e.g. Meyrat *et al.*, 2023), but its application in natural environments as done in this thesis remains limited. As proposed by Carrivick *et al.* (2010), the models should be fully calibrated using high-quality field data, which is often not available. This is underscored by the two GLOF sites exploited in this thesis, where information availability was limited to small literature and reports. Moreover, several challenges occur in retrospective modeling. Discrepancies and variabilities in model outputs can arise due to factors such as spatial resolution (Huggel *et al.*, 2008) and uncertainties in input data (Pappenberger *et al.*, 2006). The selection of suitable friction parameters, terrain and defining acceptable input volumes require more careful consideration, as the modeler must justify the values. A more careful selection of the input data would have increased the simulation results in this thesis. Therefore, future GLOF examinations with small data available should conduct field observation or rely more on GLOF sites with similar boundary conditions in their model input.

In the context of GLOF modeling, retrospective simulations applied in this thesis provided critical insights into flow behavior and inundation extent. The case studies exploited demonstrated the effectiveness of using satellite images and topographic reconstruction to validate the model results. Nevertheless, limitations such as the lack of discharge values and topographic data challenges in achieving high-accuracy reconstructions, which is also stated by Westoby *et al.* (2014). Moreover, Westoby *et al.* (2014) critique the application of these calibration techniques for retrospective and predictive GLOF

modeling, debating that each GLOF site or event is unique and the likelihood of another outburst occurring under similar conditions is low.

An emerging solution to address the retrospective modeling approach is the implementation of probabilistic approaches, which include stochastic sampling techniques and quantifying the uncertainty in simulation results (Westoby *et al.*, 2014). Such approaches have been applied in hydrological modeling and offer optimistic potential in GLOF modeling reconstructions by producing probability-weighted flood inundation maps (e.g. Blazkova and Beven, 2004; Franz and Hogue, 2011). These methods allow the incorporation of parameter ranges that yield acceptable model performance and make evaluating result equivalence in modeling results easier.

Overall, the retrospective approach conducted in this thesis has proven to be a valuable tool for understanding GLOF events and improving model results. To tackle the disadvantages, future research should focus on expanding the datasets of well-documented GLOF events to improve predictive modeling, enhancing the robustness of calibration techniques and exploring the probabilistic modeling approach. Integrating field observations in modeling techniques will further contribute to reliable simulation results and improve hazard assessments and mitigation strategies for potential GLOF regions.

5.3.3 Limitations of Digital Elevation Models (DEMs)

It is widely recognized that terrain features and channel topography significantly influence the flow dynamics in GLOF simulations (e.g. Huggel *et al.*, 2008; Westoby *et al.*, 2014), the findings of this study reinforce this understanding. The simulation results underscore the crucial role of the DEM and its sensitivity in comparison to friction parameters and input volumes, which play a subsequent role in influencing results. An accurate topographic representation of GLOF pathways is crucial for generating robust simulation results, such as inundation extents and flow heights across different input values.

However, the availability of high-quality terrain data remains a major challenge, especially in remote areas such as the South Lhonak region. The acquisition of fine-resolution data (e.g. LiDAR), which would result in higher accuracy of model outputs is often impractical due to financial and logistical limitations. Fine-resolution data would significantly increase the accuracy of the model output compared to the coarse SRTM data used in this study for South Lhonak. Despite the relatively coarse resolution of the DEM, it was sufficient for examining the flow behavior, alining with findings by Sanders (2007) and Huggel *et al.* (2008), who state that GLOF simulations conducted with coarse-resolution can yield reliable results for ad-hoc hazard assessments. Similarly, Zhang, Wang and An (2025) applied a 40 m DEM to model the South Lhonake GLOF using r.avaflow with success. However, when compared to higher-resolution DEM applied in this study and Sattar *et al.* (2021), the accuracy of simulation results is noticeably lower (Chapter 5.1.1).

While the applied simulations in South Lhonak were constrained to the village of Chungthang due to the high computational demand of large-scale GLOF simulations, the Weingarten Lake site allowed the full outflow routing. The smaller outflow valley of Weingarten Lake demanded less computational

power, making it possible to simulate the entire outflow downstream to Täsch. This discrepancy underscores the importance of an appropriate DEM selection that balances computational power with result accuracy.

To represent the actual terrain, the DEMs used in this study underwent reprocessing and modifications in QGIS (Chapters 3.3.1 and 3.4.1). However, it is important to acknowledge that processing techniques can produce misassumptions, which can only be corrected and verified through a conducted field observation. For instance, the applied interpolation methods "*r.fillnulls*" or "*r.fill.dir*", resampling techniques with the ratercalculator and error propagation during DEM processing can result in the smoothing of topographic features. These processing steps may unintentionally impact the precision of the outflow path. Especially regards the simulated values of maximum momentum, flow velocity and maximum pressure in Figure 14 underscore this challenge, as the results are not significant. On-site validation or higher-resolution DEMs could enhance the model reliability by representing finer topographic details and reducing uncertainties associated with DEM processing, which aligns with the findings of (Saritha *et al.*, 2021).

Despite the DEM challenges, the modified DEM applied in this study is considered sufficiently precise for the executed RAMMS simulations. However, future research could benefit from incorporating advanced data sources, such as LiDAR or UAV-based photogrammetry, to achieve higher accuracy and improved GLOF predictions. Nevertheless, the trade-offs between data availability, computational costs and model precision must always be carefully considered in practical engineering applications.

5.3.4 Modeling GLOFs as Cascading Processes

Natural disasters often result from cascading processes instead of isolated phenomena, and so do GLOFs (Chapter 2.1). Therefore, an integrated system approach is crucial for comprehensively understanding GLOFs and for future predictive models (Emmer *et al.*, 2022). All relevant hazards within the GLOF environment must be considered, including potential interactions and cascading effects of GLOFs.

The software RAMMS is not capable of simulating the cascading process chain as a unified model. Exclusively sequential modeling is possible, as RAMMS also offers software for rockfalls (RAMMS::Rockfall) and avalanches (RAMMS::Avalanche), enabling the simulations of possible triggering events. However, the breaching process is excluded from the capabilities and has to be modeled with a different model such as BREACH (Fread, 1988). Consequently, the sequential modeling approach allows the usage of the optimal model at each cascade, with the disadvantage of the potential mismatch of the outputs and inputs of the following models applied. Although the RAMMS is only able to simulate the sequences of the GLOF process chain, such as the outflow propagation examined in this study, the results are highly accurate regarding the back-calculation of the South Lhonak Lake and Weingarten Lake. In contrast, unified modeling is possible with the software r.avaflow simulating the process chains within a single model run. This approach, highlighted by the work of Zhang, Wang and An (2025), provides a more realistic transition between the cascading processes. Moreover, only one software has to be applied, making this approach highly user-friendly and less cost and time-intensive than sequential

modeling. However, the accuracy of the inundation extent and flow heights is not accurate compared to the RAMMS simulations and the real-world event as examined in this study.

5.4 Impact of Friction Parameters on Simulation Accuracy

Several previous studies have performed back calculations using RAMMS at various GLOF sites worldwide. The friction parameters μ and ξ used in these simulations are summarized in Figure 20. The summarized parameters not only enable a comparison of the parameters applied in this study but also offer an overview for future modeling assumptions.

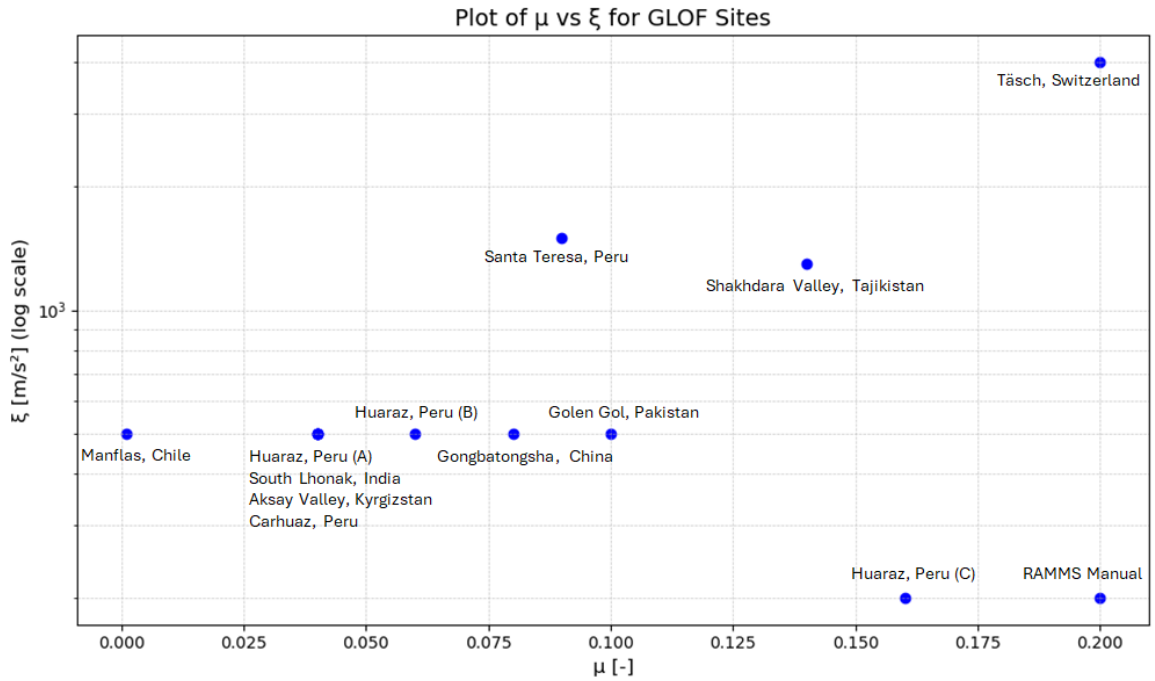

Figure 20: Friction parameters μ (x-axis) and ξ (logarithmic y-axis) from back-calculations of different GLOF events modeled with RAMMS. Data are from RAMMS manual (Bartelt et al.*, 2017); Täsch, Switzerland (conducted in this thesis); Huaraz, Peru (A) (Frey* et al.*, 2018); Huaraz, Peru (B) (Motschmann* et al.*, 2020); Huaraz, Peru (C) (Meyrat* et al.*, 2024); Carhuaz, Peru (Schneider* et al.*, 2014); South Lhonak, India (conducted in this thesis); Aksay Valley, Kyrgyzstan (Brüniger, 2023); Shakhdara Valley, Tajikistan (Mergili* et al.*, 2011); Golen Gol, Pakistan (Friz, 2021); Santa Teresa, Peru (Frey* et al.*, 2016); Manflas, Chile (Iribarren Anacona* et al.*, 2018); Gongbatongsha, China (Sattar, Haritashya,* et al.*, 2021). One has to note that the RAMMS manual default values are evaluated for debris flows and not GLOFs as the others do.*

The chosen values for South Lhonak simulations (μ = 0.04 and ξ = 500 m/s^2) are consistent with the parameters in three other GLOF modeling studies (Frey *et al.*, 2018; Schneider *et al.*, 2014; Brüniger, 2023). The parameters applied in the Täsch simulations exhibit higher ξ values than other GLOF case studies. In contrast, the μ value aligns with the default value recommended for debris flows (Bartelt *et al.*, 2017). The high ξ was chosen because, in initial simulations, the flow stopped prematurely and accelerated small values in flow height and velocities. Such high ξ are usually applied for very smooth surfaces, for example for modeling snow avalanches (e.g. Martini, Baggio and D'Agostino, 2023).

However, Frey *et al.* (2016) examined the impact of RAMMS' turbulent friction parameter ξ on multiple flow characteristics and stated that the inundation extent, height and velocity of the mass flow hardly vary with change in ξ. Therefore, reducing the friction parameter μ could have produced better simulation results, as the runout distance is more robustly governed by μ according to Iribarren Anacona *et al.* (2018).

Despite the limited number of scholars applying RAMMS for GLOF routing simulations, a clear pattern emerges regarding the most suitable friction parameters μ and ξ. Four out of 13 studies utilized the same friction parameters for μ = 0.04 and ξ = 500 m/s^2, while one study (Motschmann *et al.*, 2020) applied a slightly increased μ =0.06 while maintaining ξ = 500 m/s^2 for their best-fit approach. Although the number of modeling studies remains small, the friction parameters for μ and ξ with 0.04 respectively 500 m/s^2 seem appropriate for GLOF simulations. Especially the ξ values show great consistency in the back-calculation of GLOf events. 8 out of 13 studies applied the value of 500 m/s^2 for their ξ values. Therefore it is recommended, at least for initial simulations, to start simulations with the ξ of 500 m/s^2 and then adapt the μ values.

To support this observation, further explanation of various GLOF sites with these friction parameter settings is necessary. However, the RAMMS model parameters ultimately depend on the GLOF characteristics such as topography (DEM), rheological properties (e.g. erosion) and hydro-meteorological conditions (input volumes). Consequently, model calibration remains the optimal approach for determining the friction parameters that significantly influence simulation results. This is underscored in the work of Mikoš and Bezak (2021), who examined the friction parameters of debris flow sites across the globe.

5.5 Recommendations for Future Research

Future research and examinations of GLOF events should examine the performance of the upcoming RAMMS version which holds in the two-phase approach of Meyrat *et al.* (2023). The focus should lie on the performance of the model with a special interest in the dewatering processes and therefore the transitional behavior. Moreover, the applicability of the new version from a practical engineer's view should be examined, as the increased number of parameters not only challenges the need for further data on specific sites but also the computational power. This would benefit further examination of GLOF sites especially in rural areas and high numbers of dangerous GLOFs as such occur in HKKK (Taylor *et al.*, 2023).

A comprehensive literature review of parameters of various GLOF sites modeled with RAMMS should be applied to improve the decision-making process for using the best-fit parameters, e.g. μ and ξ. This would improve the results in retrospective and predictive modeling, as users have a reference for similar geographical and rheological GLOF sites. Moreover, it would accelerate the modeling process for finding the best-fit friction parameters, which can be a huge benefit for ad-hoc risk assessments. It is recommended to generate a table that includes information about the source (author, year), location

and year of examined GLOF event, magnitude, simulation resolution, friction parameters μ and ξ, and a short description of the study as already done in the work of Mikoš and Bezak (2021) for general modeling with RAMMS. Users could compare the GLOF site under investigation with the table and apply similar values or compare the parameters for validation purposes.

To achieve the above recommendation, a comprehensive description of the modeling process and used parameters is necessary. Future research should include a more detailed description of the simulations conducted, generating a better understanding of input volumes and friction parameters. A more detailed description would have allowed better comparison of the models in this study, as Sattar *et al.* (2021) and Zhang, Wang and An (2025) did not fully include how they modeled the outflow. An extensive description of the modeling process would allow future works to adapt and progress the parameters at study sites with the same geographical and rheological setting. Especially regarding predictive modeling, this would be a significant advantage, when no event exists for back-calculations and therefore the refinement and valuation of the parameters.

Future research should prioritize comprehensive risk assessments and mitigation strategies for South Lhonak Lake, as it remains a persistent natural hazard. Sattar *et al.* (2025) highlight the lake's ongoing susceptibility to GLOFs, including the potential outflow due to further lateral moraine failures. In addition, sediment deposits in the Teesta Valley remain exposed and could contribute to further sediment entrainment during a potential GLOF. The high sediment availability increases the likelihood of debris flow formation, emphasizing the urgent need for effective mitigation strategies. Future studies should examine a multifaced approach to risk reduction. This includes implementing structural protection measures, enhancing early warning systems, formulating evacuation plans and developing regulatory frameworks. The regulatory considerations should include hydropower development policies and socio-economic planning for villages in the Teesta region to minimize vulnerability and exposure to GLOFs. Furthermore, climate change impacts, particularly increasing extreme precipitation events and the retreat of the South Lhonak Glacier, must be systematically integrated into risk assessments. Lessons from the case study of Weingarten Lake underscore the potential effectiveness of mitigation measures, such as dam construction, in reducing GLOF risks. However, future studies should also exploit the interplay of multiple hazards, including snow avalanches and landslides that could block outflows, potentially exacerbating flood risks. Special attention should be given to the role of extreme precipitation events in altering outburst dynamics due to changing climate. Ultimately, future risk assessments should extend beyond GLOF modeling to incorporate the broader implications of climate change and socio-dynamic factors. A more holistic perspective will ensure that mitigation strategies are sustainable, robust and adaptive to elevating societal and environmental conditions.

6 Conclusion

6.1 Summary of Findings

The debris flow software RAMMS enables the simulation of GLOFs across different geographical and rheological settings with accuracy. The simulations show a correlation to the real event that happened at both study sites in Switzerland and Sikkim Himalaya, despite not replicating the exact inundation extent of the compared real event. Thus the performance of the software is given and can be recommended for further GLOF investigations across the world with small data available regarding the terrain and rheological setting. Additionally, the RAMMS software is highly user-friendly and applicable for low computational power environments. Its performance is particularly effective for regional-scale GLOF studies, allowing for the examination of the entire valley outflows and mitigation measures, as the study of Weingarten Lake has demonstrated this capability. However, compared to other models such as HEC-RAS or r.avaflow, the performance of RAMMS is limited to modeling only one process at once for the cascading process chains of GLOFs and is not able to simulate the transformation processes. On the other hand, HEC-RAS can simulate the breaching processes and outflow routing in one simulation step, excluding the process of the triggering event. R.avaflow in comparison can perform the whole process chain of a cascading GLOF, including the triggering event as well as the breaching and outflow routing. Thus the results are not that accurate, it still capture the flow behavior of the flood propagation of GLOFs.

The superordinate goal of applying RAMMS as a predictive model at potential GLOF sites remains difficult. Especially when there is no information about a past event, it remains challenging to predict GLOF routing without any field survey, direct discharge measurements or paleo-stage indicators from a past event. The difficulty of prediction is reinforced under a changing environment, where climate and rheological parameters are changing rapidly, despite having a past scenario as an indicator. The debris flow model therefore can only be used to reproduce events with tuning of flow parameters. The free parameters have to be adjusted by hand to replicate the different flows observed in real events. This “best fit” approach in retrospective modeling should be overcome in the future with more detailed back-simulations of other GLOF scenarios with the same rheological conditions. This would allow the usage of parameters for predicting GLOFs at different sites across the globe. Therefore it is recommended to apply RAMMS on various sites to examine more parameters for each rheological and geographical setting.

The DEM remains the most important input parameter when GLOF simulations are conducted. As models calculate the parameters and equations for each cell, it is crucial to apply a solid DEM. This can be both lowering and increasing the resolution, depending on the interest of usage. For instance, for simulations of a long-distance outflow GLOF routing a low-resolution DEM is recommended, whereas at a specific location of interest, a small resolution is required. This is also connected to the availability of computational power, where low-resolution DEMs need less and high resolution needs more power. The DEM is very sensitive, sinks in riverbed or nodata areas influence the simulation significantly and

can lead to false simulation results not replicating the present terrain. It is recommended that the DEM is not only evaluated with the processing tool, such as QGIS used in this thesis but also the applied modeling software. Moreover, a fragile DEM can mislead friction parameters and input hydrographs applied in the simulations.

Modeling transitional flow behaviors remains an objective in GLOF simulations. Larg-scale, destructive GLOFs can undergo multiple flow behavior changes due to variations in topography and sediment entrainment. However, the current single-phase RAMMS model is unable to replicate these transitions autonomously. In retrospective modeling, flow transitions can only be approximated by manually adjusting friction parameters in predefined sections. The upcoming two-phase RAMMS software is expected to address this limitation, offering improved capabilities for both retrospective and predictive modeling. With these advancements, transitional flow behaviors should be more accurately replicated, enhancing the reliability of future GLOF simulations.

6.2 Contributions to the Field

This thesis provides to the field of GLOF modeling by applying the RAMMS software. The findings presented offer insights for future applications, particularly in the areas of DEM processing and the fragile balance between resolution selection and computational efficiency. These contributions are essential for advancing the efficiency and advancement of GLOF simulations, providing a robust foundation for practical applications and further research.

One key aspect addressed in this thesis is the evaluation of different GLOF modeling approaches, focusing on how RAMMS performs relative to other available models. By conducting a comparison of various modeling frameworks, this research generates a brief understanding of the strengths and limitations of each approach, with a special focus on the RAMMS software. This comparative analysis assists modelers in selecting the most suitable model based on their specific objectives, such as ad-hoc simulations for hazard assessments, simulations of the whole process chain of GLOFs or mitigation measurements. The insights of this study contribute to a more informed decision-making process, enabling the chosen model to align with the available resources and desired outcomes. Furthermore, this thesis can offer guidance on the selection of key model parameters, such as friction coefficients or input volumes. These parameters play a crucial role in determining the accuracy of retrospective and predictive modeling outcomes. Through validation using real-world study cases, this research identifies the best-fit parameter ranges that enhance model reliability and performance. The findings, including additional literature, serve as a valuable reference for GLOF examinations seeking to tune their model parameters for improved predictive capabilities. A major contribution of this thesis is the demonstration of effectiveness regards mitigation strategies, highlighted in the context of Weingarten Lake. This case provides concrete evidence of how well-designed mitigation structures can significantly reduce the impact of potential GLOF events. The findings underscore the importance of integrating modeling with practical mitigation efforts to reduce vulnerabilities associated with GLOFs.

References

Bartelt, P. *et al.* (2017) 'RAMMS:: DEBRIS FLOW User Manual v1. 7.0', *WSL Institute for Snow and Avalanche Research SLF, Davos, Switzerland* [Preprint].

Batchelor, G.K. (2000) *An introduction to fluid dynamics*. Cambridge university press. Available at: https://books.google.com/books?hl=de&lr=&id=aXQgAwAAQBAJ&oi=fnd&pg=PR13&dq=Batchelor,+G.+K.+(1967).+An+Introduction+to+Fluid+Dynamics.+Cambridge:+Cambridge+University++Press.&ots=0Vb19CxR3l&sig=hNnYi2DGXtkwWlyhGWCNNLFAL3Q (Accessed: 23 January 2025).

Benn, D.I. *et al.* (2012) 'Response of debris-covered glaciers in the Mount Everest region to recent warming, and implications for outburst flood hazards', *Earth-Science Reviews*, 114(1–2), pp. 156–174.

Berger, C., McArdell, B.W. and Schlunegger, F. (2011) 'Sediment transfer patterns at the Illgraben catchment, Switzerland: Implications for the time scales of debris flow activities', *Geomorphology*, 125(3), pp. 421–432.

Blazkova, S. and Beven, K. (2004) 'Flood frequency estimation by continuous simulation of subcatchment rainfalls and discharges with the aim of improving dam safety assessment in a large basin in the Czech Republic', *Journal of Hydrology*, 292(1), pp. 153–172. Available at: https://doi.org/10.1016/j.jhydrol.2003.12.025.

Bolch, T. *et al.* (2012) 'The State and Fate of Himalayan Glaciers', *Science*, 336(6079), pp. 310–314. Available at: https://doi.org/10.1126/science.1215828.

Breien, H. *et al.* (2008) 'Erosion and morphology of a debris flow caused by a glacial lake outburst flood, Western Norway', *Landslides*, 5(3), pp. 271–280. Available at: https://doi.org/10.1007/s10346-008-0118-3.

Brüniger, C. (2023) *Uncertainties in modelling glacier lake outburst floods: Sensitivity analyses of mass movements in northern Kyrgyzstan*. Master's Thesis. University of Zurich. Available at: https://www.zora.uzh.ch/id/eprint/254348/ (Accessed: 29 January 2025).

Brunner, G.W. (2002) 'Hec-ras (river analysis system)', in *North American water and environment congress & destructive water*. ASCE, pp. 3782–3787.

Cao, Z. and Carling, P.A. (2002) 'Mathematical modelling of alluvial rivers: reality and myth. Part 1: General review', *Proceedings of the Institution of Civil Engineers - Water and Maritime Engineering*, 154(3), pp. 207–219. Available at: https://doi.org/10.1680/wame.2002.154.3.207.

Carling, P. *et al.* (2010) 'Unsteady 1D and 2D hydraulic models with ice dam break for Quaternary megaflood, Altai Mountains, southern Siberia', *Global and Planetary Change*, 70(1), pp. 24–34. Available at: https://doi.org/10.1016/j.gloplacha.2009.11.005.

Carrivick, J.L. *et al.* (2010) 'Coupled fluid dynamics-sediment transport modelling of a Crater Lake break-out lahar: Mt. Ruapehu, New Zealand', *Journal of Hydrology*, 388(3–4), pp. 399–413.

Carrivick, J.L. and Tweed, F.S. (2016) 'A global assessment of the societal impacts of glacier outburst floods', *Global and Planetary Change*, 144, pp. 1–16.

Chanson, H. (2004) *Hydraulics of open channel flow*. Elsevier. Available at: https://books.google.com/books?hl=de&lr=&id=VCNmKQI6GiEC&oi=fnd&pg=PP1&dq=Chanson,+H.,+2004.+The+Hydraulics+of+Open+Channel+Flows:+An+Introduction,+2nd+edition.+Butterworth-Heinemann,+Oxford+(630+pp.).&ots=pqO_ozd3jU&sig=hj8zJkeU3J-SWgCc1npKWLefh0w (Accessed: 22 January 2025).

Christen, M., Kowalski, J. and Bartelt, P. (2010) 'RAMMS: Numerical simulation of dense snow avalanches in three-dimensional terrain', *Cold Regions Science and Technology*, 63(1–2), pp. 1–14.

Clague, J.J. and Evans, S.G. (2000) 'A review of catastrophic drainage of moraine-dammed lakes in British Columbia', *Quaternary Science Reviews*, 19(17–18), pp. 1763–1783.

Costa, J.E. and Schuster, R.L. (1988) 'The formation and failure of natural dams', *Geological society of America bulletin*, 100(7), pp. 1054–1068.

Coussot, P. and Meunier, M. (1996) 'Recognition, classification and mechanical description of debris flows', *Earth-Science Reviews*, 40(3–4), pp. 209–227.

Cronin, S.J. *et al.* (1999) 'Dynamic interactions between lahars and stream flow: A case study from Ruapehu volcano, New Zealand', *Geological Society of America Bulletin*, 111(1), pp. 28–38.

Cui, P. *et al.* (2010) 'Debris Flows Resulting From Glacial-Lake Outburst Floods in Tibet, China', *Physical Geography*, 31(6), pp. 508–527. Available at: https://doi.org/10.2747/0272-3646.31.6.508.

Emmer, A. *et al.* (2020) '70 years of lake evolution and glacial lake outburst floods in the Cordillera Blanca (Peru) and implications for the future', *Geomorphology*, 365, p. 107178.

Emmer, A. *et al.* (2022) 'Progress and challenges in glacial lake outburst flood research (2017–2021): a research community perspective', *Natural Hazards and Earth System Sciences Discussions*, 2022, pp. 1–34.

Frank, F. *et al.* (2015) 'The importance of entrainment and bulking on debris flow runout modeling: examples from the Swiss Alps', *Natural Hazards and Earth System Sciences*, 15(11), pp. 2569–2583.

Frank, F. *et al.* (2017) 'Debris-flow modeling at Meretschibach and Bondasca catchments, Switzerland: sensitivity testing of field-data-based entrainment model', *Natural hazards and earth system sciences*, 17(5), pp. 801–815.

Franz, K.J. and Hogue, T.S. (2011) 'Evaluating uncertainty estimates in hydrologic models: borrowing measures from the forecast verification community', *Hydrology and Earth System Sciences*, 15(11), pp. 3367–3382.

Fread, D.L. (1988) 'BREACH: AN EROSION MODEL FOR EARTHEN DAM FAILURES', *Hydrologic Research Laboratory, National Weather Service, NOAA*, 855.

Frey, H. *et al.* (2016) 'A robust debris-flow and GLOF risk management strategy for a data-scarce catchment in Santa Teresa, Peru', *Landslides*, 13(6), pp. 1493–1507. Available at: https://doi.org/10.1007/s10346-015-0669-z.

Frey, H. *et al.* (2018) 'Multi-source glacial lake outburst flood hazard assessment and mapping for Huaraz, Cordillera Blanca, Peru', *Frontiers in Earth Science*, 6, p. 210.

Friz, C. (2021) *Numerical Debris Flow Modeling of GLOF Events Golen Gol*. Available at: https://doi.org/10.13140/RG.2.2.21836.54403.

Gaume, J. *et al.* (2018) 'Dynamic anticrack propagation in snow', *Nature communications*, 9(1), p. 3047.

Grove, J.M. (2019) *The little ice age*. Routledge. Available at: https://www.taylorfrancis.com/books/mono/10.4324/9780203505205/little-ice-age-jean-grove (Accessed: 22 January 2025).

Harrison, S. *et al.* (2018) 'Climate change and the global pattern of moraine-dammed glacial lake outburst floods', *The Cryosphere*, 12(4), pp. 1195–1209.

Hazra, P. and Krishna, A.P. (2022) 'Assessment of Proglacial Lakes in Sikkim Himalaya, India for Glacial Lake Outburst Flood (GLOF) Risk Analysis using HEC-RAS and Geospatial Techniques', *Journal of the Geological Society of India*, 98(3), pp. 344–352. Available at: https://doi.org/10.1007/s12594-022-1986-1.

HEC-RAS User's Manual (2025). Available at: https://www.hec.usace.army.mil/confluence/rasdocs/rasum/latest (Accessed: 23 January 2025).

Hegg, C. *et al.* (2002) 'Unwetterschäden in der Schweiz im Jahre 2001', *Wasser, Energie, Luft*, pp. 99–105.

Heller, V. and Hager, W.H. (2011) 'Wave types of landslide generated impulse waves', *Ocean Engineering*, 38(4), pp. 630–640.

Heller, V., Hager, W.H. and Minor, H.-E. (2008) 'Scale effects in subaerial landslide generated impulse waves', *Experiments in Fluids*, 44(5), pp. 691–703. Available at: https://doi.org/10.1007/s00348-007-0427-7.

Huggel, C. *et al.* (2002) 'Remote sensing based assessment of hazards from glacier lake outbursts: a case study in the Swiss Alps', *Canadian Geotechnical Journal*, 39(2), pp. 316–330. Available at: https://doi.org/10.1139/t01-099.

Huggel, C. *et al.* (2003) 'Regional-scale models of debris flows triggered by lake outbursts', *Natural Hazards and Earth System Sciences*, 3(6), pp. 647–662.

Huggel, C. *et al.* (2004) 'An assessment procedure for glacial hazards in the Swiss Alps', *Canadian Geotechnical Journal*, 41(6), pp. 1068–1083. Available at: https://doi.org/10.1139/t04-053.

Huggel, C. *et al.* (2008) 'Evaluation of ASTER and SRTM DEM data for lahar modeling: A case study on lahars from Popocatépetl Volcano, Mexico', *Journal of Volcanology and Geothermal Research*, 170(1), pp. 99–110. Available at: https://doi.org/10.1016/j.jvolgeores.2007.09.005.

Hungr, O. (2000) 'Analysis of debris flow surges using the theory of uniformly progressive flow', *Earth Surface Processes and Landforms*, 25(5), pp. 483–495. Available at: https://doi.org/10.1002/(SICI)1096-9837(200005)25:5<483::AID-ESP76>3.0.CO;2-Z.

Hungr, O., Leroueil, S. and Picarelli, L. (2014) 'The Varnes classification of landslide types, an update', *Landslides*, 11(2), pp. 167–194. Available at: https://doi.org/10.1007/s10346-013-0436-y.

IBER (2010) 'Two-dimensional modeling of free surface shallow water flow. Hydraulic Reference Manual.'

Iribarren Anacona, P. *et al.* (2018) 'Dynamics of an outburst flood originating from a small and high-altitude glacier in the Arid Andes of Chile', *Natural Hazards*, 94(1), pp. 93–119. Available at: https://doi.org/10.1007/s11069-018-3376-y.

Iverson, R.M. (1997) 'The physics of debris flows', *Reviews of Geophysics*, 35(3), pp. 245–296. Available at: https://doi.org/10.1029/97RG00426.

Iverson, R.M. (2009) 'Elements of an improved model of debris-flow motion', in *AIP Conference Proceedings*. American Institute of Physics, pp. 9–16. Available at: https://pubs.aip.org/aip/acp/article-abstract/1145/1/9/847199 (Accessed: 22 January 2025).

Iverson, R.M. *et al.* (2011) 'Positive feedback and momentum growth during debris-flow entrainment of wet bed sediment', *Nature Geoscience*, 4(2), pp. 116–121.

Kershaw, J.A., Clague, J.J. and Evans, S.G. (2005) 'Geomorphic and sedimentological signature of a two-phase outburst flood from moraine-dammed Queen Bess Lake, British Columbia, Canada', *Earth Surface Processes and Landforms*, 30(1), pp. 1–25. Available at: https://doi.org/10.1002/esp.1122.

Kidson, R.L., Richards, K.S. and Carling, P.A. (2006) 'Hydraulic model calibration for extreme floods in bedrock-confined channels: case study from northern Thailand', *Hydrological Processes*, 20(2), pp. 329–344. Available at: https://doi.org/10.1002/hyp.6086.

King, O. *et al.* (2019) 'Glacial lakes exacerbate Himalayan glacier mass loss', *Scientific Reports*, 9(1), p. 18145.

Klimeš, J. *et al.* (2014) 'The reconstruction of a glacial lake outburst flood using HEC-RAS and its significance for future hazard assessments: an example from Lake 513 in the Cordillera Blanca, Peru', *Natural Hazards*, 71(3), pp. 1617–1638. Available at: https://doi.org/10.1007/s11069-013-0968-4.

Kumar, B. and Murugesh Prabhu, T.S. (2012) 'Impacts of climate change: Glacial lake outburst floods (GLOFs)', *Climate change in sikkim patterns, impacts and initiatives. Information and public relations department, Government of Sikkim, Gangtok* [Preprint]. Available at: http://sikkimforest.gov.in/climate-change-in-sikkim/6-Chapter-Impact%20of%20Climate%20Change%20%20Glacier%20Lake%20Outburst%20Floods%20(GLOFs).pdf (Accessed: 22 January 2025).

Kumar, P. *et al.* (2020) 'Climatic variability at Gangtok and Tadong weather observatories in Sikkim, India, during 1961–2017', *Scientific reports*, 10(1), p. 15177.

Lala, J.M., Rounce, D.R. and McKinney, D.C. (2018) 'Modeling the glacial lake outburst flood process chain in the Nepal Himalaya: reassessing Imja Tsho's hazard', *Hydrology and Earth System Sciences*, 22(7), pp. 3721–3737. Available at: https://doi.org/10.5194/hess-22-3721-2018.

Manville, V., Major, J.J. and Fagents, S.A. (2013) 'Modeling lahar behavior and hazards', *Modeling volcanic processes: the physics and mathematics of volcanism*, pp. 300–330.

Martini, M., Baggio, T. and D'Agostino, V. (2023) 'Comparison of two 2-D numerical models for snow avalanche simulation', *Science of The Total Environment*, 896, p. 165221. Available at: https://doi.org/10.1016/j.scitotenv.2023.165221.

Massey, C.I. *et al.* (2010) 'Out-burst flood (lahar) triggered by retrogressive landsliding, 18 March 2007 at Mt Ruapehu, New Zealand—a successful early warning', *Landslides*, 7(3), pp. 303–315. Available at: https://doi.org/10.1007/s10346-009-0180-5.

McArdell, B.W., Bartelt, P. and Kowalski, J. (2007) 'Field observations of basal forces and fluid pore pressure in a debris flow', *Geophysical Research Letters*, 34(7), p. 2006GL029183. Available at: https://doi.org/10.1029/2006GL029183.

Mergili, M. *et al.* (2011) 'Glacial lake outburst floods in the Pamir of Tajikistan: challenges in prediction and modelling', *Italian journal of engineering geology and environment*, pp. 973–982.

Mergili, M. (2014) *r.avaflow - The mass flow simulation tool. r.avaflow 2.4 User manual.* Available at: https://www.avaflow.org/manual.php (Accessed: 8 January 2025).

Mergili, M. *et al.* (2020) 'Reconstruction of the 1941 GLOF process chain at lake Palcacocha (Cordillera Blanca, Peru)', *Hydrology and Earth System Sciences*, 24(1), pp. 93–114.

Meyrat, G. *et al.* (2022) 'A dilatant, two-layer debris flow model validated by flow density measurements at the Swiss illgraben test site', *Landslides*, 19(2), pp. 265–276. Available at: https://doi.org/10.1007/s10346-021-01733-2.

Meyrat, G. *et al.* (2023) 'Voellmy-type mixture rheologies for dilatant, two-layer debris flow models', *Landslides*, 20(11), pp. 2405–2420. Available at: https://doi.org/10.1007/s10346-023-02092-w.

Meyrat, G. *et al.* (2024) 'Simulating glacier lake outburst floods (GLOFs) with a two-phase/layer debris flow model considering fluid-solid flow transitions', *Landslides*, 21(3), pp. 479–497. Available at: https://doi.org/10.1007/s10346-023-02157-w.

Meyrat, G., Bartelt, P. and McArdell, B. (2023) 'A dilatant two-phase debris flow model with erosion validated by full-scale field data from the Illgraben test station', in *E3S Web of Conferences*. EDP Sciences, p. 01015. Available at: https://www.e3s-conferences.org/articles/e3sconf/abs/2023/52/e3sconf_dfhm82023_01015/e3sconf_dfhm82023_01015.html (Accessed: 24 January 2025).

Mikoš, M. and Bezak, N. (2021) 'Debris Flow Modelling Using RAMMS Model in the Alpine Environment With Focus on the Model Parameters and Main Characteristics', *Frontiers in Earth Science*, 8. Available at: https://doi.org/10.3389/feart.2020.605061.

Mitchell, A. *et al.* (2022) 'Variable hydrograph inputs for a numerical debris-flow runout model', *Natural Hazards and Earth System Sciences*, 22(5), pp. 1627–1654.

Motschmann, A. *et al.* (2020) 'Losses and damages connected to glacier retreat in the Cordillera Blanca, Peru', *Climatic Change*, 162(2), pp. 837–858. Available at: https://doi.org/10.1007/s10584-020-02770-x.

Narama, C. *et al.* (2018) 'Large drainages from short-lived glacial lakes in the Teskey Range, Tien Shan Mountains, Central Asia', *Natural Hazards and Earth System Sciences*, 18(4), pp. 983–995.

Nath, S.K. (2005) 'An initial model of seismic microzonation of Sikkim Himalaya through thematic mapping and GIS integration of geological and strong motion features☆', *Journal of Asian Earth Sciences*, 25(2), pp. 329–343.

Nauser, M. (2016) *Das Wallis angesichts des Klimawandels – Auswirkungen und Anpassungsoptionen in den Bereichen Wasserbewirtschaftung und Naturgefahren (Synthesepapier)*. Sion: Dienststelle für Wald und Landschaft, Sektion Naturgefahren.

Neogi, S., Dasgupta, S. and Fukuoka, M. (1998) 'High P–T polymetamorphism, dehydration melting, and generation of migmatites and granites in the Higher Himalayan Crystalline Complex, Sikkim, India', *Journal of Petrology*, 39(1), pp. 61–99.

O'Brien, J.S., Julien, P.Y. and Fullerton, W.T. (1993) 'Two-Dimensional Water Flood and Mudflow Simulation Journal of Hydraulic Engineering 119 (2): 244-261'.

Osti, R., Bhattarai, T.N. and Miyake, K. (2011) 'Causes of catastrophic failure of Tam Pokhari moraine dam in the Mt. Everest region', *Natural Hazards*, 58(3), pp. 1209–1223. Available at: https://doi.org/10.1007/s11069-011-9723-x.

Pappenberger, F. *et al.* (2006) 'Influence of uncertain boundary conditions and model structure on flood inundation predictions', *Advances in Water Resources*, 29(10), pp. 1430–1449. Available at: https://doi.org/10.1016/j.advwatres.2005.11.012.

Pierson, T.C. *et al.* (1996) 'Flow and deposition of posteruption hot lahars on the east side of Mount Pinatubo, July–October 1991', *Fire and Mud: eruptions and lahars of Mount Pinatubo, Philippines*, pp. 921–950.

Pierson, T.C. (2020) 'Flow behavior of channelized debris flows, Mount St. Helens, Washington', in *Hillslope processes*. Routledge, pp. 269–296. Available at: https://www.taylorfrancis.com/chapters/edit/10.4324/9781003028840-13/flow-behavior-channelized-debris-flows-mount-st-helens-washington-thomas-pierson (Accessed: 22 January 2025).

Pitman, E.B. *et al.* (2013) 'Two phase simulations of glacier lake outburst flows', *Journal of Computational Science*, 4(1–2), pp. 71–79.

Pudasaini, S.P. (2012) 'A general two-phase debris flow model', *Journal of Geophysical Research: Earth Surface*, 117(F3), p. 2011JF002186. Available at: https://doi.org/10.1029/2011JF002186.

Pudasaini, S.P. (2020) 'A full description of generalized drag in mixture mass flows', *Engineering Geology*, 265, p. 105429.

Pudasaini, S.P. and Fischer, J.-T. (2020) 'A mechanical erosion model for two-phase mass flows', *International Journal of Multiphase Flow*, 132, p. 103416.

Pudasaini, S.P. and Krautblatter, M. (2021) 'The mechanics of landslide mobility with erosion', *Nature Communications*, 12(1), p. 6793. Available at: https://doi.org/10.1038/s41467-021-26959-5.

Pudasaini, S.P. and Mergili, M. (2019) 'A Multi-Phase Mass Flow Model', *Journal of Geophysical Research: Earth Surface*, 124(12), pp. 2920–2942. Available at: https://doi.org/10.1029/2019JF005204.

Raj, K.B.G., Remya, S.N. and Kumar, K.V. (2013) 'Remote sensing-based hazard assessment of glacial lakes in Sikkim Himalaya', *Current Science*, pp. 359–364.

Richardson, S.D. and Reynolds, J.M. (2000) 'An overview of glacial hazards in the Himalayas', *Quaternary International*, 65, pp. 31–47.

Rickenmann, D. (1999) 'Empirical Relationships for Debris Flows', *Natural Hazards*, 19(1), pp. 47–77. Available at: https://doi.org/10.1023/A:1008064220727.

Rickenmann, D. *et al.* (2006) 'Comparison of 2D debris-flow simulation models with field events', *Computational Geosciences*, 10(2), pp. 241–264. Available at: https://doi.org/10.1007/s10596-005-9021-3.

Rinzin, S. *et al.* (2024) 'Exploring implications of input parameter uncertainties on GLOF modelling results using the state-of-the-art modelling code, r. avaflow', *EGUsphere*, 2024, pp. 1–38.

Rounce, D.R. *et al.* (2016) 'A new remote hazard and risk assessment framework for glacial lakes in the Nepal Himalaya', *Hydrology and Earth System Sciences*, 20(9), pp. 3455–3475.

de Saint-Venant, A.B. (1871) 'Théorie et équations générales du mouvement non permanent des eaux courantes', *Comptes Rendus des séances de l'Académie des Sciences*, 17(3), pp. 147–154.

Salm, B. (1993) 'Flow, flow transition and runout distances of flowing avalanches', *Annals of Glaciology*, 18, pp. 221–226.

Salm, B., Burkhard, A. and Gubler, H.U. (1990) *Berechnung von Fliesslawinen: eine Anleitung für Praktiker mit Beispielen*. Eidgenössisches Institut für Schnee-und Lawinenforschung, Weissfluhjoch/Davos. Available at: https://www.dora.lib4ri.ch/wsl/islandora/object/wsl%3A26106/datastream/PDF/Salm-1990-Berechnung_von_Fliesslawinen_eine_Anleitung-%28published_version%29.pdf (Accessed: 28 January 2025).

Sanders, B.F. (2007) 'Evaluation of on-line DEMs for flood inundation modeling', *Advances in Water Resources*, 30(8), pp. 1831–1843. Available at: https://doi.org/10.1016/j.advwatres.2007.02.005.

Saritha, G. *et al.* (2021) 'Digital elevation model and terrain mapping using LiDAR', *Materials Today: Proceedings*, 46, pp. 3979–3983.

Sattar, A., Goswami, A., *et al.* (2021) 'Future glacial lake outburst flood (GLOF) hazard of the South Lhonak Lake, Sikkim Himalaya', *Geomorphology*, 388, p. 107783.

Sattar, A., Haritashya, U.K., *et al.* (2021) 'Modeling lake outburst and downstream hazard assessment of the Lower Barun Glacial Lake, Nepal Himalaya', *Journal of Hydrology*, 598, p. 126208.

Sattar, A. *et al.* (2022) 'Transition of a small Himalayan glacier lake outburst flood to a giant transborder flood and debris flow', *Scientific reports*, 12(1), p. 12421.

Sattar, A. *et al.* (2025) 'The Sikkim flood of October 2023: drivers, causes and impacts of a multi-hazard cascade', *Science* [Preprint].

Sattar, A., Goswami, A. and Kulkarni, A.V. (2019a) 'Application of 1D and 2D hydrodynamic modeling to study glacial lake outburst flood (GLOF) and its impact on a hydropower station in Central Himalaya', *Natural Hazards*, 97(2), pp. 535–553. Available at: https://doi.org/10.1007/s11069-019-03657-6.

Sattar, A., Goswami, A. and Kulkarni, A.V. (2019b) 'Hydrodynamic moraine-breach modeling and outburst flood routing-A hazard assessment of the South Lhonak lake, Sikkim', *Science of the total environment*, 668, pp. 362–378.

Schneider, D. *et al.* (2014) 'Mapping hazards from glacier lake outburst floods based on modelling of process cascades at Lake 513, Carhuaz, Peru', *Advances in Geosciences*, 35, pp. 145–155.

Schürch, P. *et al.* (2011) 'Dynamic controls on erosion and deposition on debris-flow fans', *Geology*, 39(9), pp. 827–830.

Sharma, R.K. *et al.* (2018) 'Remote sensing and in situ-based assessment of rapidly growing South Lhonak glacial lake in eastern Himalaya, India', *Natural Hazards*, 93(1), pp. 393–409. Available at: https://doi.org/10.1007/s11069-018-3305-0.

Singh, V.P. (1996) 'Comparative Evaluation of Dam-Breach Models', in V.P. Singh (ed.) *Dam Breach Modeling Technology*. Dordrecht: Springer Netherlands, pp. 220–231. Available at: https://doi.org/10.1007/978-94-015-8747-1_8.

Smith, G.A. and Lowe, D.R. (1991) 'Lahars: volcano-hydrologic events and deposition in the debris flow—hyperconcentrated flow continuum'.

Somos-Valenzuela, M.A. *et al.* (2016) 'Modeling a glacial lake outburst flood process chain: the case of Lake Palcacocha and Huaraz, Peru', *Hydrology and Earth System Sciences*, 20(6), pp. 2519–2543.

Stock, J.D. and Dietrich, W.E. (2006) 'Erosion of steepland valleys by debris flows', *Geological Society of America Bulletin*, 118(9–10), pp. 1125–1148.

Stolz, A. and Huggel, C. (2008) 'Debris flows in the Swiss National Park: the influence of different flow models and varying DEM grid size on modeling results', *Landslides*, 5(3), pp. 311–319. Available at: https://doi.org/10.1007/s10346-008-0125-4.

Stricker, B. (2010) *Murgänge im Torrente Riascio (TI): Ereignisanalyse, Auslösefaktoren und Simulation von Ereignissen mit RAMMS*. PhD Thesis. Geographisches Institut der Universität Zürich. Available at: https://www.researchgate.net/profile/Benjamin-Stricker-Zirfass/publication/232060352_Murgange_im_Torrente_Riascio_TI_Ereignisanalyse_Auslosefaktoren_und_Simulation_von_Ereignissen_mit_RAMMSDebris_flows_in_Torrente_Riascio_TI_Quantitative_analysis_of_past_events_triggering_factors_and_/links/0912f507448aaece6a000000/Murgaenge-im-Torrente-Riascio-TI-Ereignisanalyse-Ausloesefaktoren-und-Simulation-von-Ereignissen-mit-RAMMSDebris-flows-in-Torrente-Riascio-TI-Quantitative-analysis-of-past-events-triggering-factors.pdf (Accessed: 28 January 2025).

Taylor, C. *et al.* (2023) 'Glacial lake outburst floods threaten millions globally', *Nature Communications*, 14(1), p. 487.

Voigt, T. *et al.* (2010) 'Impacts of climate change on snow, ice, and permafrost in Europe: observed trends, future projections, and socio- economic relevance', *European Topic Centre on Air and Climate Change* [Preprint]. Available at: https://doi.org/10.5167/uzh-53485.

Wang, Y., Hutter, K. and Pudasaini, S.P. (2004) 'The Savage-Hutter theory: A system of partial differential equations for avalanche flows of snow, debris, and mud', *ZAMM - Journal of Applied Mathematics and Mechanics / Zeitschrift für Angewandte Mathematik und Mechanik*, 84(8), pp. 507–527. Available at: https://doi.org/10.1002/zamm.200310123.

Westoby, M.J. *et al.* (2014) 'Modelling outburst floods from moraine-dammed glacial lakes', *Earth-Science Reviews*, 134, pp. 137–159.

Worni, R. *et al.* (2012) 'Analysis and dynamic modeling of a moraine failure and glacier lake outburst flood at Ventisquero Negro, Patagonian Andes (Argentina)', *Journal of Hydrology*, 444, pp. 134–145.

Worni, R. *et al.* (2014) 'Coupling glacial lake impact, dam breach, and flood processes: A modeling perspective', *Geomorphology*, 224, pp. 161–176.

Yu, Y. *et al.* (2024) 'Retrospective analysis of glacial lake outburst flood (glof) using ai earth insar and optical images: A case study of south lhonak lake, sikkim', *Remote Sensing*, 16(13), p. 2307.

Zemp, M. *et al.* (2015) 'Historically unprecedented global glacier decline in the early 21st century', *Journal of glaciology*, 61(228), pp. 745–762.

Zhang, T., Wang, W. and An, B. (2025) 'A massive lateral moraine collapse triggered the 2023 South Lhonak Lake outburst flood, Sikkim Himalayas', *Landslides*, 22(2), pp. 299–311. Available at: https://doi.org/10.1007/s10346-024-02358-x.

Ziegler, A.D. *et al.* (2014) 'Pilgrims, progress, and the political economy of disaster preparedness – the example of the 2013 Uttarakhand flood and Kedarnath disaster', *Hydrological Processes*, 28(24), pp. 5985–5990. Available at: https://doi.org/10.1002/hyp.10349.

Appendix

A) Dam Implementation According to “SWISSIMAGE Zeitreise”

Dam west, located at the apex of the fan

2000

2006

Dam east, located before the river Rotbach enters Täschalp

2000

2012

B) Geology Map of Weingarten Lake

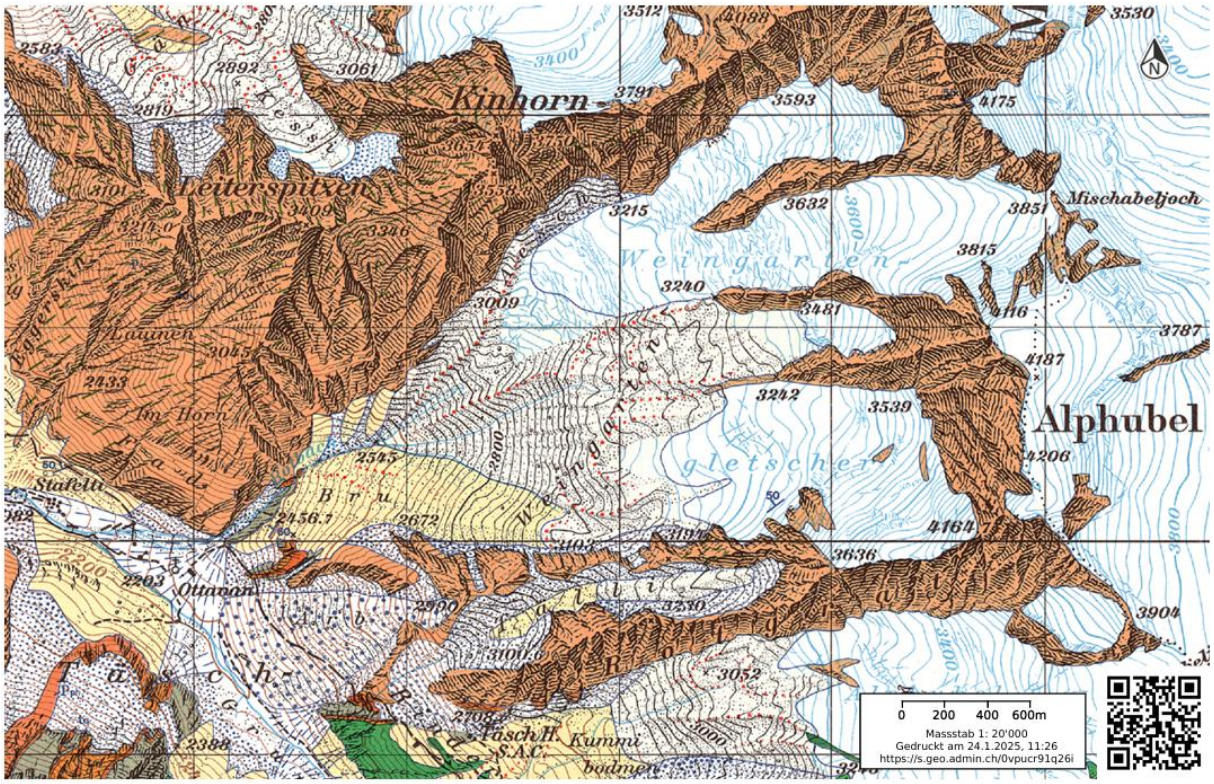

C) Permafrost Layer Weingarten Lake

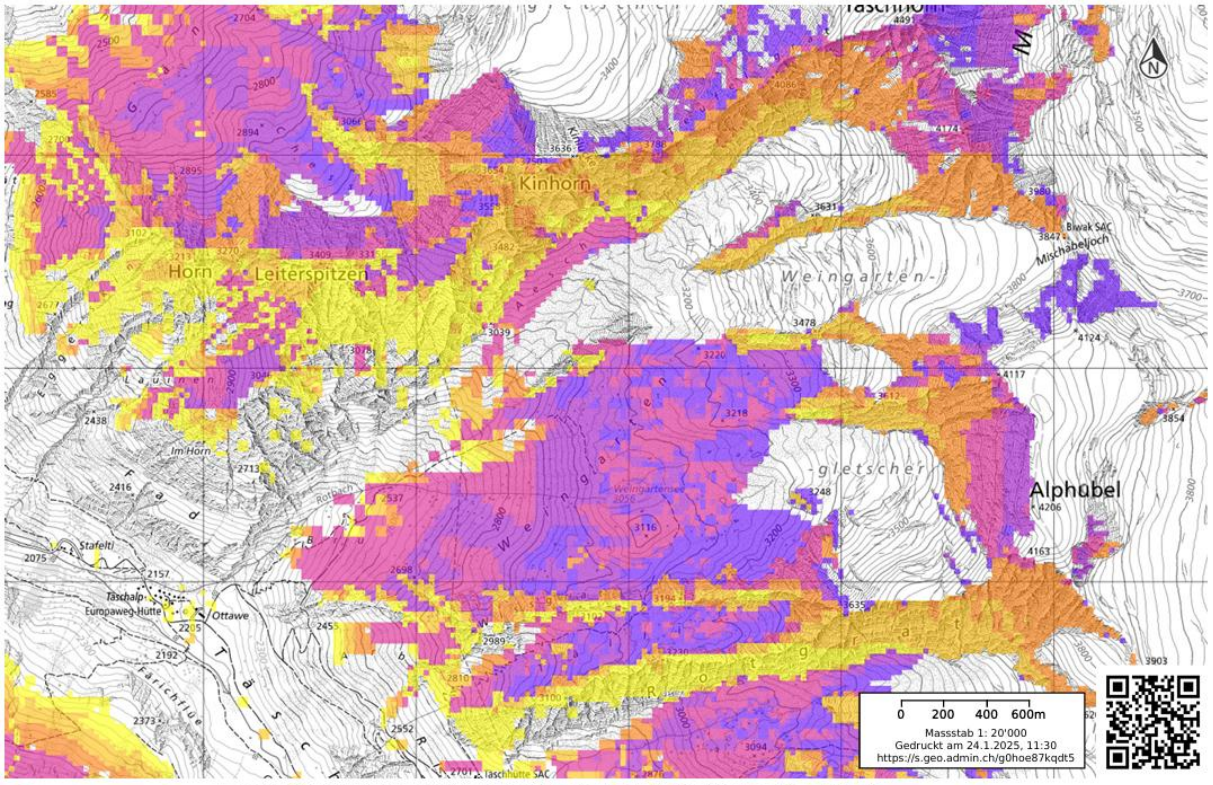

Legende

- Permafrost lokal möglich, fleckenhaft, punktuell
- Permafrost lokal möglich, fleckenhaft häufig
- Permafrost lokal möglich, fleckenhaft bis grossflächig
- Permafrost flächenhaft wahrscheinlich
- Permafrost flächenhaft wahrscheinlich, Mächtigkeit zunehmend
- Permafrost flächenhaft wahrscheinlich, z.T. grosse Mächtigkeiten bis über 100 m

D) Socio-Economic Development

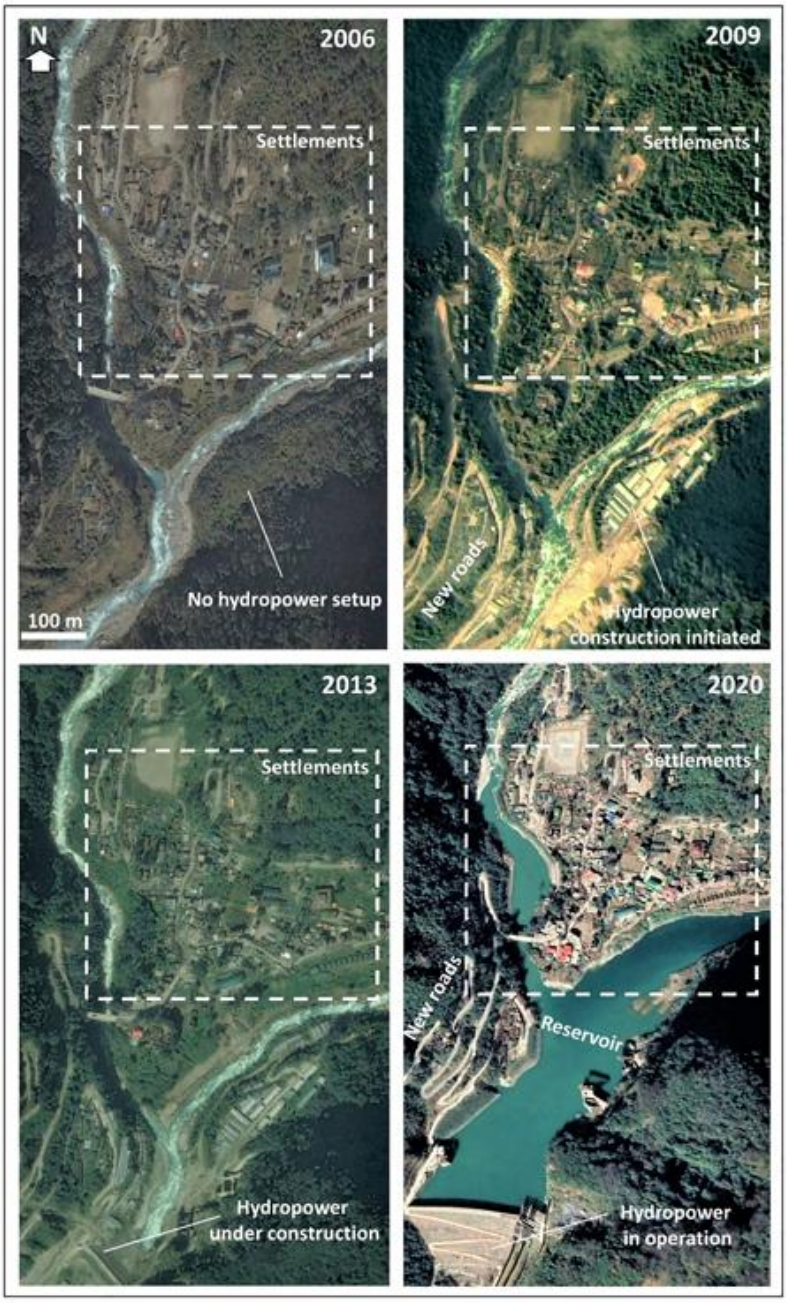

Fig. 14. Evolution of the Chungthang town. The rapid growth of the infrastructure is seen after the establishment of the hydropower setup.

Map of Sattar *et al.* (2021) highlighting the socio-economic development.

E) Utilized Parameters for r.avaflow simulations

Parameter	Default values	Range of values
Density of solid (ρS)	2700 kg·m^{-3}	2500–2900 kg·m^{-3}
Density of fluid (ρF)	1000 kg·m^{-3}	1000–1200 kg·m^{-3}
Entrainment coefficient (C_E)	10^{-7}	10^{-6}–10^{-8}
Basal friction of solid (δ)	35°	8°–20°
Internal friction of solid (φ)	20°	20°–35°
Fluid friction number (C_{FF})	0.05	0–0.1
Kinematic viscosity of fluid (C_{KV})	−3 m^2·s^{-1}	−1–5 m^2·s^{-1}
Yield strength of fluid (C_{YC})	0 Pa	0–10 Pa
Shear velocity coefficient (C_{SV})	0.05	0–0.05
Ambient drag coefficient (C_{AD})	0	0–0.2
Maximum water fraction of deposited material (C_{WF})	0.333	0–0.333

The table shows the 11 utilized parameters for the r.avaflow simulations conducted by Zhang, Wang and An (2025). 6 of them were identified as sensitive.

F) Simulation of the whole South Lhonak GLOF

Simulation stopped because of high computational power.

Personal Declaration

I hereby declare that the submitted thesis results from my own independent work. All external sources are explicitly acknowledged in the thesis.

I further acknowledge that ChatGPT and Grammarly were utilized during the completion of this thesis to assist with grammar, syntax and content refinement.

Zurich, January 31, 2025

Noël Baumann